②

US Army Corps of Engineers

AD-A209 527

MILITARY HYDROLOGY

Report 16

ASSESSMENT OF SHUTTLE IMAGING RADAR AND LANDSAT IMAGERY FOR GROUND-WATER EXPLORATION IN ARID ENVIRONMENTS

by

Harold C. MacDonald, Brent C. Clark, Doug S. Taylor
Gregory L. Rainwater, Verne H. Kaupp, William P. Waite

University of Arkansas
Fayetteville, Arkansas 72701

DTIC
ELECTE
JUN 27 1989
S E D

June 1989
Report 16 of a Series

89 6 27 016

Unclassified

SECURITY CLASSIFICATION OF THIS PAGE

REPORT DOCUMENTATION PAGE		*Form Approved* *OMB No 0704 0188* *Exp Date Jun 30, 1986*

1a REPORT SECURITY CLASSIFICATION Unclassified	1b RESTRICTIVE MARKINGS
2a SECURITY CLASSIFICATION AUTHORITY	3 DISTRIBUTION/AVAILABILITY OF REPORT Approved for public release; distribution unlimited.
2b DECLASSIFICATION/DOWNGRADING SCHEDULE	

4 PERFORMING ORGANIZATION REPORT NUMBER(S)	5 MONITORING ORGANIZATION REPORT NUMBER(S) Miscellaneous Paper EL-79-6

6a NAME OF PERFORMING ORGANIZATION University of Arkansas	6b OFFICE SYMBOL *(If applicable)*	7a NAME OF MONITORING ORGANIZATION USAEWES Environmental Laboratory

6c ADDRESS (City State, and ZIP Code) Fayetteville, AR 72701	7b ADDRESS (City, State, and ZIP Code) PO Box 631 Vicksburg, MS 39181-0631

8a NAME OF FUNDING/SPONSORING ORGANIZATION US Army Corps of Engineers	8b OFFICE SYMBOL *(If applicable)*	9 PROCUREMENT INSTRUMENT IDENTIFICATION NUMBER Contract No. DACA39-85-C-0013

8c ADDRESS (City, State, and ZIP Code) Washington, DC 20314-1000	10. SOURCE OF FUNDING NUMBERS			
	PROGRAM ELEMENT NO.	PROJECT NO. See reverse.	TASK NO CO	WORK UNIT ACCESSION NO 017

11. TITLE *(Include Security Classification)*
Military Hydrology; Report 16, Assessment of Shuttle Imaging Radar and Landsat Imagery for Ground-Water Exploration in Arid Environments

12. PERSONAL AUTHOR(S)
See Reverse.

13a. TYPE OF REPORT Report 16 of a series	13b TIME COVERED FROM _____ TO _____	14. DATE OF REPORT (Year, Month, Day) June 1989	15 PAGE COUNT 89

16. SUPPLEMENTARY NOTATION
Available from National Technical Information Service, 5285 Port Royal Road, Springfield, VA 22161.

17	COSATI CODES		18. SUBJECT TERMS *(Continue on reverse if necessary and identify by block number)*
FIELD	GROUP	SUB-GROUP	See reverse.

19. ABSTRACT *(Continue on reverse if necessary and identify by block number)*

Remote sensor imagery interpretation can provide valuable guides for ground-water exploration. Imagery interpretation affords a reliable, rapid, and cost-effective technique for the identification and analysis of ground-water resources of a given area and is particularly useful in areas for which data or access is limited. Shuttle imaging radars (SIR-A and -B) are part of the National Aeronautics and Space Administration's continuing program of basic and applied research to explore the utility of radar imaging techniques for Earth observations. The shuttle radar of the eastern Sahara provided imagery that allowed for the detection of previously unknown buried stream channels ("radar rivers"). Mapping of such drainage patterns in desert environments can sometimes provide a regional guide to potential ground-water resources. However, the shuttle radar did not provide complete coverage of the eastern Sahara, and in fact, many of the desert areas of the world were not imaged. On the other hand, Landsat data are available for most of the arid and semiarid regions of the Earth,
(Continued)

20 DISTRIBUTION/AVAILABILITY OF ABSTRACT ☒ UNCLASSIFIED/UNLIMITED ☐ SAME AS RPT ☐ DTIC USERS	21 ABSTRACT SECURITY CLASSIFICATION Unclassified	
22a NAME OF RESPONSIBLE INDIVIDUAL	22b TELEPHONE (Include Area Code)	22c OFFICE SYMBOL

DD FORM 1473, 84 MAR | 83 APR edition may be used until exhausted
 All other editions are obsolete | SECURITY CLASSIFICATION OF THIS PAGE
 Unclassified

10. PROJECT NO. (Continued).

4A762719AT40

12. PERSONAL AUTHORS (Continued).

MacDonald, Harold C.; Clark, Brent C.; Taylor, Doug S.; Rainwater, Gregory L.; Kaupp, Verne H.; Waite, William P.

18. SUBJECT TERMS (Continued).

Aircraft radars; Arid terrain; Ground-water exploration; Imaging radar, Landsat; Radar remote sensing; "Radar rivers," Relict fluvial channels; Satellite remote sensing; Shuttle radars.

19. ABSTRACT (Continued).

although the use of Landsat imagery to detect "radar rivers" in those areas where no spaceborne radar coverage is available has not been adequately addressed prior to this study.

- This report provides: (a) an evaluation of the suitability of Landsat imagery to bridge the gap between shuttle radar flight lines; (b) a discussion of the circumstances under which either remote sensor may be superior for detecting relict drainage systems; and (c) an assessment of the value of imaging radar for ground-water exploration in arid regions.

This investigation indicates that relict fluvial channels initially inferred on shuttle imagery can be extended and mapped on a regional basis if the Landsat imagery data base is properly selected and processed. In addition, short wavelength aircraft radars may have considerable applicability in sand-covered terrains where differences in surface morphology and texture define relict fluvial channels. Used in a complementary mode, radar imagery and Landsat data can provide an important ground-water exploration technique in arid regions throughout the world.

Success of military operations in such desert areas depends on the location of sufficient quantities of water to sustain the force. The utility of SIR and Landsat imagery for mapping relict fluvial channels in arid regions is therefore important to the military, particularly with the attention currently being directed toward Southwest Asia.

PREFACE

The work reported herein was performed by personnel at the University of Arkansas, Fayetteville, AR, for the US Army Engineer Waterways Experiment Station (WES) under Contract No. DACA39-85-C-0013. Serving as Principal Investigator for the University was Dr. Harold C. MacDonald, Professor of Geology. Messrs. Brent C. Clark, Doug S. Taylor, and Gregory L. Rainwater, graduate students in the Department of Geology, assisted Dr. MacDonald in conducting the research. This report was prepared by Dr. MacDonald, Messrs. Clark, Taylor, and Rainwater, as well as Drs. Verne H. Kaupp and William P. Waite, Professors of Electrical Engineering at the University. Acknowledgment is made to Dr. Paul G. Harrison, Cities Service Company, Tulsa, OK, for providing Landsat digital data and enhanced imagery products; students of the Image Simulation Laboratory, Engineering Experiment Station, University of Arkansas, for generating enhanced Landsat images; Mr. Ronald H. Gelnett, MARS and Associates, Inc., Phoenix, AZ, who made radar imagery of the Sudan available to the researchers; and Dr. Gerald G. Schaber, Chief, Branch of Astrogeology, US Geological Survey (USGS), Flagstaff, AZ, for allowing graduate students from the University of Arkansas to visit his facility and for briefing them on current USGS work with shuttle imaging radar in desert regions.

The effort was funded by Headquarters, US Army Corps of Engineers (HQUSACE), under Department of the Army Project No. 4A762719AT40, "Mobility and Weapons Effects Technology," Task Area CO, Work Unit 017, "Remote Procedures for Locating Water Supplies." Mr. Austin A. Owen was the HQUSACE Technical Monitor.

Principal Investigators of Work Unit 017 were Messrs. Elba A. Dardeau, Jr., and John G. Collins, Environmental Constraints Group (ECG), Environmental Systems Division (ESD), Environmental Laboratory (EL), WES. Mr. Dardeau also served as Contracting Officer's Representative. The work unit was conducted under the general supervision of Mr. Malcolm P. Keown, Chief, ECG; Dr. Victor E. LaGarde III, Chief, ESD; and Dr. John Harrison, Chief, EL. This report was edited by Ms. Lee T. Byrne of the Information Technology Laboratory.

COL Dwayne G. Lee, EN, is the Commander and Director of WES.

Dr. Robert W. Whalin is the Technical Director.

This report should be cited as follows:

MacDonald, H. C., Clark, B. C., Taylor, D. S., Rainwater, G. L.,
Kaupp, V. H., and Waite, W. P. 1989. "Military Hydrology; Report 16,
Assessment of Shuttle Imaging Radar and Landsat Imagery for Ground-Water
Exploration in Arid Environments," Miscellaneous Paper EL-79-6, US Army
Engineer Waterways Experiment Station, Vicksburg, MS.

Accession For		
NTIS GRA&I	☒	
DTIC TAB	☐	
Unannounced	☐	
Justification		
By		
Distribution/		
Availability Codes		
Dist	Avail and/or Special	
A-1		

CONTENTS

MILITARY HYDROLOGY

ASSESSMENT OF SHUTTLE IMAGING RADAR AND LANDSAT IMAGERY FOR GROUND-WATER EXPLORATION IN ARID ENVIRONMENTS

PART I: INTRODUCTION

Background

1. Military hydrology is a specialized field of study that deals with the effects of surface and subsurface water on the planning and conduct of military operations. In 1977, Headquarters, US Army Corps of Engineers, approved a military hydrology research program; management responsibility was subsequently assigned to the Environmental Laboratory, US Army Engineer Waterways Experiment Station, Vicksburg, MS.

2. The objective of military hydrology research is to develop an improved hydrologic capability for the Armed Forces with emphasis on applications in the tactical environment. To meet this overall objective, research is being conducted in four thrust areas: (a) weather-hydrology interactions, (b) state of the ground, (c) streamflow, and (d) water supply.

3. Previously published Military Hydrology reports are listed on the inside of the back cover. This report is the seventh that contributes to the water-supply thrust area, which is oriented toward the development of an integrated approach for rapidly locating and evaluating ground-water supplies, particularly in arid regions. Specific work efforts include: (a) the compilation of guidelines for the expedient location of water for human survival, (b) the development of remote imagery interpretation procedures for detecting and evaluating ground-water sources, (c) the adaptation of suitable geophysical methods for detecting and evaluating ground-water sources, and (d) the development of water-supply analysis and display concepts.

4. Remote sensor imagery interpretation is a valuable tool for ground-water exploration; it is a reliable, rapid, and cost-effective technique for the identification and analysis of ground-water resources of a given area and is particularly useful in areas for which data or access is limited. Since 1972, the National Aeronautics and Space Administration's (NASA's) Landsat

satellite remote sensing systems have been acquiring high-quality imagery of the Earth's surface on a repetitive basis. These data have been used for worldwide ground-water exploration. However, Landsat sensors are adversely affected by cloud cover and associated weather conditions. Recently, Shuttle Imaging Radars-A and -B (SIR-A and -B) have provided images from many parts of the world. Unlike Landsat imagery, shuttle radar imagery is not affected by weather conditions or solar illumination. Shuttle radar imagery interpretation has made possible the detection of previously unmapped stream channels beneath the extremely dry sand sheets, dunes, and drift sands of the eastern Sahara.

5. Shuttle imaging radars are part of NASA's continuing program of basic and applied research to explore the utility of radar imaging techniques for Earth observations. SIR-B is viewed by the geoscience community as an interim step in developing an Earth-orbiting microwave sensor system capable of routinely imaging global resources.

6. The shuttle radar imagery of the eastern Sahara allowed for the detection of previously unknown buried stream channels ("radar rivers"). Mapping of such drainage patterns in desert environments can sometimes provide a regional guide to potential ground-water resources. However, the shuttle radar did not provide complete coverage of the eastern Sahara; in fact, many of the desert areas of the world were not imaged. Landsat data, on the other hand, are available for most of the Earth's arid and semiarid regions, although the use of Landsat imagery to detect "radar rivers" in those areas where no spaceborne radar coverage is available has not been adequately addressed.

Objectives

7. The objectives of this investigation were to: (a) evaluate the suitability of Landsat imagery to bridge the gap between shuttle radar flight lines, (b) determine under what circumstances one remote sensor may be superior to the other for detecting relict drainage systems, (c) assess the value of imaging radar for ground-water exploration in arid regions, (d) determine the optimum enhancement techniques for defining desert landforms and surface texture, and (e) assess the suitability of this approach for military applications.

Scope

8. The investigation reported herein includes six major parts. Part I
is an introduction. Part II is a review of spaceborne imaging radar tech-
niques, including previous radar interpretation studies in arid environments.
Selection criteria, location, and pertinent geologic and hydrologic parameters
for each test site are provided in Part III. Part IV contains a comparison of
the interpretative data content of the spaceborne radar imagery versus that of
Landsat imagery and an evaluation of the relative merits of each sensor for
ground-water exploration. An aspect of ground-water resource evaluation that
has not been previously recognized, i.e., the potential for using aircraft
radar for the detection of "radar rivers," is presented in Part V. Contrast
enhancement of digital Landsat data is addressed in Part VI. Conclusions and
recommendations comprise Part VII.

PART II: REVIEW OF SPACEBORNE IMAGING RADAR TECHNIQUES

9. The concept of using reflected radio waves for remote target location purposes evolved in several countries prior to World War II with the development of systems that transmitted from ground to airborne targets. By the end of the war, the techniques (collectively called radar, an acronym for radio detection and ranging) and their basic principles had been developed to a high degree.

10. Radar is unique among the commonly used remote sensors because it provides its own illumination, electromagnetic energy of radio or microwave frequencies. For the simplest mode of operation (i.e., ground to air), a transmitter on the ground emits electromagnetic radiation in the form of radio frequency (RF) energy. When the RF energy is interrupted by any object, such as an aircraft, part of the energy is reflected back to a receiver. The reflection or reradiation of energy returned to the receiver is referred to as an "echo," and the object reflecting or reradiating the signal is called the target. If, however, reradiation is returned from the surrounding terrain, which makes selecting the desired target difficult, the unwanted return signals are termed "clutter." This "clutter" is what the interpreter must analyze.

11. Imaging radars were first developed in the early fifties as incoherent side-looking airborne radars (SLAR) for high-resolution remote sensing; by 1969, SLAR surveys were commercially available. In parallel with SLAR exploitation, the coherent imaging radar or synthetic aperture radar (SAR) was also being developed--first with the experiments in the early fifties by Carl Wiley of the Goodyear Aircraft Corporation and later at the Universities of Illinois and Michigan (MacDonald 1980). The SAR makes use of the Doppler phase history of the backscattered radiation from natural targets to synthesize an effective along-track aperture, which is much larger than the real aperture, thereby permitting fine along-track resolution without the need for an impractically long antenna.

12. Spaceborne imaging radars were first made available for Earth observation with the launch of Seasat in 1978. The promising results of the Seasat imagery helped shift interest of the remote sensing community toward the microwave field. Two SAR experiments have been conducted aboard space shuttle flights, SIR-A in 1981 and SIR-B in 1984. In addition, a number of

imaging radar satellite programs are in advanced stages of planning, SIR-C (United States), ERS-1 and -2 (European Space Agency), JERS-1 (Japan), RADSAT (Canada), and the Venus radar mapping mission Magellan (United States).

Radar Principles

13. The resolutions of spaceborne imaging radar systems do not match those of photography; however, these same systems have the unique ability to delineate physical characteristics of the Earth's surface by providing an image of "photographic" quality independent of visibility or weather conditions. This operational advantage is related to the fact that radars utilize the microwave band of the electromagnetic spectrum, which can penetrate clouds, smoke, fog, and most precipitation. Radar mapping surveys can thus be conducted at virtually any time.

Operational frequencies

14. Conventional radars use the frequency range from 230 to 40,000 MHz, although neither end of this range is truly definitive of the frequency limitation for radar operation. A letter code of frequency-wavelength bands was arbitrarily selected to ensure military security in the early development stages of radar and has continued in use for convenience. Figure 1 shows the subdivisions of the microwave spectrum, letter designations, and the frequencies and wavelengths used for most imaging radar systems. The SAR systems used on Seasat, SIR-A, and SIR-B were relatively long wavelength radars (L-band, 23.5 cm), which made them virtually independent of weather conditions including the effects of precipitation.

Terminology significant to radar imagery interpretation

15. An antenna is positioned in the azimuth or along-track direction of an aircraft or spacecraft and, of course, moves at the velocity of the craft. Through this fixed antenna, pulses of radar energy are propagated outward in the across-track direction. The across-track direction is also referred to as the range or look direction. The line-of-sight distance measured from the antenna to an observation point on the ground is the slant range (R in Figure 2), whereas ground range is the horizontal distance measured along the surface from the ground track (Figure 2) to some point or object on the terrain. For SAR, that portion of the imaged terrain surface closest to the
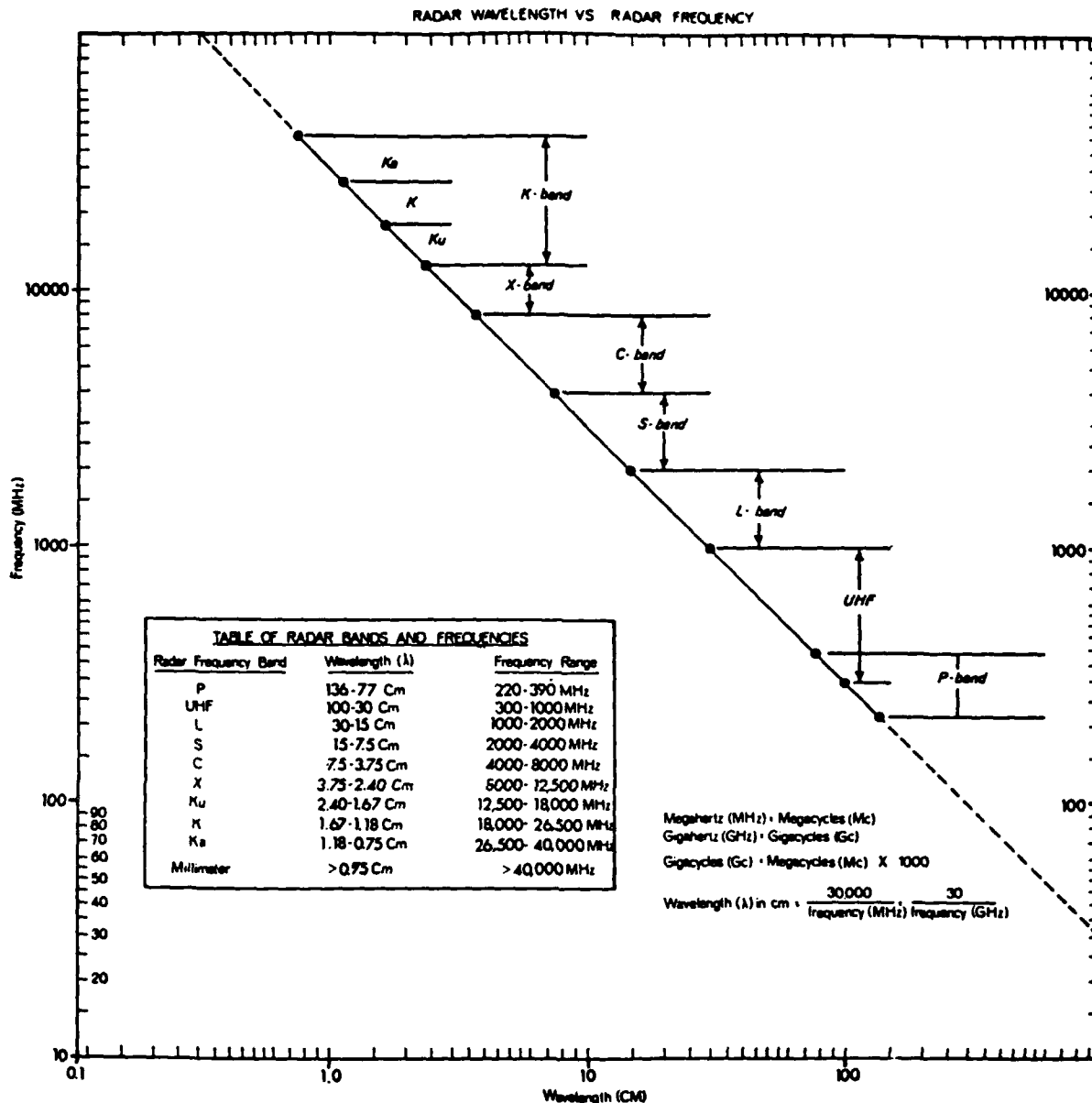
TABLE OF RADAR BANDS AND FREQUENCIES

Radar Frequency Band	Wavelength (λ)	Frequency Range
P	136-77 Cm	220-390 MHz
UHF	100-30 Cm	300-1000 MHz
L	30-15 Cm	1000-2000 MHz
S	15-7.5 Cm	2000-4000 MHz
C	7.5-3.75 Cm	4000-8000 MHz
X	3.75-2.40 Cm	5000-12,500 MHz
Ku	2.40-1.67 Cm	12,500-18,000 MHz
K	1.67-1.18 Cm	18,000-26,500 MHz
Ka	1.18-0.75 Cm	26,500-40,000 MHz
Millimeter	>0.75 Cm	>40,000 MHz

Megahertz (MHz) · Megacycles (Mc)
Gigahertz (GHz) · Gigacycles (Gc)
Gigacycles (Gc) · Megacycles (Mc) X 1000

$$\text{Wavelength } (\lambda) \text{ in cm} = \frac{30{,}000}{\text{frequency (MHz)}} = \frac{30}{\text{frequency (GHz)}}$$

Frequency (MHz) vs Wavelength (CM)

Figure 1. Radar frequencies and wavelength bands (after MacDonald 1969)

ground track is the near range, and that portion farthest from the ground track is the far range.

16. The angle between a line from the radar antenna to an observation point on the terrain and a horizontal plane passing through the antenna is the depression angle (β in Figure 2). The angle of incidence Θ is formed by an impinging beam of radar energy (propagational vector, which is perpendicular to the radar wave front) and a perpendicular at the point of incidence. The
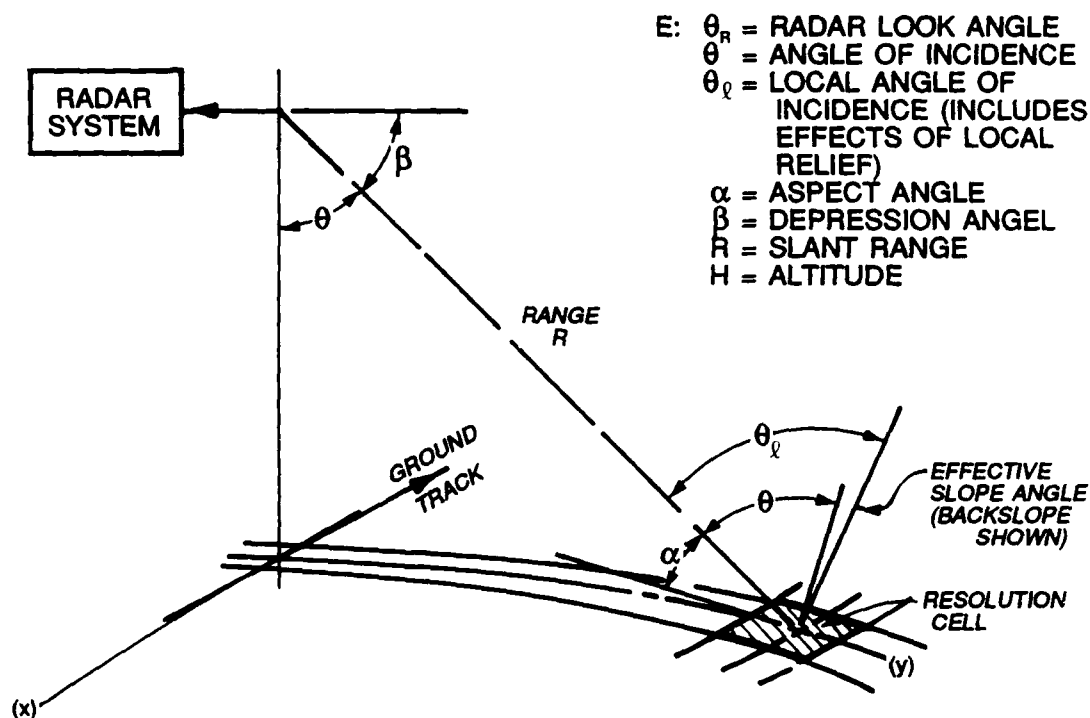
9

E: θ_R = RADAR LOOK ANGLE
θ = ANGLE OF INCIDENCE
θ_ℓ = LOCAL ANGLE OF INCIDENCE (INCLUDES EFFECTS OF LOCAL RELIEF)
α = ASPECT ANGLE
β = DEPRESSION ANGEL
R = SLANT RANGE
H = ALTITUDE

Figure 2. Side-looking radar geometry (after Kaupp, Waite, and MacDonald 1982)

look angle θ_R is measured in a vertical plane from nadir (point on the ground directly beneath the antenna) to the radar beam. For level terrain, the look and incidence angles will be equal (Figure 2). However, under more typical operational conditions, a local angle of incidence θ_ℓ must be defined (Figure 2). Measured between the radar beam and the normal to local surface, θ_ℓ accounts for the variation in terrain slope at the place on the ground where the imaging takes place (Kaupp, Waite, and MacDonald 1982).

SAR geometric characteristics

17. Pravdo et al. (1983) have summarized the geometric effects related to elevation variations in the terrain that result in nonrecoverable ambiguities or distortions of the image. These include foreshortening, layover, and shadowing. If a surface were perfectly flat, surface elements in the near range of the SAR would be illuminated and reflect the radar signals before surface elements in the far range. Thus, the signals would be received from near-range to far-range elements progressively in time. However, if a surface element is elevated relative to its surroundings, it will intercept the radar

10

signal sooner and appear in the radar image to be closer than it is. Figure 3a illustrates how foreshortening causes an apparent reduction of slopes inclined toward the radar (i.e., slope AB appears in the radar image as shortened slope A'B'). The "radar image plane" in the figure is a geometric representation (a right-angle projection) of the conversion between target range and location on the resulting image. For extreme cases of relief displacement (Figure 3b), the ordering of surface elements on the radar image is the reverse of the ordering on the ground (i.e., B' appears at a nearer range than A', whereas A is actually at a nearer range than B). This is known as "layover." The elevated element can also prevent the radar signal from illuminating elements in its shadow (Figure 3c).

Radar return strength and image tone

18. The SAR image is a measure of the radar backscatter or the reflectivity of the target scene. The strength of radar return and hence image tone are primarily influenced by the following terrain and radar system parameters:

      a. Ground parameters.

          (1) Terrain slope.
          (2) Surface roughness.
          (3) Complex dielectric constant.
          (4) Terrain feature orientation.

      b. Radar system parameters.

          (1) Frequency/wavelength.
          (2) Radar look angle/depression angle.
   (3) Antenna look direction.
          (4) Polarization.

19. Tone on radar imagery is the shade of gray recorded for the signal returned from each resolution cell (or instantaneous field of view) on the ground. On positive imagery prints, high intensities representing strong return signals appear as light or bright tones, whereas low intensities, or low return signals, appear as dark tones. Although tone is a basic recognition element for imagery interpretation, it is highly system dependent. For example, both the brightest and darkest radar imagery tones (other than radar shadow) are generally influenced by the specular reflection. In specular reflection, the surface from which the reradiation occurs is essentially smooth or has a surface roughness about 10 times smaller than the wavelength of incident radar radiation. Strongest returns occur when such a smooth surface is oriented essentially perpendicular to the incident radiation so that a
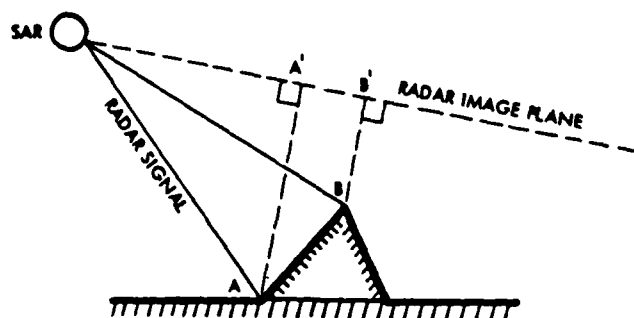
a. Foreshortening
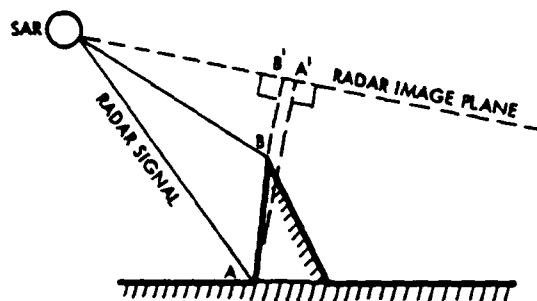
b. Layover
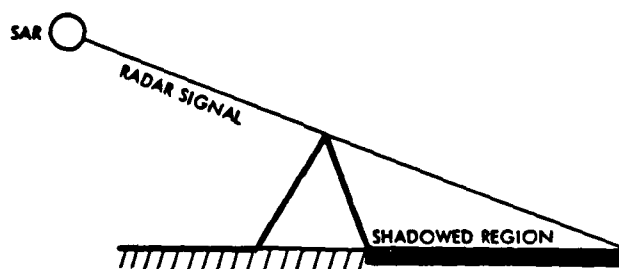
c. Shadowing

Figure 3. SAR geometric characteristics
and the effects of surface height varia-
tions (after Pravdo et al. 1983)

major part of the energy is returned to the radar. Conversely, weakest
returns occur when such a surface slopes away from or essentially is parallel
to the incident radiation, allowing only a small percentage to be returned to
the radar. If the surface is rough relative to the wavelength of the imping-
ing radar energy (i.e., has a roughness scale greater than the wavelength),
reradiation will occur in many directions. A rough surface produces diffuse
reflection, which in turn, produces a broad range of tones on the imagery.

12

Spaceborne Imaging Radars

Seasat SAR

20. The Seasat satellite was launched on 26 June 1978 into a near polar orbit (108-deg orbital inclination) at an altitude of 800 km. Among other sensors, Seasat carried an L-band SAR that was designed to image the ocean surface. The Seasat SAR was a fixed parameter system with a 23-deg angle of incidence. Such a small incidence angle was selected because it is ideally suited for imaging the ocean; however, images were also collected over land areas. On 10 October 1978, Seasat failed as a result of a short in the satellite electrical system. During its 100 days of acquisition, the Seasat SAR collected almost 42 hr of data, equivalent to about 100 million sq km of coverage. Nearly all of the Seasat data were optically processed, and certain selected scenes, representing 100- by 100-km regions, were also digitally processed. Two major conclusions resulted from the evaluation of the Seasat SAR data: (a) for certain types of terrains, resultant 23-deg incidence angle images were found to be very useful for geologic applications; and (b) digitally processed images were superior to optically processed images for most applications. For a complete description of the Seasat SAR and discussions of SAR imagery interpretation, see Ford et al. (1980) and Pravdo et al. (1983).

SIR-A

21. The second space shuttle (STS-2) was launched 12 November 1981 into a shallow (38-deg orbital inclination), circular orbit at an altitude of 268 km. The major payload was the OSTA-1 experiment pallet carrying the SIR-A, the first in a planned sequence of increasingly complex experimental microwave sensors building on the experience gained from Seasat. Even though shuttle power problems ended the mission after only 2 days, nearly 8 hr of SAR images equivalent to approximately 10 million sq km of areal coverage were collected. The data were recorded optically on film (SAR holograms) and converted into images via optical processing techniques.

22. The SIR-A was an L-band system with fixed parameters. The sensor was a derivative of the Seasat SAR, and it used the same type of antenna panels, transmitter, modulator, and receiver. However, the SIR-A angle of incidence was 47 deg, compared with 23 deg for the Seasat SAR. For a complete description of the SIR-A experiment, see Elachi et al. (1982). Discussions of SIR-A imagery interpretations are provided by Ford, Cimino, and Elachi (1983).

SIR-B

23. SIR-B was derived from the SIR-A hardware. It was also an L-band system, but major parts were redesigned to accommodate the angle diversity experiment, which was central to the program. The antenna system was redesigned, with the formatter and associated electronic system being built to accommodate different angles of incidence. The coherent return signal was digitized, and data were telemetered via the Tracking Data Relay Satellite System (TDRSS) to the ground for digital image processing. For a description of the SIR-B experiment, see Ford et al. (1986).

24. On 5 October 1984, NASA launched SIR-B on space shuttle Mission 41-G. The orbit was inclined at 57 deg (the largest inclination possible from Cape Canaveral, FL) and had a final altitude of approximately 230 km. Unlike previous space shuttle missions, SIR-B acquired digital radar image coverage of varied terrains and ocean surfaces through a range of incidence angles. Approximately 7 hr of digital data covering about 6.5 million sq km of the Earth's surface was obtained between latitudes 60-deg N and 60-deg S.

25. The mission was plagued with troubles. The first was a failure in the shuttle's K-Band telemetry link to the TDRSS. The second involved a metal particle that contaminated the SIR-B transmission path, which caused a large loss in transmitted power output and thereby reduced the signal-to-noise ratio. Finally, the last 100 m of tape from the onboard high-density tape recorders was lost. The composite result was that only about 20 percent of the planned data were actually obtained.

Previous Studies Involving Spaceborne Imaging Radar in Arid Regions

26. The majority of investigations involving the interpretation of data from the SIR experiments in the hyperarid eastern Sahara have been directed by scientists at the US Geological Survey's (USGS's) Branch of Astrogeology in Flagstaff, AZ. For example, a study by McCauley et al. (1982) compared SIR-A and Landsat to emphasize the superiority of radar for penetrating surface sediments and imaging relict fluvial patterns. The study incorporated ground truth from field work, and certain radar responses were successfully matched with the corresponding sediment types. Field data collection also enabled construction of a radar signal backscatter model for accurately studying variation in the tone on the radar images. McCauley et al. (1982) concluded that

"the most striking result of the experiment in the eastern Sahara is that the SIR-A pictures, even with only preliminary processing, and the radar terrain maps made from them show unambiguously the presence of major subjacent features that are not detectable even on specially processed Landsat pictures at the same scale."

27. Breed (1983) reported that the Egyptian desert is an ideal environment for radar signal penetration and encouraged the application of radar as a regional guide for ground-water exploration to reduce expensive geophysical exploration programs. Blom, Crippen, and Elachi (1984) documented the advantage of penetration offered by Seasat imagery obtained in a different arid environment, the Mojave Desert of southern California. Igneous dikes buried beneath as much as 2 m of alluvium and revealed by the Seasat radar were not evident in the field or on aerial photographs.

28. Elachi, Roth, and Schaber (1984) provided theoretical considerations verifying that SIR-A imagery radar can image subsurface features. For penetration to occur, the surface layer must have a very low loss tangent, which implies a very low moisture content (less than 1 percent). The authors presented a simple backscatter model to show that for a thin sand layer with a low loss tangent, the presence of the covering layer enhances the capability to image the subsurface interface, particularly at large incidence angles.

29. An in-depth study of radar penetration and backscatter characteristics of the shuttle radar over the eastern Sahara was reported by Schaber et al. (1985). They discussed the influence of sediments in and around the relict fluvial channels on signal response and provided detailed descriptions of the sediments analyzed in their study. Most recently, Schaber et al. (1986) have concluded that signal penetration and subsurface backscatter from shallow dielectric interfaces in the upper metre of the sand sheet are enhanced not only by the operational characteristics of the spaceborne radar but also by the physical and chemical characteristics of the surficial deposits. Pertinent physical characteristics probably include: (a) a favorable distribution of particle sizes, (b) a low density of materials, (c) a low clay content, and (d) an extremely low moisture content. The authors also concluded that the sand sheet is virtually "transparent" to the SIR signals for centimetre-to-metre depths over vast areas throughout the eastern Sahara, whereas it "obscures from optical sensing (i.e., Landsat Multispectral

Scanner) a substantial amount of underlying information related to past
fluvial activity."

PART III: GEOLOGY AND HYDROLOGY OF THE TEST SITES

30.   Shuttle radar and Landsat images were obtained for 10 test sites.
Site selection criteria included:

a.   Availability of shuttle radar coverage.

b.   Availability of Landsat imagery coverage, preferably for
more than 1 year and season.

c.   Evidence of sand-covered terrain that might allow for
penetration of radar energy and delineation of subsurface
features.

d.   Proximity to areas where recent scientific expeditions have
provided information on terrain conditions.

The 10 test sites selected are in four different geographic areas.   Test site
and area characteristics are briefly discussed in the following paragraphs.

Northeastern Chad, Northwestern Sudan, and South-Central Egypt

31.   Test sites 1 through 5 (Figure 4) are on the southernmost edge of
the Western Desert, a subdivision of the eastern Sahara Desert.   The region is
characterized by a flat topographic surface that is covered with wind-sorted
sand (i.e., eolian) deposits.

Geology

32.   The geology of test sites 1 through 5 is relatively simple, with
varying combinations and thicknesses of sand colluvium, pea gravel, and cali-
chified colluvium lying unconformably under the thin (10-cm) eolian deposits.
At depths below approximately 10 m, the Nubian Sandstone, a Cretaceous
sequence of cross-bedded sandstone and shale, underlies the entire area.
Occasionally, small outcrops of wind-pitted and grooved gneiss of the African
Shield occur.

Hydrology

33.   Despite the extreme aridity of the region around test sites 1
through 5, the upper fringe of the water table is as shallow as 3 m (McCauley
et al. 1982).   Productive wells have been drilled into the alluvium of a
"radar river" at a depth of about 150 m.   Fossil water has also been found at
a depth of about 500 m in the Nubian Sandstone, the major aquifer of the
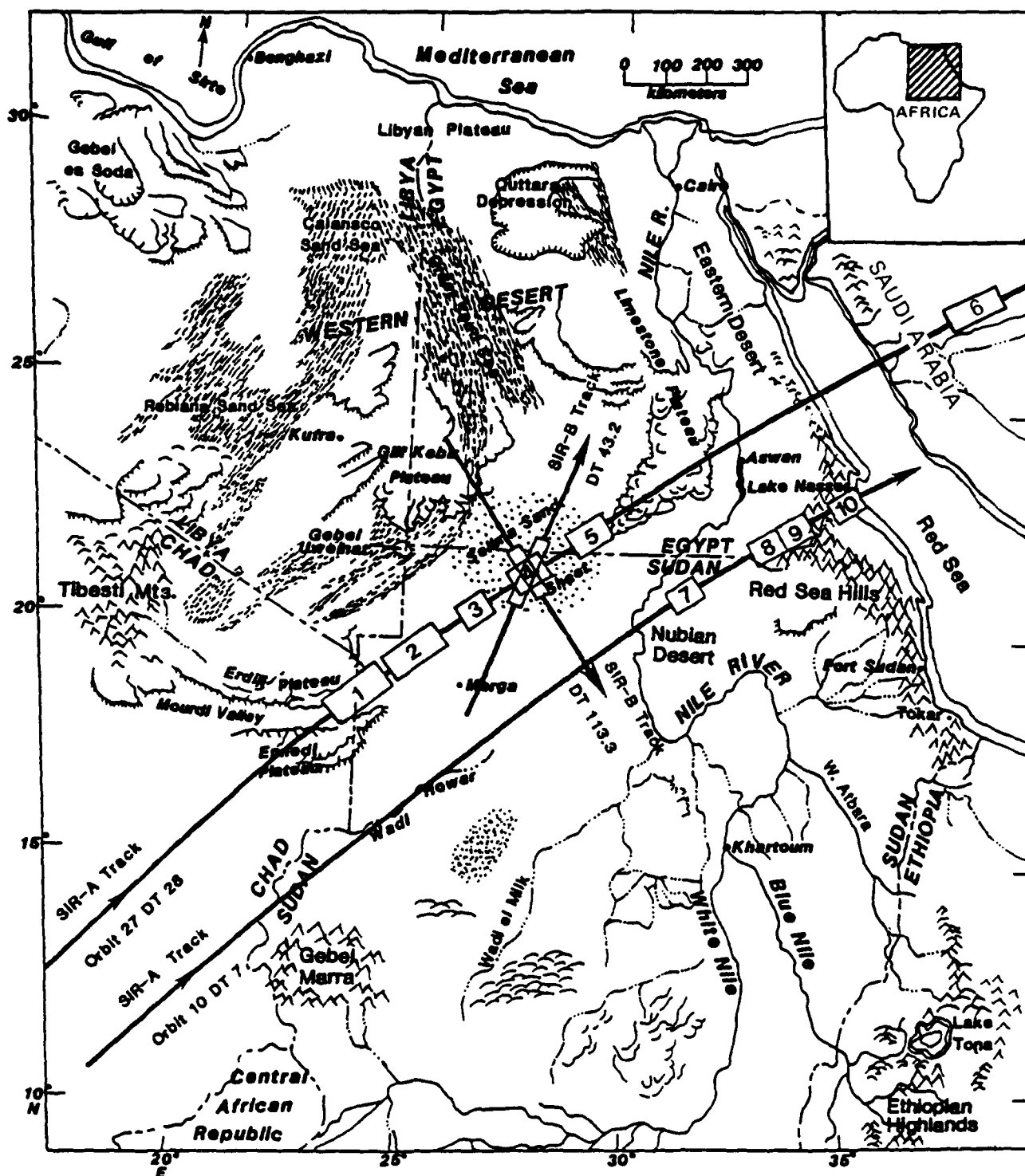
Figure 4. Test site locations (modified from McCauley et al. 1982)

18

eastern Sahara.* The quality of the fossil ground water is good (Shata 1982), with the age being roughly 30,000 years BP (i.e., Before Present) (Wright et al. 1982). Ground-water recharge is relatively slow with an apparent movement from south to north (Salama 1976).

Northwestern Saudi Arabia

34. Test site 6 (Figure 4) is centered in a large sand desert, the An Nafud (or Great Nafud). This desert is a predominately flat, sandy basin with occasional sand dunes.

Geology

35. The near surface geology of the An Nafud is characterized by varying thicknesses of Quaternary alluvium deposits, including coarse lag gravels, fine-grained gravels, calichelike sediments, and barchan dunes. Underlying the Quaternary deposits is the Tabuk Formation (Lower Ordivician through Lower Devonian), composed of an alternating sequence of fine- to medium-grained, micaceous sandstone and gray, silty shale. The Tabuk is exposed in the western half of test site 6. The Cambrian System Saq Sandstone lies conformably beneath the Tabuk. The Saq is a coarse- to medium-grained, cross-bedded sandstone with shale stringers. The entire region is floored by a Precambrian Basement Complex. Regional slope is to the northeast (Jado and Zotl 1984).

Hydrology

36. The hydraulically connected sandstones of the Tabuk Formation and the Saq Sandstone are the most productive aquifers in northern Saudi Arabia. Well data, although scarce, indicate that water quality is good (Jado and Zotl 1984). Recharge is from the southwest.

Northeastern Sudan and Southeastern Egypt

37. Test sites 7 through 9 (Figure 4) are within the northern Red Sea Hills region, located between the Nubian Desert and the Red Sea. This terrain is considered an inselberg-and-plains topography. The relative extent of the

---

* Personal Communication, 1986, Dr. Gerald G. Schaber, Chief, Branch of Astrogeology, USGS, Flagstaff, AZ.

lowland plains versus that of the residual inselbergs depends chiefly on the stage of the geomorphic evolution of the region.

Geology

38. Previous geologic work conducted in this area has been limited. The few published geologic maps of northeastern Sudan and southeastern Egypt have large sections simply labeled as unexplored. The major geologic formations of this area can be divided into those rocks consisting of the Precambrian Basement Complex, the Cretaceous Nubian Sandstone, Quaternary alluvium, and Recent surficial deposits.

39. The Precambrian Basement Complex exposed in the study area is known as the Red Sea Hills. This Basement Complex consists of a variety of igneous, metamorphic, and sedimentary rocks that are overlain by the horizontal and subhorizontal Paleozoic and Mesozoic sedimentary and igneous rocks (Whiteman 1971). These strata were altered, folded, intruded, and then denuded to form the sub-Nubian surface. The outcrops are deeply weathered and contain fissures, faults, and joints and occur commonly as inselbergs, which are steep-sloped residuals rising above the surrounding plains. The inselbergs tend to become partly drowned in sediment and form rugged hills where stream erosion has cut deep into the rock.

Hydrology

40. Within test sites 7 through 9, ground water--in this case, fossil ground water--is considered to have accumulated from infiltration during the Quaternary fluvial period some 10,000 years BP. These waters are considered a nonrenewable resource because currently there appears to be little or no recharge. Rain rarely falls; thus, wells are the main source of water. Approximately 80 percent of the inhabitants depend upon ground water for their existence most of the year (Rodis, Hassan, and Wahadan 1963). The majority of the wells are hand dug. The primary aquifers consist of

    a. Recent surficial deposits.

    b. The Nubian Sandstone.

    c. The weathered Precambrian Basement Complex.

41. Alluvia along the channels of wadis and slope-wash deposits are the principal sources of water in the surficial deposits. Ground water occurs occasionally in surficial sand deposits but only as a result of major storm events in those areas underlain by impermeable strata.

42. By far, the most important aquifer is the Nubian Sandstone. Water in the Nubian is largely under low artesian pressure, with the permeable sandstones and conglomerates comprising the main aquifers. The upper surface of the zone of saturation ranges from about 65 m to more than 165 m below the land surface, with individual aquifers within this zone being up to 35 m thick (Rodis and Iskander 1963). Because the more permeable units grade both laterally and vertically into less permeable rock, individual aquifers generally are of limited areal and stratigraphic extent. The chemical quality of the water is usually good with an average total dissolved solids content of about 200 ppm (Rodis and Iskander 1963).

43. The rocks of the Precambrian Basement Complex are relatively impermeable; however, secondary porosity and permeability can be present in faulted and fractured units. Weathering within these fracture zones can substantially improve water transmissibility as well as enlarge the reservoir capacity. Consequently, fracture and fault zones are generally more prolific producers of ground water than is the surrounding unfractured bedrock.

44. Based on published data (Russell and Zall 1981), most of the wells that tap ground water from the Precambrian Basement Complex have only moderate yields and are dry during parts of the year. The water quality ranges from fair to poor, being brackish or salty and containing a large quantity of dissolved solids (Rodis, Hassan, and Wahadan 1963).

Egypt-Sudan Border

45. Test site 10 (Figure 4) lies on the Egypt-Sudan border on the western side of the Red Sea. The western shore of the Red Sea consists of Tertiary sediments called the Coastal Deposits of the Red Sea Margin. These Tertiary sediments dip gently seaward at less than 30 deg. Local fold structures occur with some faulting, and dips of 20 deg or more near the faults are common. Inselberg-and-plains topography is present in the inland areas farther from the Red Sea.

Geology

46. The Tertiary beds of the Coastal Deposits of the Red Sea Margin consist of continental and marine limestones (often shelly or coralline), shales, marls, clays, grits, conglomerates, and gypsum beds. The thickness of the series, measured on low hills of the coastal plain, is over 100 m

(Whiteman 1971). The igneous and metamorphic rocks of the Precambrian Basement Complex lie partially buried in the Recent windblown sands that are scattered through the area. Surface outcrops of the Precambrian rocks become more common with increased distance from the Red Sea.

Hydrology

47. Very little is known about the ground-water potential of the Tertiary Coastal Deposits of the Red Sea Margin. These beds are folded and faulted in many places and covered by Recent surficial deposits, which may hold promise for future hydrologic investigation.

PART IV: SPACEBORNE RADAR AND LANDSAT IMAGERY COMPARISONS

Northeastern Chad, Northwestern Sudan, and
South-Central Egypt

Test site 1

48. Test site 1 (Figure 4), which lies on the Chad-Sudan border, is centered near latitude 18°45' N, longitude 24°15' E. A Landsat Multispectral Scanner (MSS) band 4 (see Table 1) image of this area (Figure 5) reveals a thin, discontinuous sheet of eolian deposits that now cover the local outcrops of Nubian Sandstone (location A) and Carboniferous marine deposits in the southwestern one-third of the scene (dark areas near the arrow). The scarp at B marks the northeastern edge of the Erdiji Plateau (Figure 4). Tonal variations on the Landsat scene are attributed to varying thicknesses of sand cover and scattered bedrock exposures. The lighter areas at C and D correspond to thicker areas of sand cover, and the darker areas indicate exposed or nearly exposed bedrock. Thin, east-west trending streaks across the image are processing defects.

Table 1

Spectral Wavelength Intervals Detected by the Landsat -1,
-2, and -3 Satellite Remote Sensing Systems

System	Type of Radiation	Wavelength, μm	NASA Designation
RBV	Visible blue-green	0.474-0.575	Band 1
RBV	Visible green-red	0.580-0.680	Band 2
RBV	Visible red, near IR	0.690-0.830	Band 3
RBV*	Panchromatic, visible to IR	0.505-0.830	
MSS	Visible green	0.5-0.6	Band 4
MSS	Visible red	0.6-0.7	Band 5
MSS	Visible red, near IR	0.7-0.8	Band 6
MSS	Near IR	0.8-1.1	Band 7
MSS**	Thermal IR	10.4-12.6	Band 8

* Landsat-3, not on Landsat-1 and -2.
** The thermal IR band on Landsat-3 never became operational.
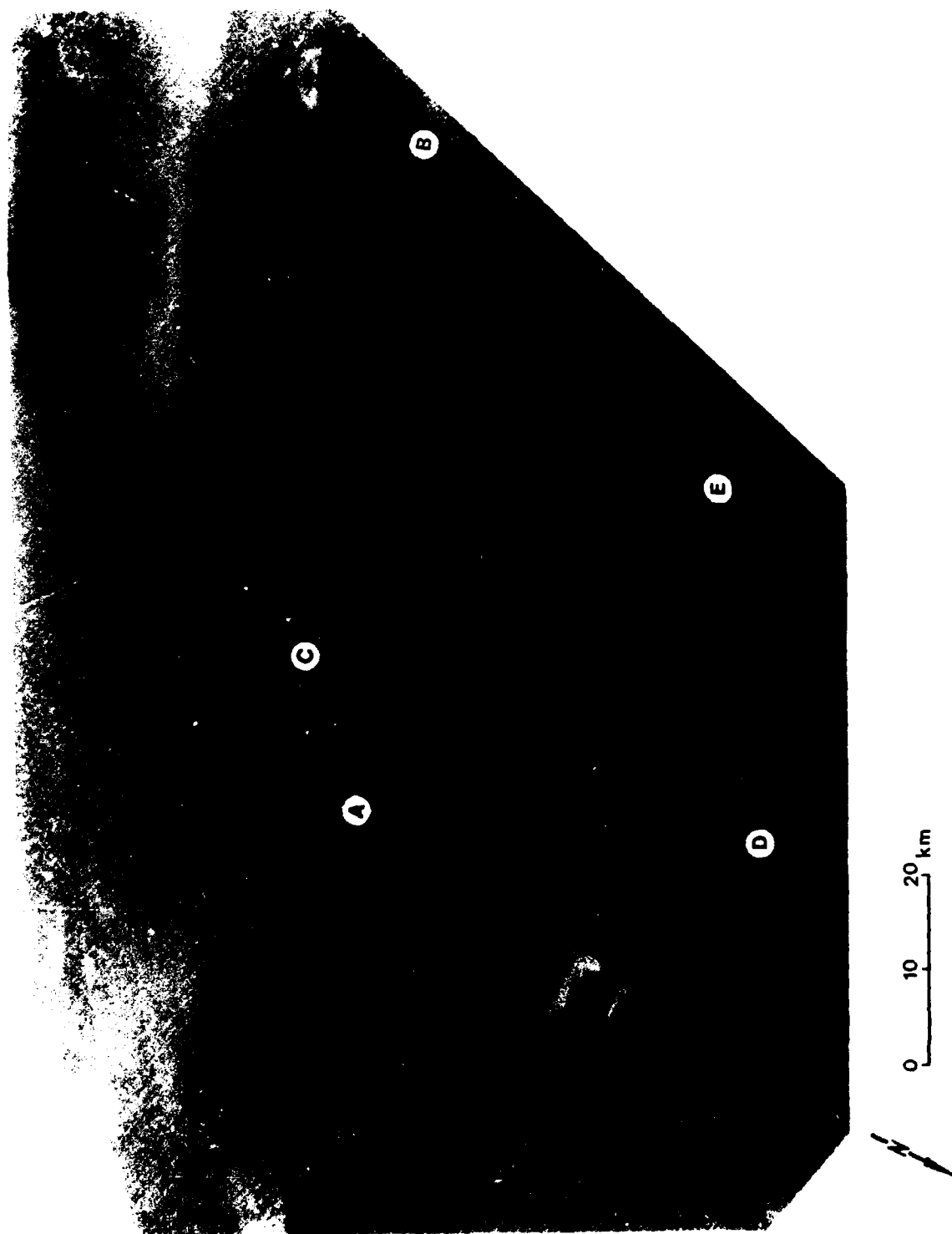
Figure 5. Landsat-2 imagery of test site 1, 18 January 1976, MSS band 4, solar elevation 36°, solar azimuth 135°, ID 82361080010500

24

49. The SIR-A radar image of the same area (Figure 6) shows an incised dendritic fluvial system. On the radar image, the scarp at B is very light toned because it has a nearly perpendicular orientation to the radar look direction, resulting in a strong return signal. The brighter return from the rock units at A probably indicates a difference in lithology from the units around E. Many of the stream channels are 2 to 3 km wide, and some at C and D are 5 to 10 km wide. A drainage divide along a line from A to D separates the larger systems. The general direction of "flow" of these sand-filled channels appears to be toward the southeast. Orientation of the smaller, incised channels between D and E appears to be partially controlled by fractures and joints in the bedrock as depicted by their rectangular pattern or abrupt 90-deg changes in course.

50. Although the Landsat and SIR-A images (Figures 5 and 6, respectively) appear distinctly different, subtle correlation can be made between the two images. For example, the light areas at C and D on the Landsat image correspond to the locations of the two largest channels on the radar image. An inference that the lighter tones indicate buried fluvial systems would be difficult to make using only the Landsat image. However, the apparent ability of radar to penetrate the sand cover leaves no doubt as to where the channels are located.

Test site 2

51. Test site 2, located in northwestern Sudan, is centered near latitude 19°45' N, longitude 25°30' E (Figure 4). The SIR-A imagery of this area (Figure 7) reveals numerous relict stream valleys, one of which is greater than 15 km wide. Two channels A1 and A2 appear to be incised. The larger incised channel A2 flows toward the southeast, emptying into a broad valley in the upper left part of the image (indicated by dashed lines and arrows, Figure 7).

52. Landsat imagery of test site 2 (Figure 8) shows low-lying, partially sand-covered exposures of Nubian Sandstone at D. The Nubian Sandstone is also exposed in the darkest area on the image located along the bottom edge left of center; in that area, it has little or no eolian cover. The dark tone is related to the high absorption and low reflection (low albedo) characteristics of the sandstone exposure when imaged using the MSS band 7 (near infrared) detectors. The length and width of the incised channels (A) are less defined on this Landsat image than on the radar image (Figure 7). The areas
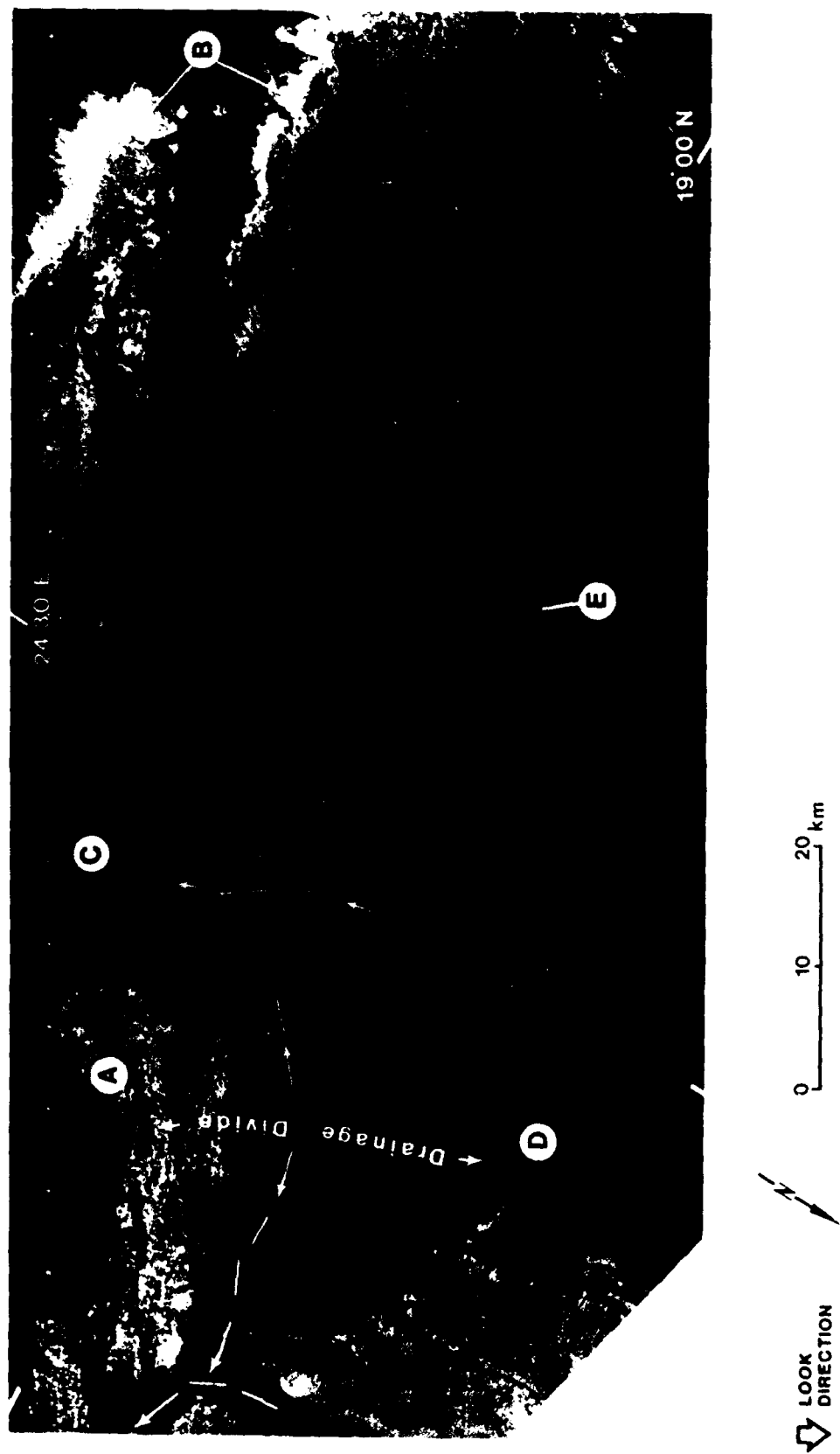
Figure 6. SIR-A imagery of test site 1, 13 November 1981, orbit 27, data take 28
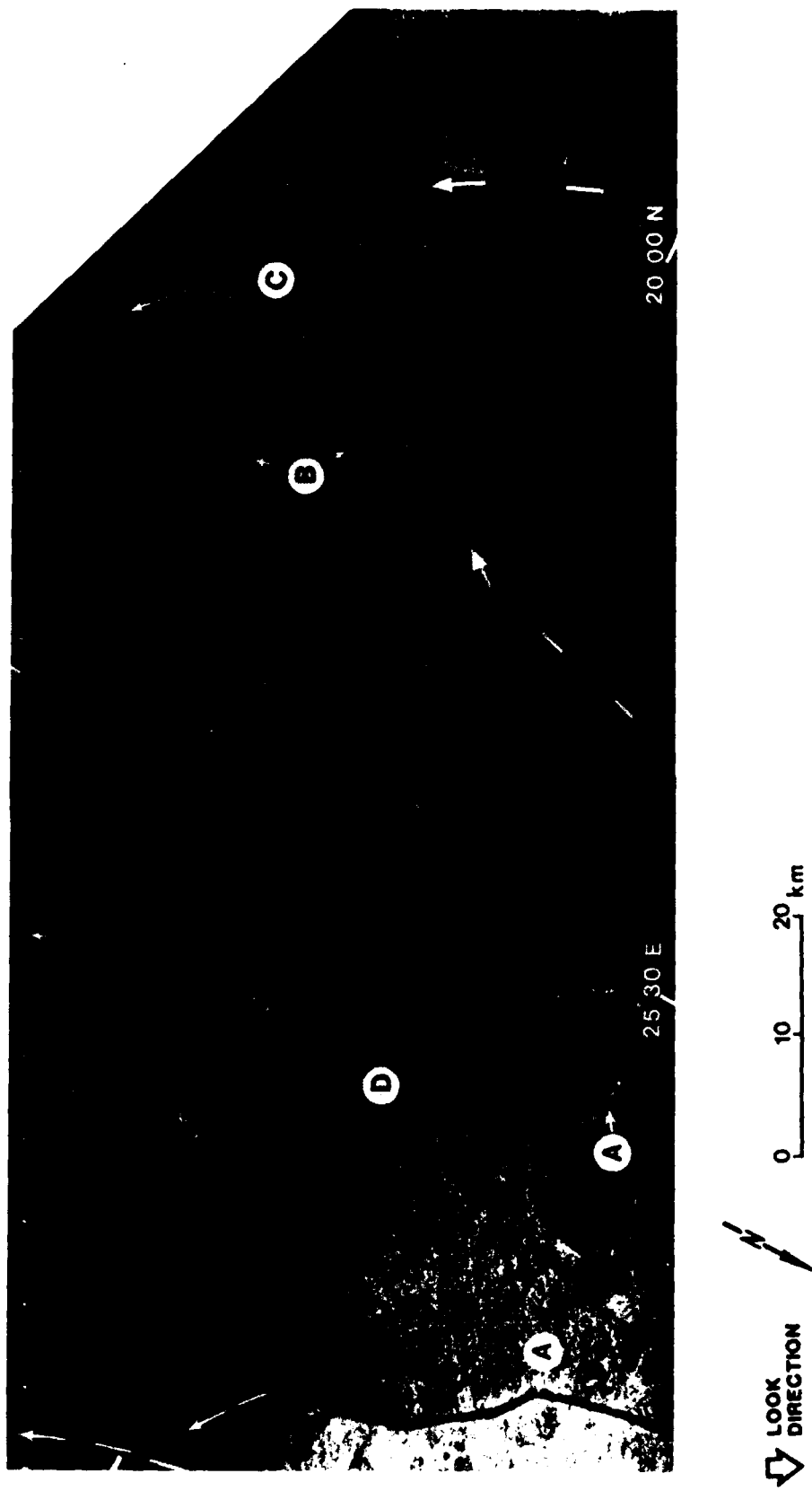
Figure 7. SIR-A imagery of test site 2, 13 November 1981, orbit 27, data take 28
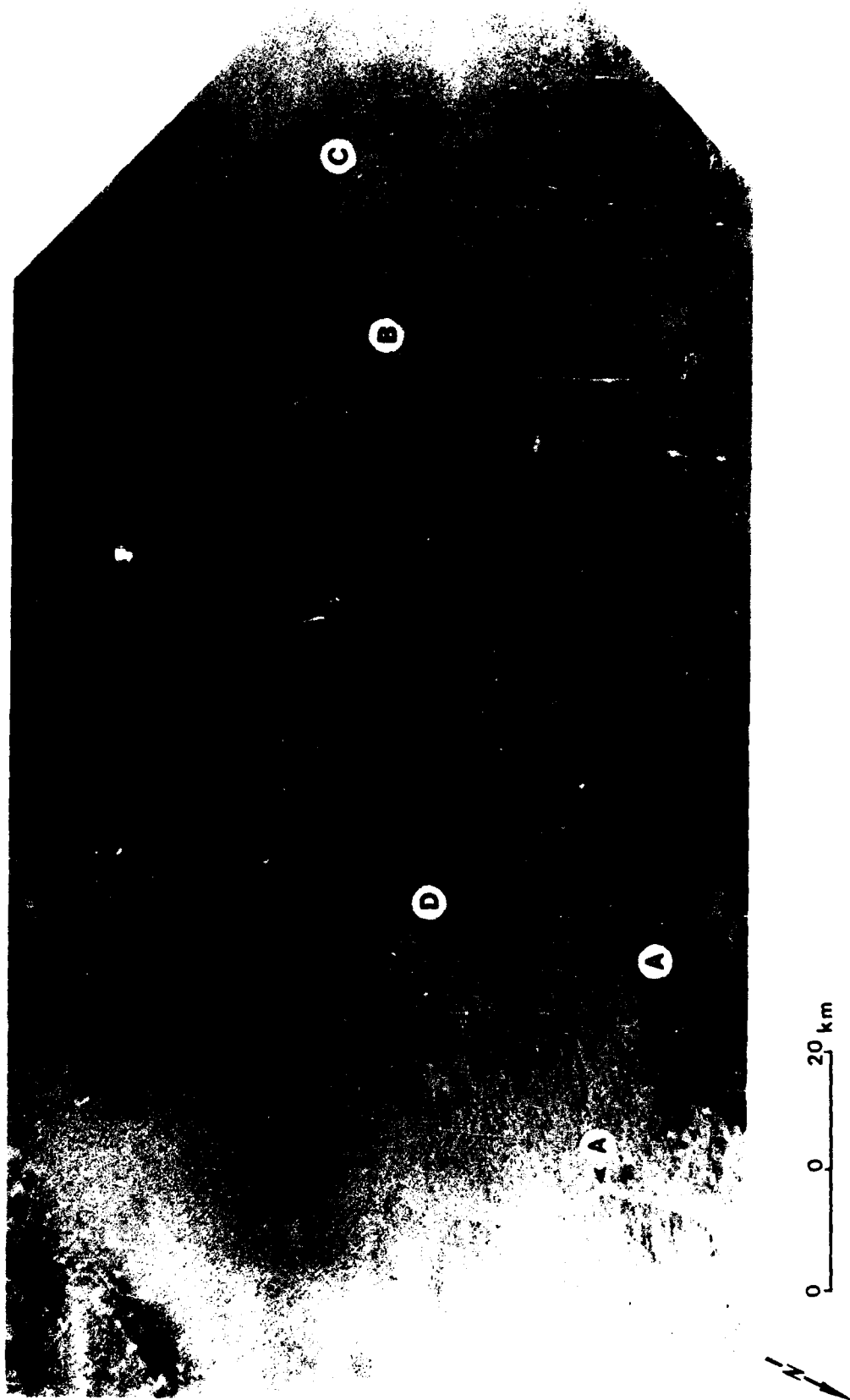
LOOK DIRECTION

25 30 E

20 00 N

0   10   20 km

Figure 8. Landsat-3 imagery of test site 2, 7 November 1980, MSS band 7, solar elevation 41°, solar azimuth 135°, ID No. 8309780749 3X0

that appear dark at B and C on the SIR-A image correspond to the location of the large relict stream valleys that apparently contain sufficient amounts of surficial windblown sand to allow absorption of the radar energy.

53. The larger valleys of test site 2 have been interpreted to be part of a regional, south-flowing fluvial system, possibly originating in the highlands near the Gilf Kebir Plateau (Figure 4). Shallow (1 to 2 m) pits dug into the alluvium of the large valleys in test site 2 contain stream-rounded pebbles and cobbles, evidence of relatively high-flow regimes in some of the Tertiary (?) System channels (McCauley et al. 1982).

Test site 3

54. Figures 9 and 10 allow for comparisons of Landsat and SIR-A images in the vicinity of test site 3, which is located in northwestern Sudan on the southwestern edge of the Selima Sand Sheet, centered near latitude 21°00' N, longitude 27°00' E (Figure 4). The radar image (Figure 10) shows a variety of features, many of which are difficult to identify accurately. What appears to be a valley at C is actually the location of a dune train. The radar signal loses its effective strength before encountering any reflective surface in these 10- to 15-m-thick sand dunes, which results in no signal return and a dark image tone (McCauley et al. 1982). A subtle fault scarp at B can effectively dam any ground water present in the 2-km-wide trough on its southern edge. The dark, featureless area in the northwestern third of the image is the edge of the incredibly flat Selima Sand Sheet. The bright returns at D and around A and B at the top of the image are low-relief exposures of Nubian Sandstone. The intermediate returns that cover most of the radar image reflect bedrock covered with a thin sand sheet. Two narrow incised valleys at A in the western part of the SIR-A image (upper part Figure 10) can be inferred. A larger (5-km-wide) valley trends from east to west between A and D in the bottom right corner of the SIR-A image.

55. The importance of using Landsat and shuttle imagery as complementary data sets is especially evident when examining Figures 9 and 10. For example, the channels at A and the scarp at B, which are evident on the radar imagery, can be located on the original Landsat imagery using the radar as a guide, but their expression is very subtle. Also, without the Landsat imagery, the 50-km-long dune train previously mentioned might have been erroneously interpreted as a "radar river."

Figure 9. Mosaic of Landsat-1 (left) and Landsat-3 images of test site 3, 12 November 1972/12 December 1980, MSS bands 4, solar elevations 42°/34°, solar azimuths 144°/139°, ID No. 81120808550

Figure 10. SIR-A imagery of test site 3, 13 November 1981, orbit 27, data take 28
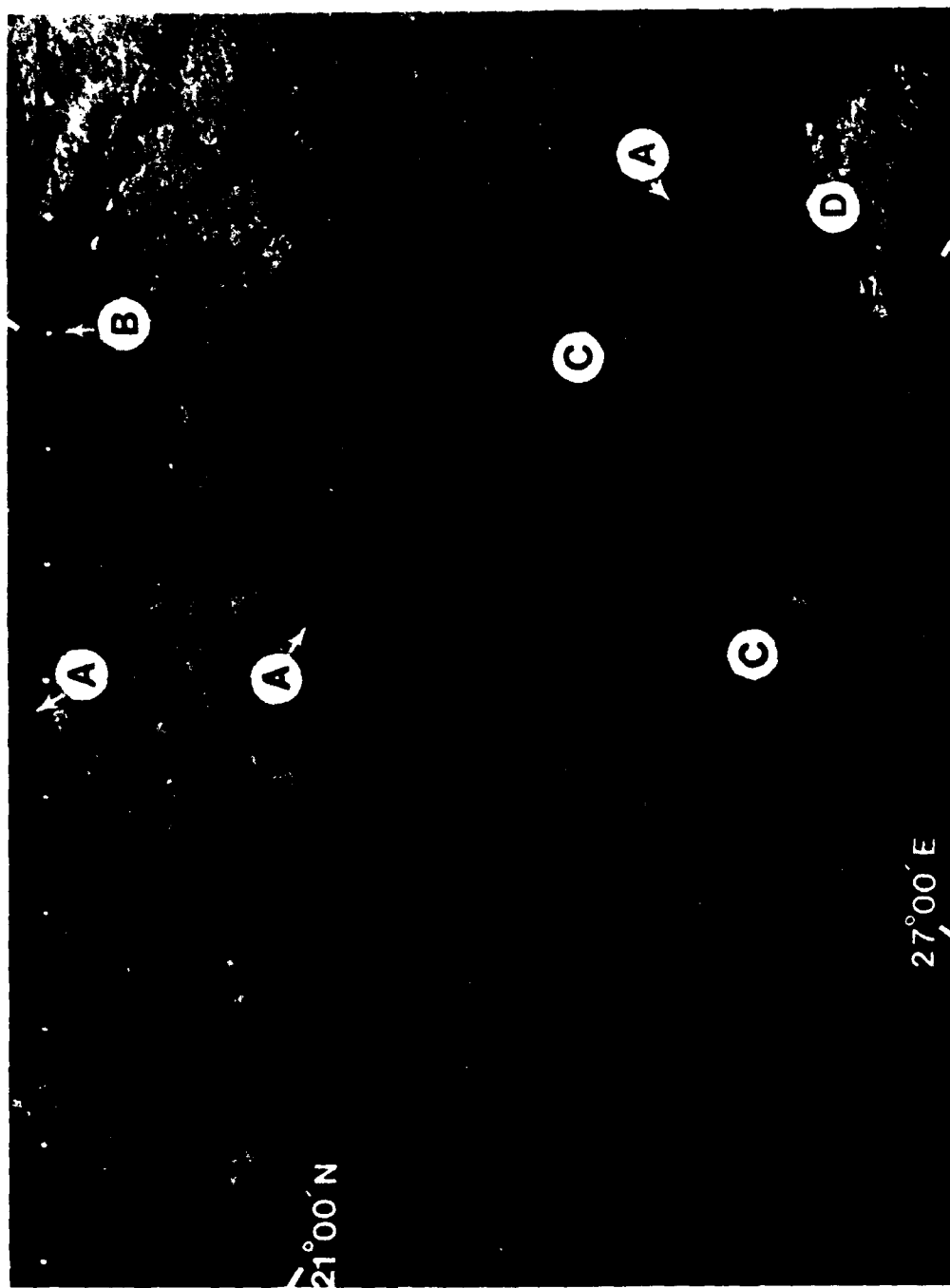
Test site 4

56.   Figure 11 provides Landsat coverage of test site 4, which is centered near latitude 21°45' N, longitude 28°14' E (Figure 4). SIR-A imagery of part of the area of test site 4 is shown in Figure 12; the bright area around A is shallowly buried Nubian strata, and the dark area at B is the radar expression of an exceptionally thick dune train. The radar signal apparently penetrates the extraordinarily flat sand sheet that blankets the area and images buried fluvial systems that range from incised channels at A and C, to wide valleys, to the braided streams at H. Flow direction arrows are indicated between H and E. The bright, curvilinear feature at E is a stream-carved terrace that deflected the flow of the stream from the northwest toward the west. The terrace around C separates the flow of the braided system H on the north side from three larger valleys that merge on the south side (dashed arrows). When they are identifiable on the Landsat image, the features clearly seen on the SIR-A image can at best be described as subtle (Figure 11). The small, incised channel (A) and the curved stream terrace (E) are recognizable on the Landsat imagery but could not be accurately identified as such without first being observed on the radar image.

57.   The Landsat image in Figure 11 shows numerous light-toned, north-trending dune trains such as the one between B and E. A unique mottled appearance of the sand can be seen on the Landsat image near H. This pattern "flows" along the dashed lines that split at C and continues around the stream-carved terrace. A significant correlation can be made between the location of the mottled sand pattern on Landsat and the fluvial system revealed on the SIR-A image. Specifically, the mottled pattern is present only in the areas on the Landsat that overlie the buried valleys inferred from radar interpretation. Regionally, SIR-A and SIR-B radar images southwest of test site 4 are dark and featureless, but the mottled pattern on the Landsat image can be followed into the area southwest of the test site for more than 75 km.

58.   Figure 13 is the SIR-B image that tracks southwest to northeast across test site 4 (Figure 14). The fluvial valleys previously identified on the SIR-A imagery (Figure 12) are also apparent on the SIR-B imagery, thus suggesting that the fluvial systems continue into the adjacent area. The very bright radar return at F is a stream-carved scarp that formed the northwest

32
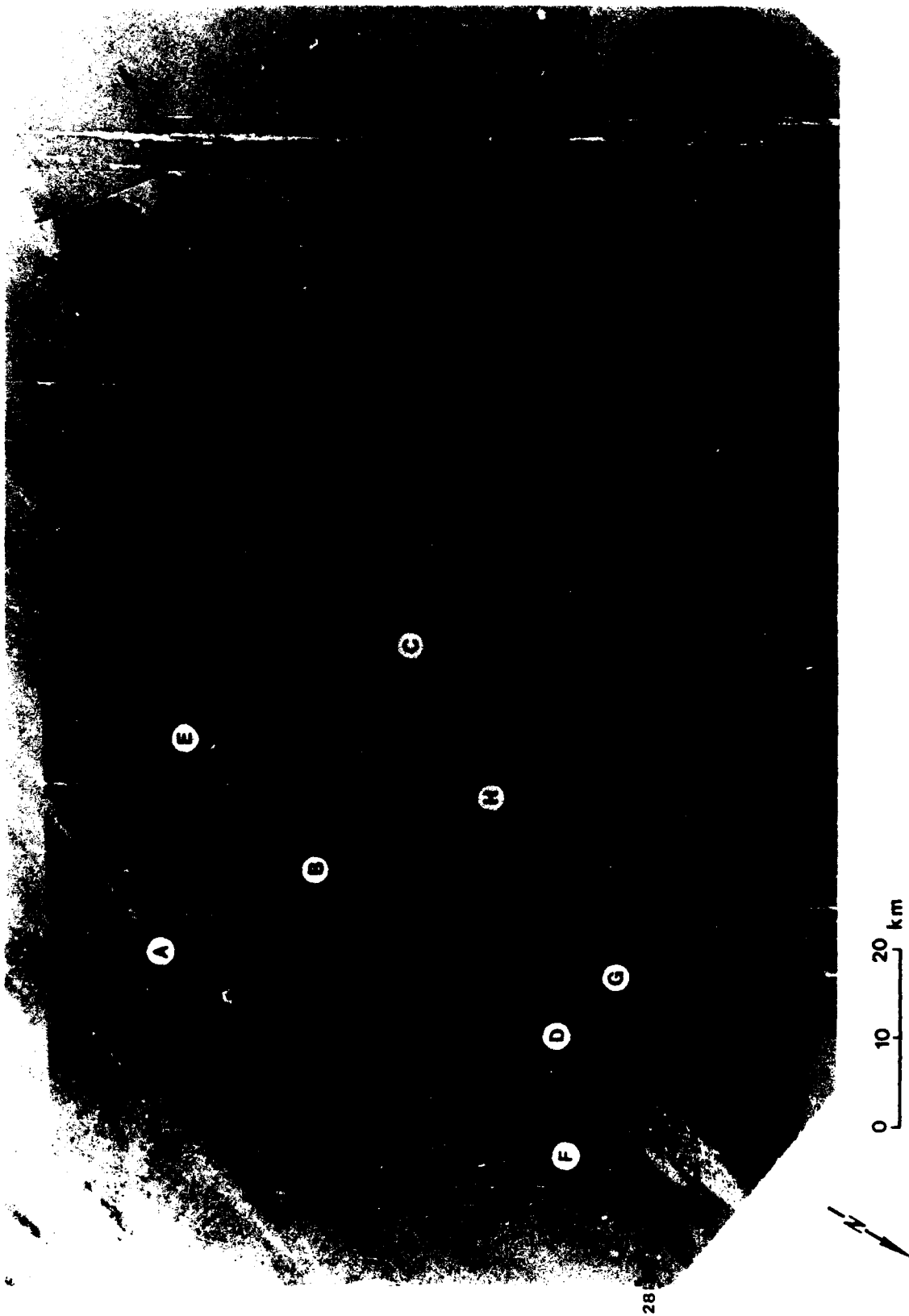
Figure 11. Landsat-5 images of test site 4, 2 February 1985, MSS band 4, solar elevation 38°, solar azimuth 135°, ID No. 85038082500 (both images)

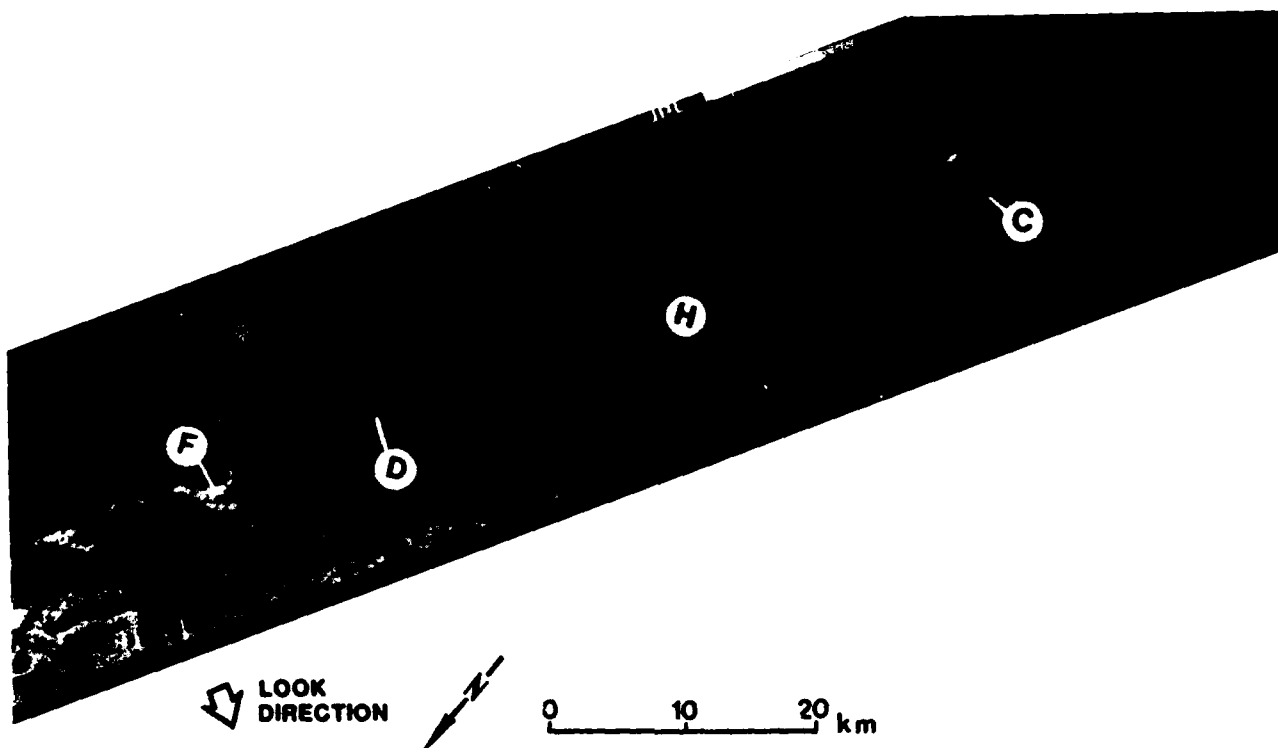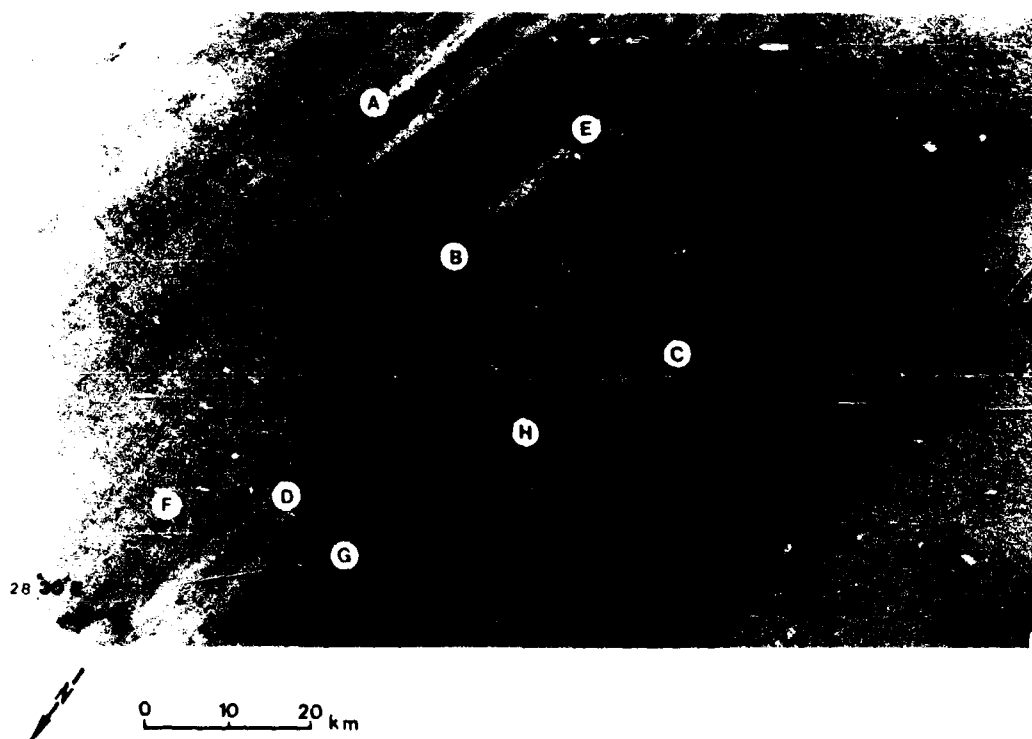Figure 12. SIR-A imagery of test site 4, 13 November 1981, orbit 27, data take 28

34

LOOK DIRECTION

0   10   20 km

Figure 13. SIR-B imagery of part of test site 4, 14 November 1984, data
take 43.2, scenes 5 and 6, incidence angle of 43.6°

0   10   20 km

Figure 14. Landsat-5 images of test site 4, 2 February 1985, MSS
band 4, solar elevation 38°, solar azimuth 135°, ID
No. 850338082500 (both images)

bank of the valley.* The perpendicular alignment of the scarp with respect to the SIR-B look direction and the curved surface facing towards the radar make it an ideal radar reflector. The scarp, once identified on the radar imagery, can then be located on the Landsat imagery (Figure 14).

Test site 5

59. Test site 5 (Figures 15 and 16) is located just north of the Chad-Sudan border and marks the boundary between the plains of the Selima Sand Sheet and the highlands of the Limestone Plateau (Figure 4). This test site is centered near latitude 22°15' N, longitude 28°45' E. The SIR-A image (Figure 16) shows a prominent scarp at B called the Kiseiba Scarp (McCauley et al. 1982). Although this scarp is not a stream-carved feature, it does contain some springs, such as the oasis Bir Keseiba near B, that support vegetation (bright dots). The most important hydrologic features are the braided stream channels at A. Even though flow direction is difficult to determine with the SIR-A imagery (Figure 16), the regional flow patterns observed on other images would indicate a probable flow direction toward the southwest (dashed arrows). On the SIR-A imagery, an incised channel at C appears to cut into the Nubian bedrock. There is no trace of any fluvial patterns or Nubian outcrops on the sand-covered plain between C and A on the Landsat image (Figure 15).

Northwestern Saudi Arabia, Test Site 6

60. Test site 6 (Figure 17) is on the western edge of the An Nafud and is centered near latitude 27°30' N, longitude 37°00' E (Figure 4). The very bright radar return at A is an isolated, and probably high-relief, exposure of the Tabuk Formation. The bright area around E is probably the identical lithology present in the darker area east of D, but it is blanketed by a much thinner sand cover and thus reflects a stronger signal. The very dark area surrounding B corresponds to a dune field of the An Nafud sand desert where the radar signal is scattered and lost in the thick sand cover. The bright, elongated patches in the dune field were first inferred to be steep dune
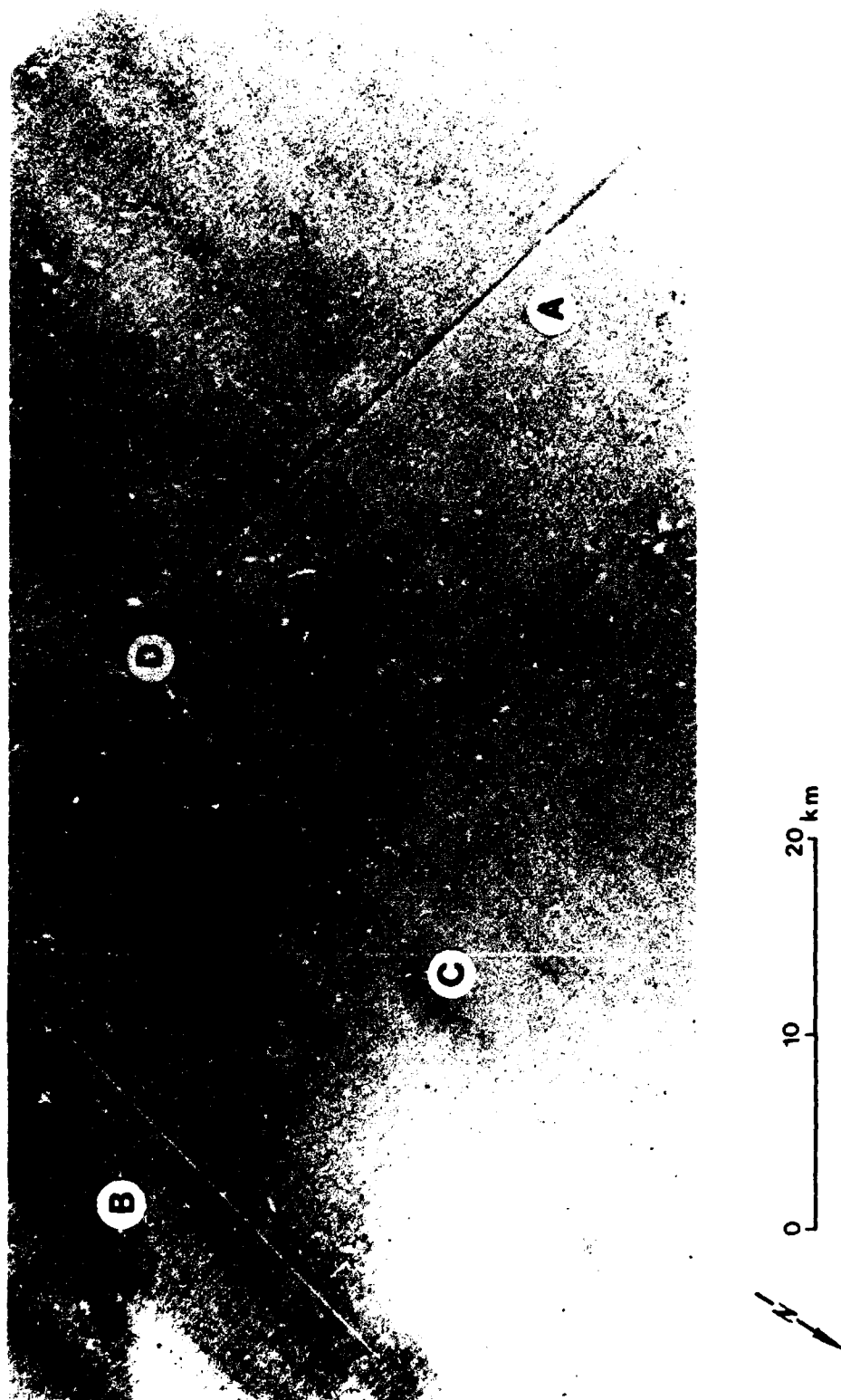
Figure 15. Landsat-1 images of test site 5, left 9 February 1973, MSS band 4, solar elevation 39°, solar azimuth 135°, ID No. 81201802500; right 9 May 1973, MSS band 4, solar elevation 61°, solar azimuth 96°, ID No. 81290075571500

37
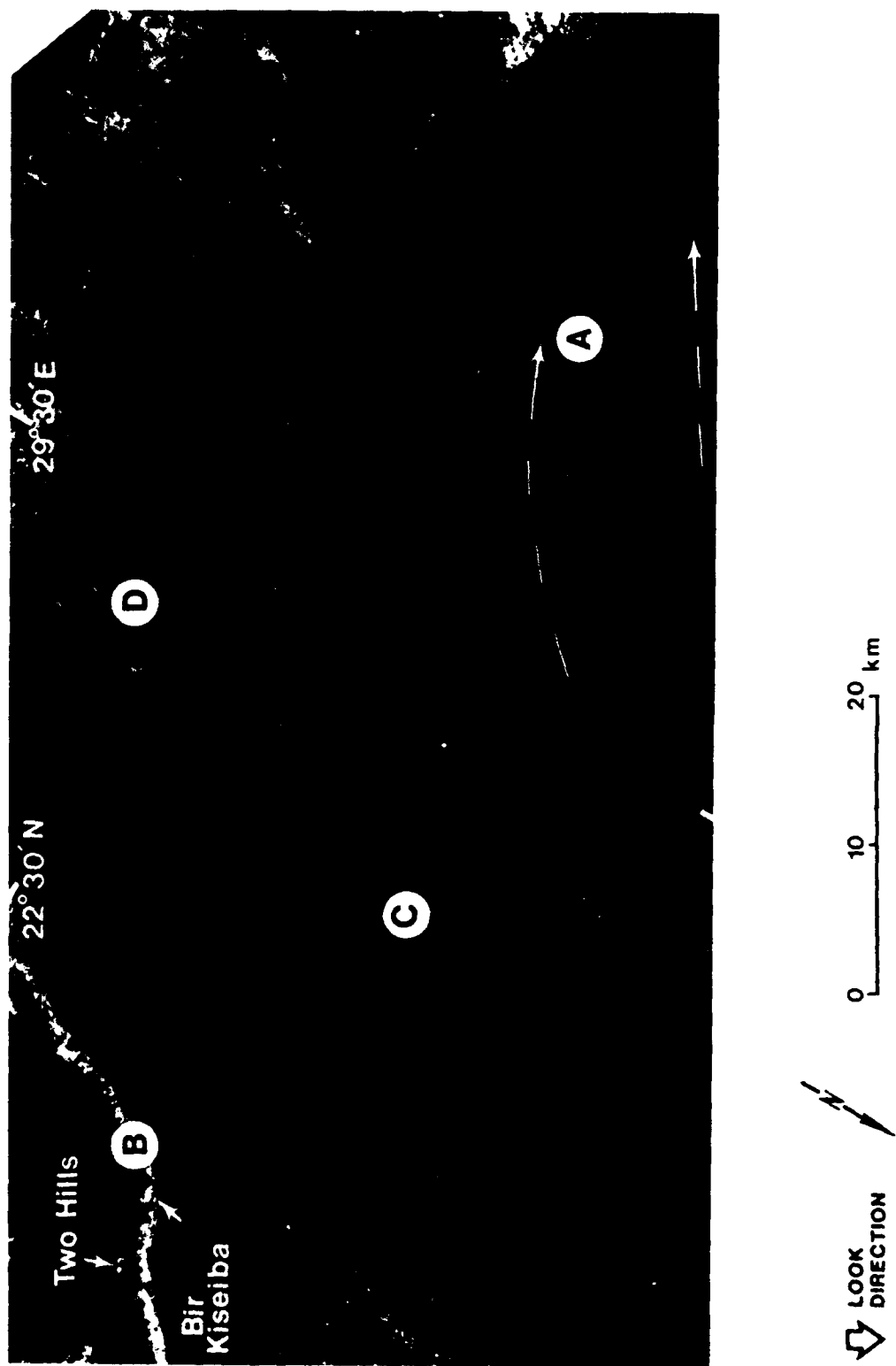
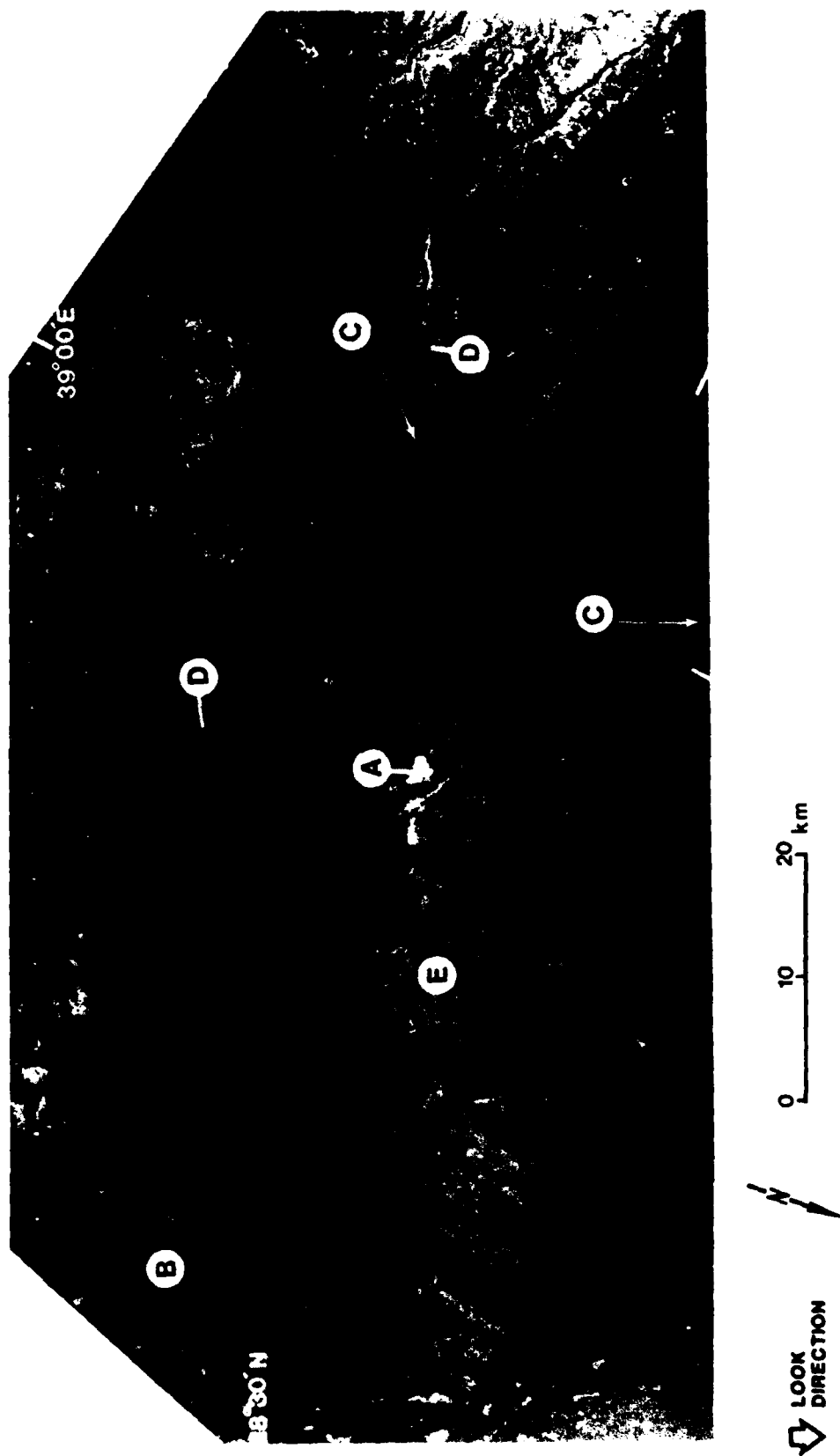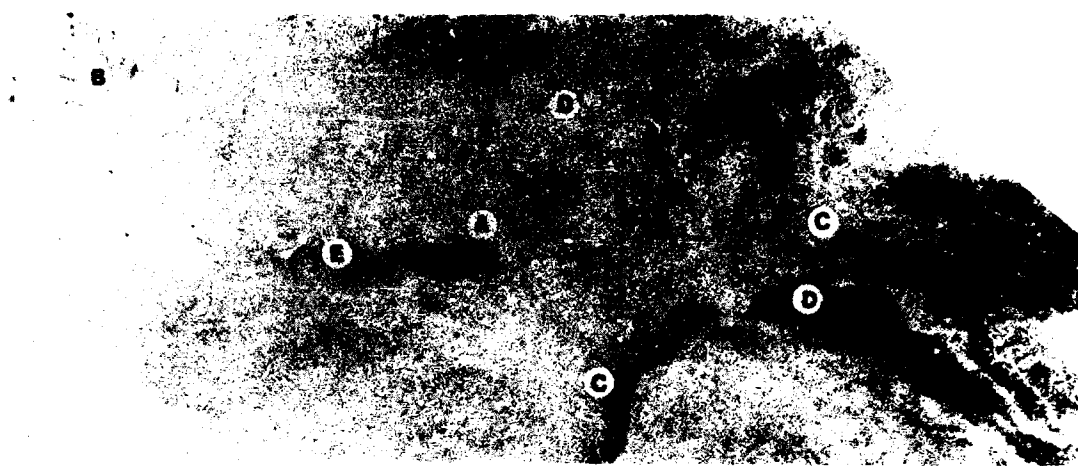Figure 16. SIR-A imagery of test site 5, 13 November 1981, orbit 27, data take 28

Figure 17. SIR-A imagery of test site 6, 13 November 1981, orbit 27, data take 28

faces; however, later examination of Landsat imagery (Figure 18) revealed that interdune outcrops appear to be responsible for many of the returns.

61. Hydrologically, the most important feature observable on the SIR-A image (Figure 17) is a relict river valley (C) fed by multiple channels (D). The pattern of the fluvial system and the fact that most of the tributaries flow into the valley from the south are strong indicators that the flow in the main valley is to the north (dashed arrows).

62. The three Landsat MSS images of test site 6 (Figure 18) show marked contrast with the SIR-A image (Figure 17) and with each other. Surprisingly, the tonal contrasts between these Landsat images are attributable to differences in processing at EROS Data Center, not acquisition times. The three images were reproduced from the same negative; however, they were processed at different times by EROS Data Center. The upper Landsat image (Figure 18a) appears to be overexposed and has a "washed-out" look. The middle Landsat image (Figure 18b) also lacks contrast, but appears to be underexposed. The bottom image (Figure 18c) has the best tonal contrast and compares favorably with the terrain information that can be interpreted from the SIR-A image (Figure 17). For example, the large stream valley that can be identified on the SIR-A image at C can also be located on all three of the Landsat images; however, this feature is best defined on the lower Landsat image (Figure 18c). Similarly, small tributary channels (D in Figure 17) are easiest to detect on the bottom Landsat image (Figure 18c). Although an isolated exposure of the Tabuk Formation can be inferred on all three Landsat images (A), sand cover makes location of the boundary between the dune field (B) and the thinly veiled Tabuk Formation (E) very difficult.

63. The Landsat Return Beam Vidicon (RBV) imagery of test site 6 (Figure 19) provides terrain information somewhat similar to the SIR-A imagery (Figure 20) but significantly better than the MSS images (Figure 18) of the same area. The RBV system records imagery that has different spatial and spectral resolution when compared with the MSS imagery illustrated in Figure 18. Spatial resolution is a measure of the smallest angular or linear separation between two objects that can be resolved by the sensor. Spectral resolution refers to the dimension and number of specific wavelength intervals in the electromagnetic spectrum to which a sensor is sensitive. The Landsat-3 RBV system (Figure 19) has a 30-m spatial resolution and records in a broad spectral band from 0.51 to 0.75 µm. The Landsat-1 MSS imagery illustrated in

a. Overexposure
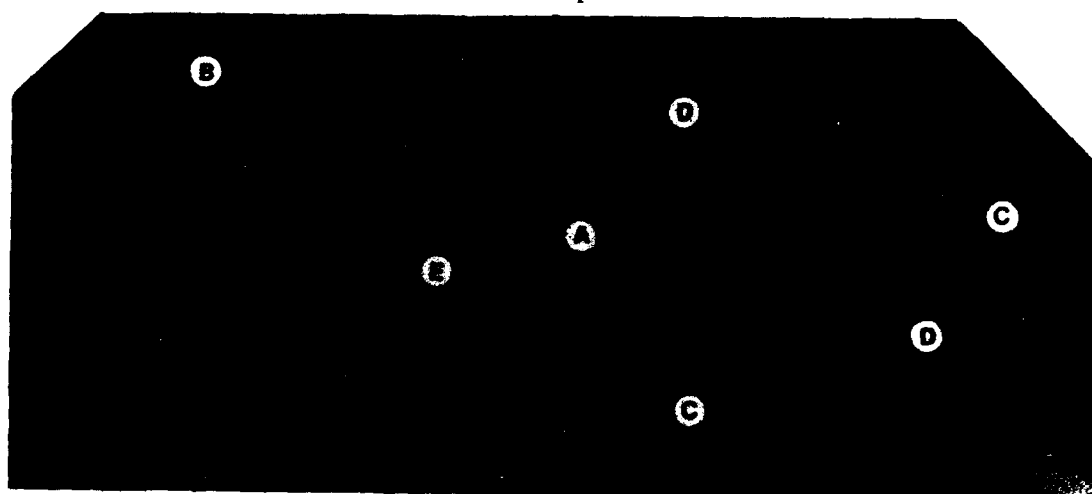
b. Underexposure

c. Optimal

0   10   20 km
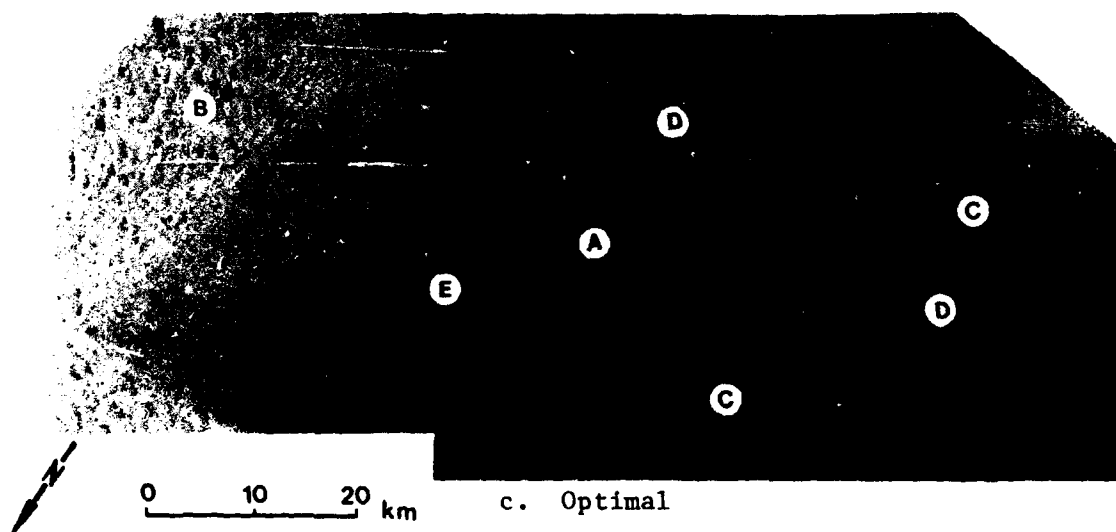
Figure 18. Landsat-1 images of test site 6, 15 July 1973, MSS band 7,
solar elevation 61°, solar azimuth 97°, ID No. 8135707260500,
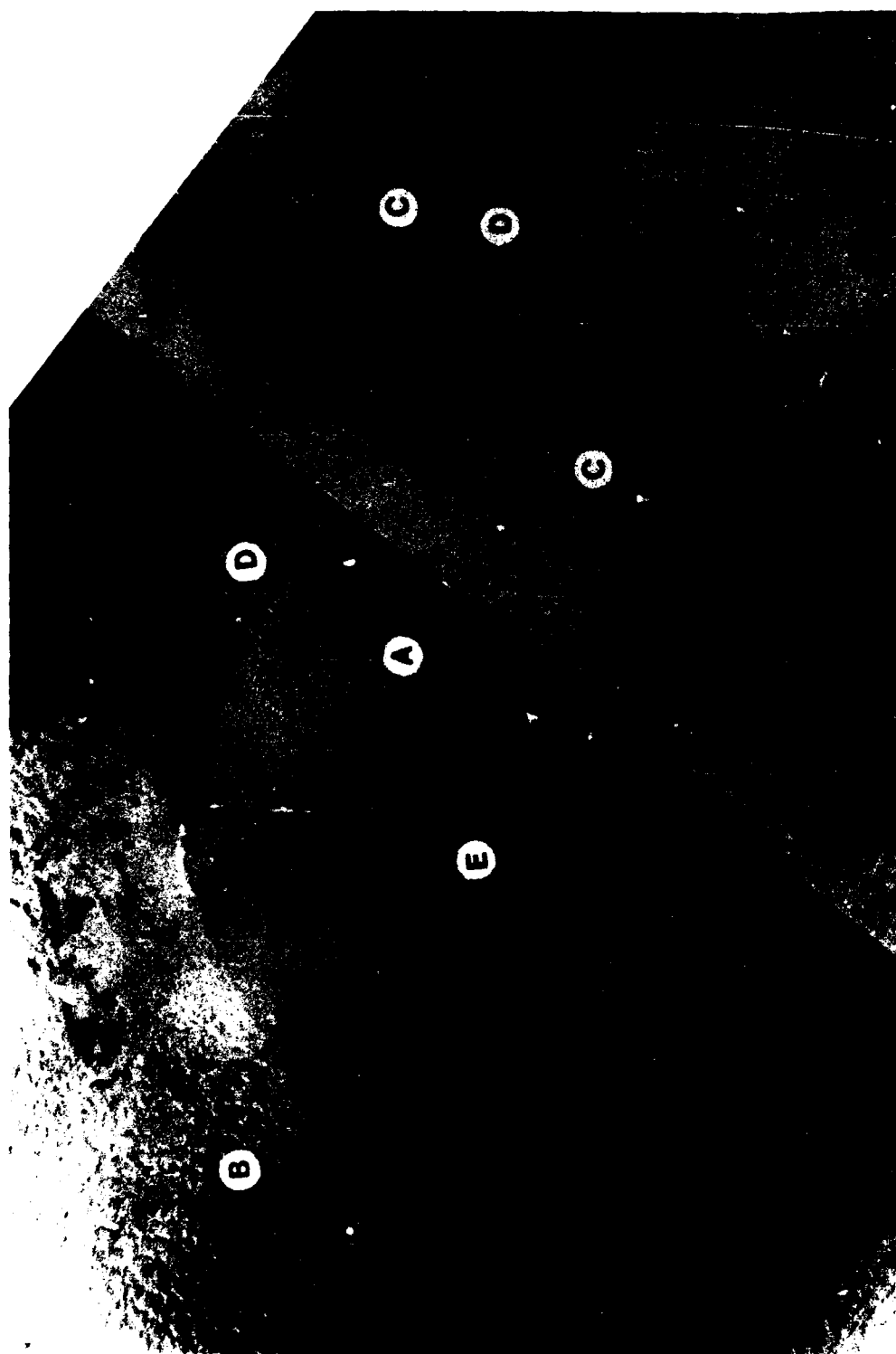demonstrating differences due to processing

41

Figure 19. Landsat-3 images of test site 6, left 12 October 1980, spectral band 0.5 to 0.75 μm, solar elevation 42°, solar azimuth 134°, ID No. 83095207021XD; right 5 December 1980, spectral band 0.5 to 0.75 μm, solar elevation 29°, solar azimuth 144°, ID No. 83100607024XC

42
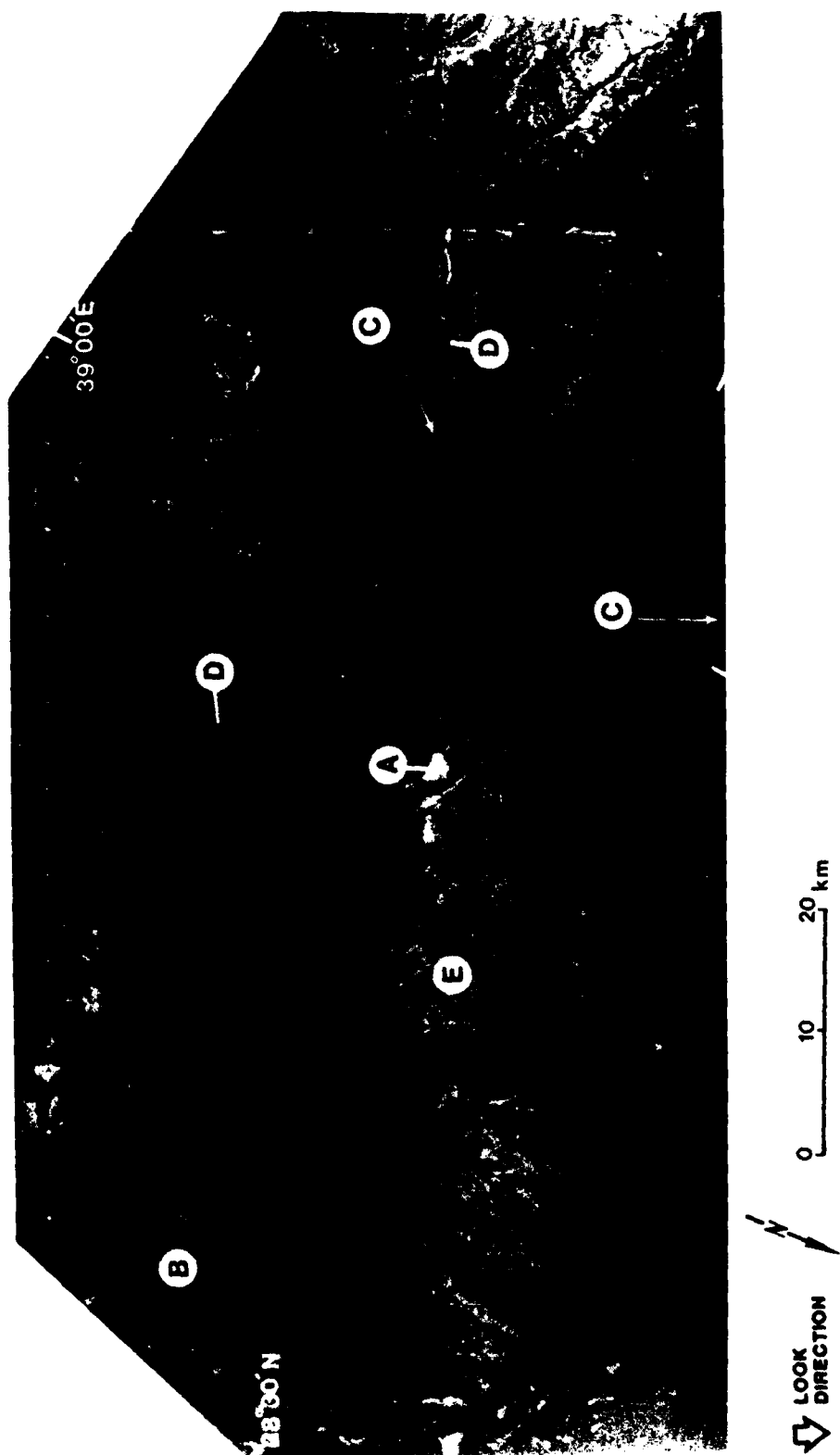
Figure 20. SIR-A imagery of test site 6, 13 November 1981, orbit 27, data take 28

43

Figure 18 was recorded in the photographic, near-infrared spectral band with a spatial resolution of 79 m.

64. Evidence of RBV improvement in spatial resolution is immediately apparent when comparing Figures 18 and 19. The sand dunes at B are clearly visible on the RBV imagery (Figure 19). The dune field is much easier to delineate on the RBV imagery than on either the MSS or SIR-A imagery. In addition. the improved tonal contrast provided by the broad spectral band of the RBV allows for the mapping of considerably more terrain detail than could be interpreted from MSS imagery.

65. Because the RBV imagery of test site 6 allowed for the mapping of most of the river valleys that could be inferred from the interpretation of the SIR-A imagery (Figure 20), a mosaic of RBV images was constructed (Figure 21) to investigate the feasibility of mapping fluvial systems in areas adjacent to shuttle radar coverage. A major fluvial channel, which was initially inferred between the two C's on the SIR-A imagery (Figure 20), can be extended over 70 km to the north using the RBV mosaic (Figure 21). The channel becomes less distinct at G where it merges with a wide plain of eolian deposits. The ancient flow (dashed arrows, Figure 21) in this wide valley apparently split at F, with smaller channels draining toward the northwest.

Northeastern Sudan and Southeastern Egypt

Test site 7

66. Test site 7 is between the eastern edge of the northern Red Sea Hills and the western edge of the Nubian Desert; it is centered at approximately latitude 20°04' N, longitude 32°00' E (Figure 4). Using available geologic data (Vail 1978), Landsat imagery (Figure 22), and SIR-A imagery (Figure 23), a reconnaissance geologic map was constructed (Figure 24). On the Landsat image, the Precambrian outcrops (A) were inferred by the dark tones, whereas on the SIR-A image, these rocks could be identified by bright radar returns that are related to the very rough outcrop surface. On the radar imagery, Recent deposits (B) appear dark-toned with numerous bright areas (C) that are probably related to concentrations of carbonate nodules and rhizoliths (calcified root casts) in the sandy alluvium (Schaber et al. 1986). The Nubian Sandstone has been inferred by an intermediately mottled gray tone.

Figure 21. Landsat-3 RBV mosaic of test site 6 and vicinity, two upper left subscenes, 12 October 1980, solar elevation 42°, solar azimuth 134°, ID Nos. 83095207021XB/83095207021XD, two lower right subscenes, 5 December 1980, solar elevation 29°, solar azimuth 144°, ID Nos. 83100607024XC/83100607024XD
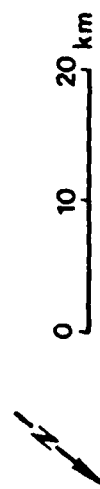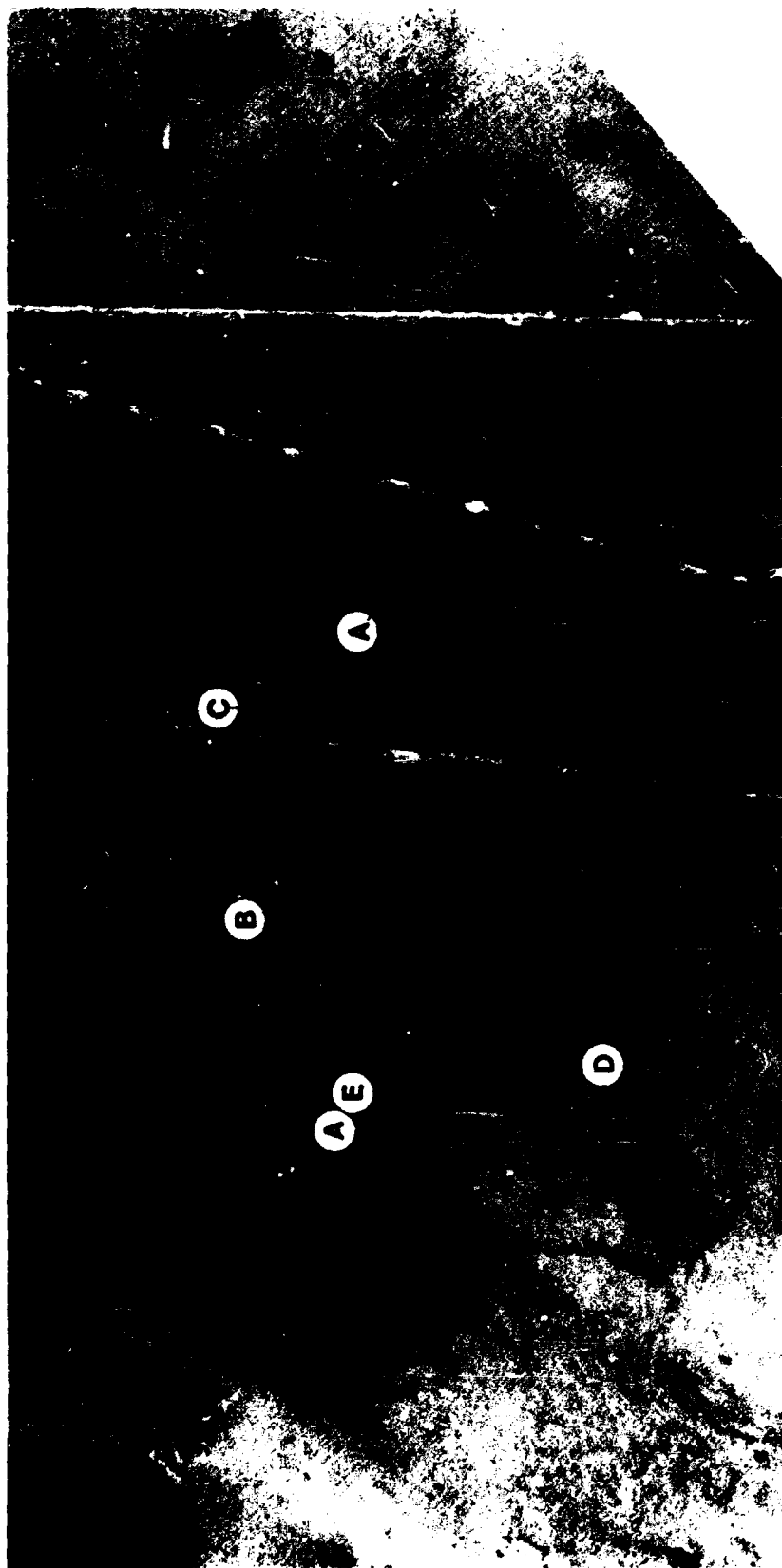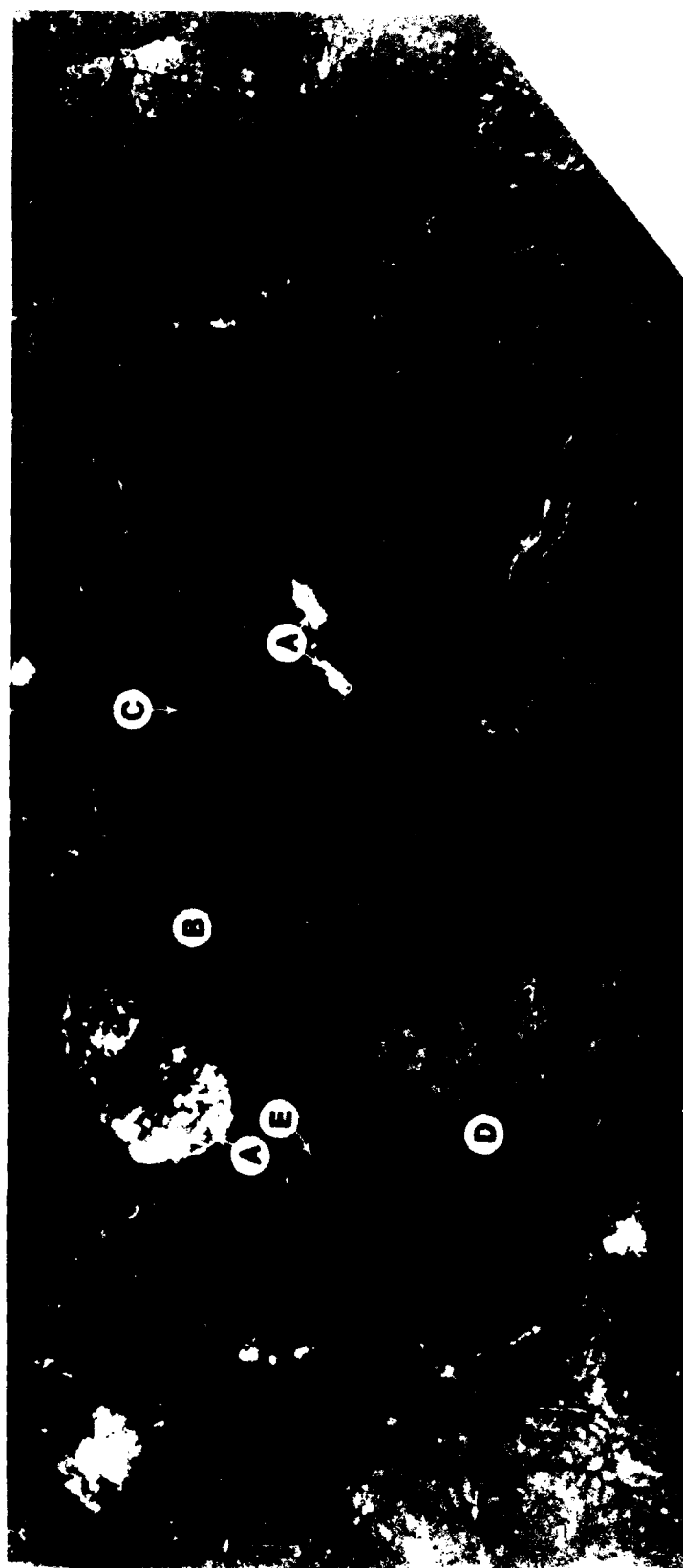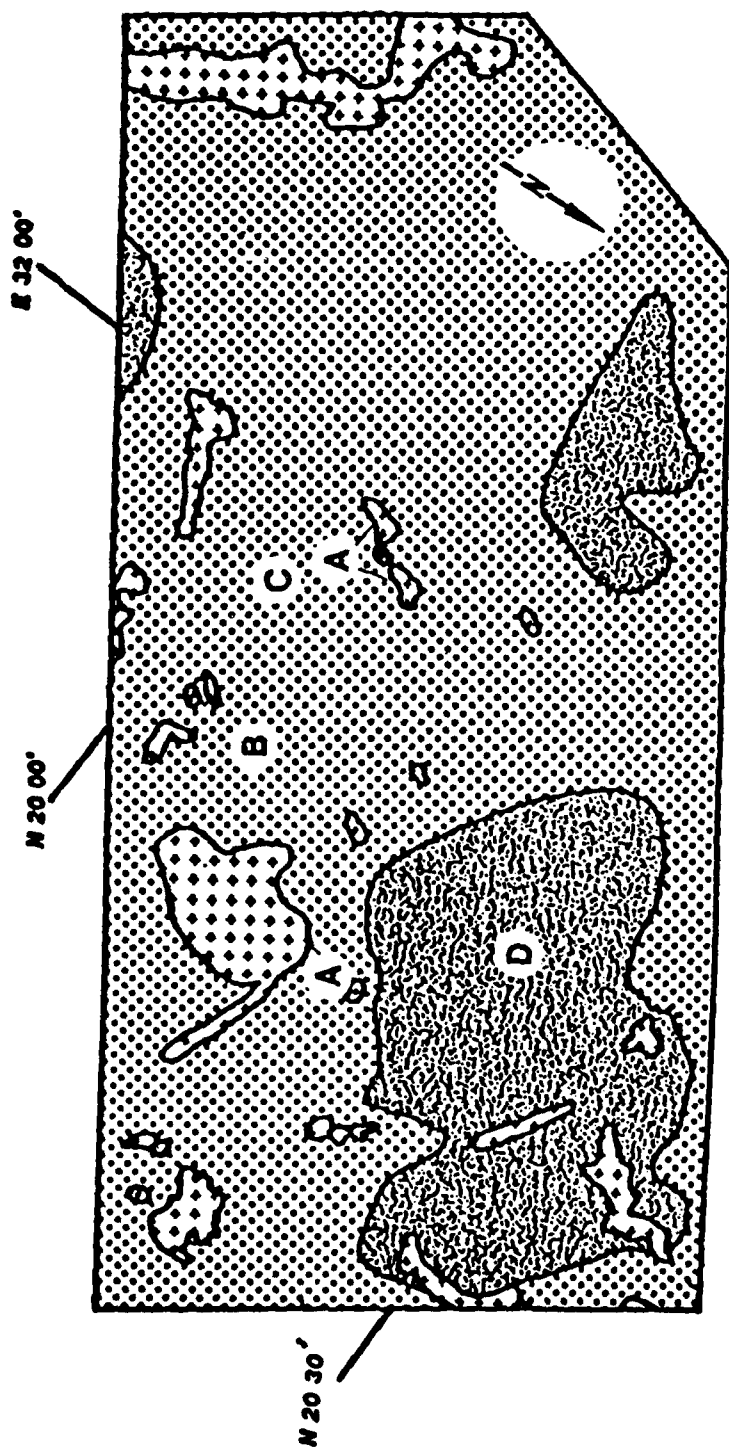
Figure 22. Landsat-2 imagery of test site 7, 13 January 1979, MSS band 7, solar elevation 35°, solar azimuth 137°, ID No. 8235607320500

Figure 23. SIR-A imagery of test site 7, 12 November 1981, orbit 10/11, data take 7

Figure 24. Reconnaissance geologic map of test site 7 inferred from the
12 November 1981 SIR-A imagery

LEGEND

QUATERNARY/RECENT WINDBLOWN SANDS AND SURFICIAL DEPOSITS

CRETACEOUS UNDIFFERENTIATED NUBIAN SANDSTONE

PRECAMBRIAN BASEMENT COMPLEX

Not apparent on the Landsat imagery are numerous fluvial channels and line-
aments that can be mapped on the SIR-A imagery in the vicinity of B and D.

Test site 8

67. Test site 8 is centered at approximately latitude 21°23' N, longi-
tude 33°35' E (Figure 4), on the northwestern edge of the northern Red Sea
Hills adjacent to the Nubian Desert. Proximity to the desert has allowed for
large amounts of windblown materials to accumulate in low-lying areas. Litho-
logically, the area can be separated into outcrops of the Precambrian Basement
Complex and Recent windblown sands and surficial deposits. Lithologic differ-
entiation can be made on the Landsat imagery (Figure 25) primarily by using
tonal variations where the Precambrian exposures appear darkest and the sand
sheet and surficial deposits exhibit highest reflectance. Figure 26 provides
a reconnaissance geologic map generated from Landsat interpretation.

68. On the SIR-A radar imagery (Figure 27), the Recent deposits (A) are
identified by their characteristic dark tones that are related to their rela-
tively smooth surfaces. Conversely, the very rough nature of the Precambrian
Basement Complex exposures results in a very bright radar return on the
imagery. Figure 28 illustrates the geologic units inferred from SIR-A imagery
interpretation.

69. Lineament patterns have been mapped using both Landsat (Figure 29)
and SIR-A (Figure 30) imagery. Lineaments, as used in this report and
inferred from Landsat or shuttle imagery, are naturally occurring, continuous
straight-line features, regardless of length, which may be manifested in the
forms of tonal, vegetative, stream pattern, or landform alignments. Because
these features commonly reflect subsurface zones of increased porosity and
permeability, lineament analysis has become an important technique used for
ground-water exploration. Significantly greater yields have been obtained
from water wells located at the intersection of or in proximity to lineaments.
Many of the topographically expressed lineaments mapped on the radar imagery
are also present on the Landsat imagery (C and D, Figures 29 and 30); however,
on the radar, these linear terrain elements are more numerous and can be
inferred over greater distances, especially in the regions of sand sheet and
surficial deposits. Similarly, relict drainage channels are much more appar-
ent on the SIR-A imagery. For example, on the Landsat image in the vicinity
of the north arrow (Figure 27), there is little evidence to support the

49

Figure 25. Landsat-2 imagery of test site 8, 7 December 1975, MSS band 5, solar elevation 35°, solar azimuth 143°, ID No. 8231907261500
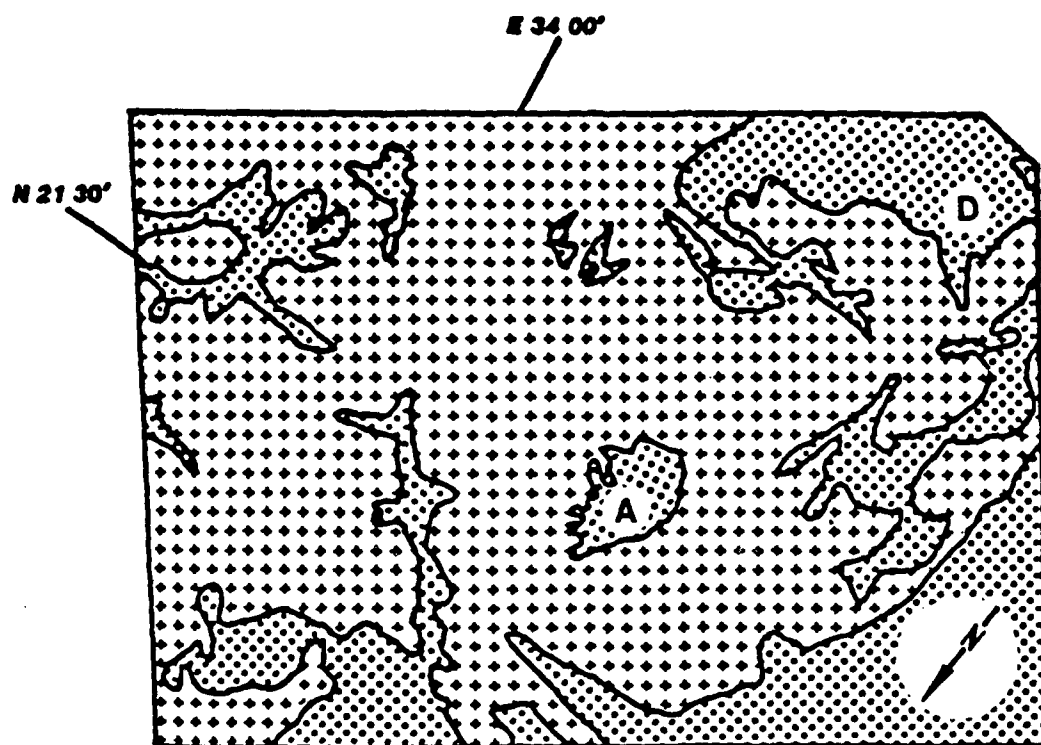
50

LEGEND

 QUATERNARY/RECENT WINDBLOWN SANDS AND SURFICIAL DEPOSITS

 PRECAMBRIAN BASEMENT COMPLEX

Figure 26. Reconnaissance geologic map of test site 8 inferred from the
7 December 1975 Landsat-2 imagery

mapping of drainage patterns. However, for this same area, a vast channel
network is revealed on the SIR-A image.

Test site 9

70. Test site 9, located in the heart of the northern Red Sea Hills, is
centered at latitude 21°43' N, longitude 34°44' E (Figure 4). Similar to the
geologic mapping techniques used in the test site 8 area, lithologic differen-
tiation on the Landsat (Figure 31) and SIR-A (Figure 32) imagery can be made

Figure 27. SIR-A imagery of test site 8, 12 November 1981, orbit 10/11, data take 7
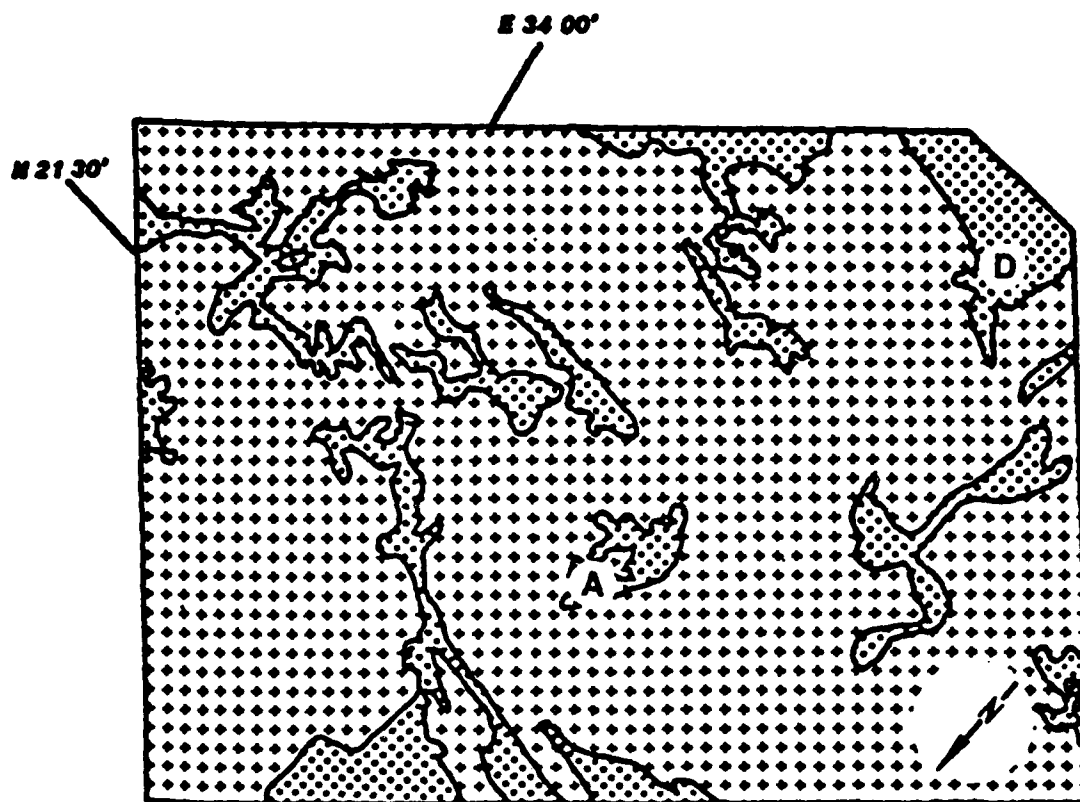
LEGEND

 QUATERNARY/RECENT WINDBLOWN SANDS AND SURFICIAL DEPOSITS

 PRECAMBRIAN BASEMENT COMPLEX

Figure 28. Reconnaissance geologic map of test site 8 inferred from the
12 November 1981 SIR-A imagery

primarily using tonal variations. On the Landsat image, the dark-toned area
at A corresponds to the light-toned area on the SIR-A image and is character-
istic of the Precambrian rock exposures. In preparing a reconnaissance geo-
logic map of the area (Figure 33), difficulties were encountered.
Differentiation between the Quaternary alluvium and Recent surficial deposits
was difficult when using the Landsat image because these units display similar
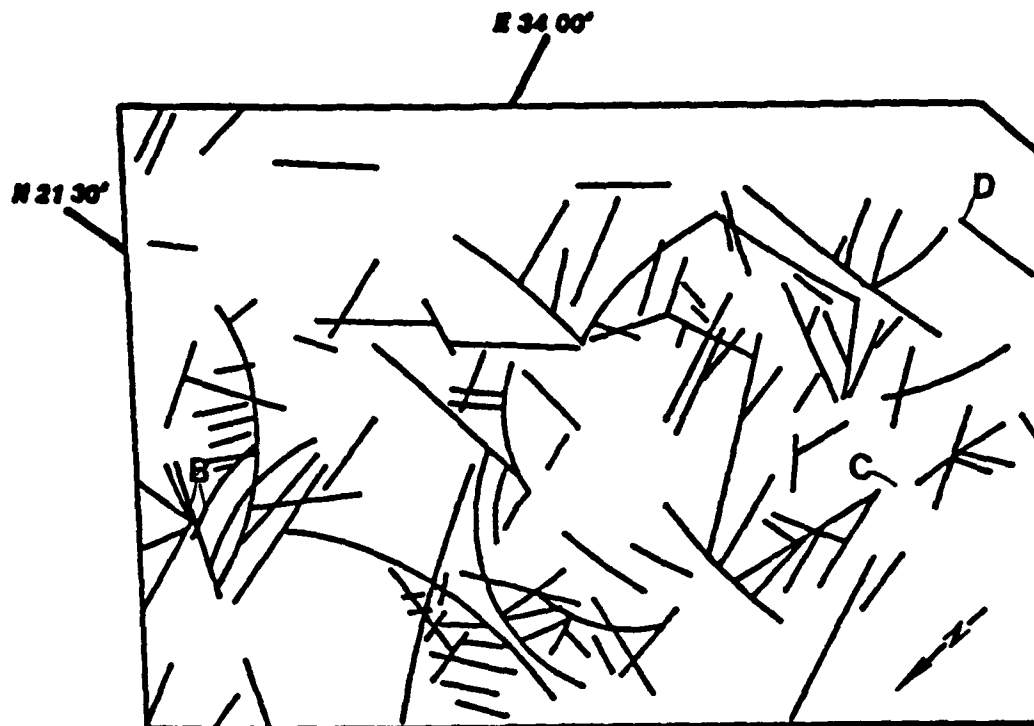
Figure 29.   Interpretation of linear and curvilinear features
detectable on the 7 December 1975 Landsat-2 imagery
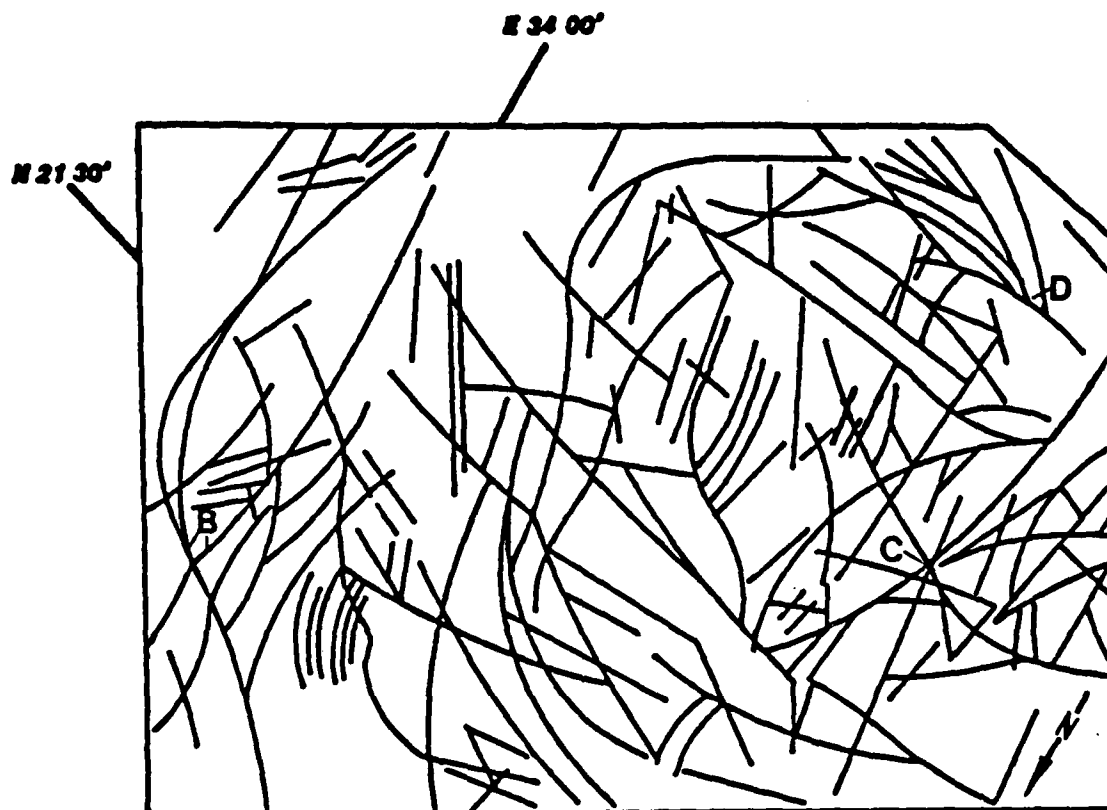
Figure 30.   Interpretation of linear and curvilinear features
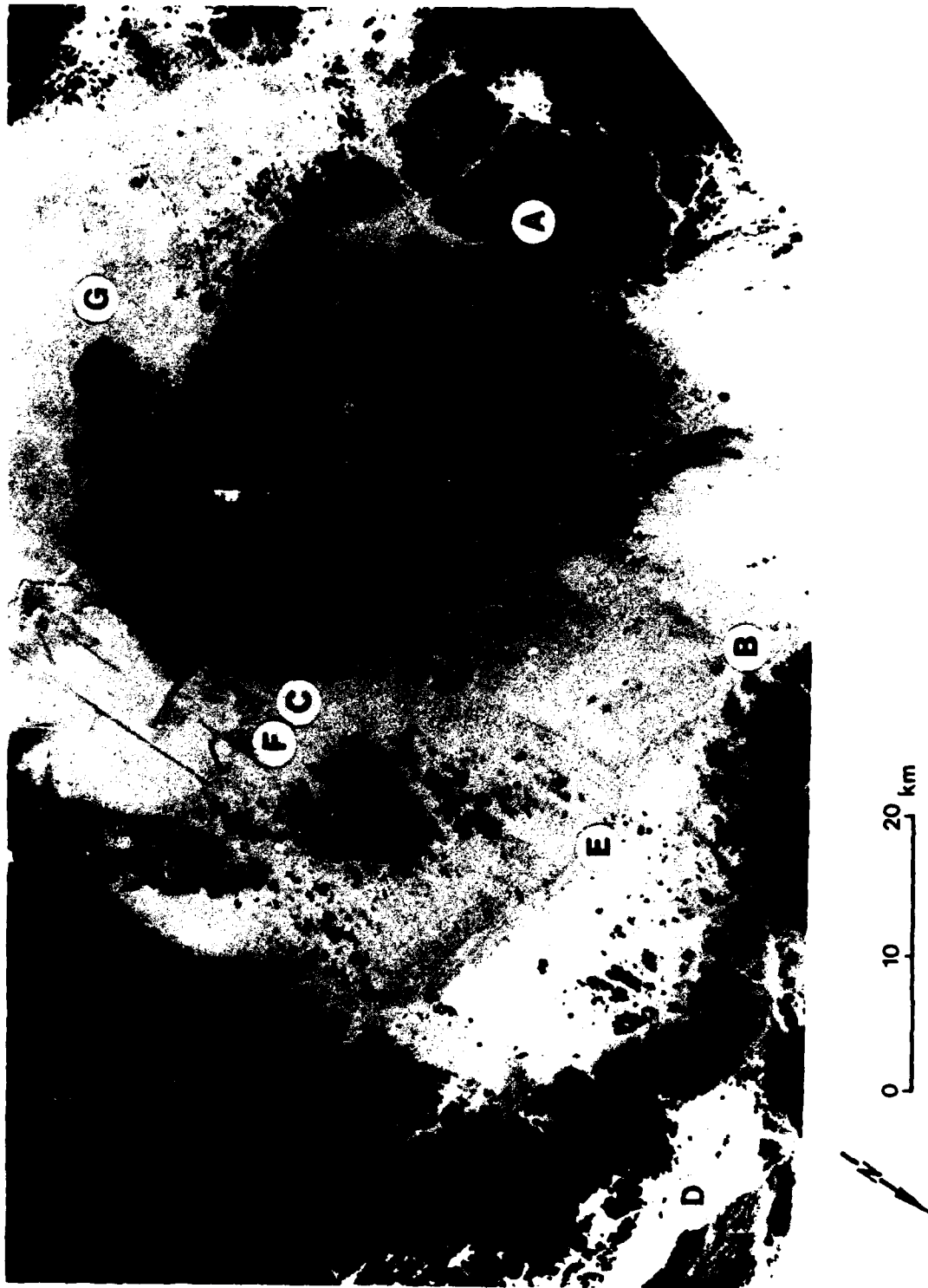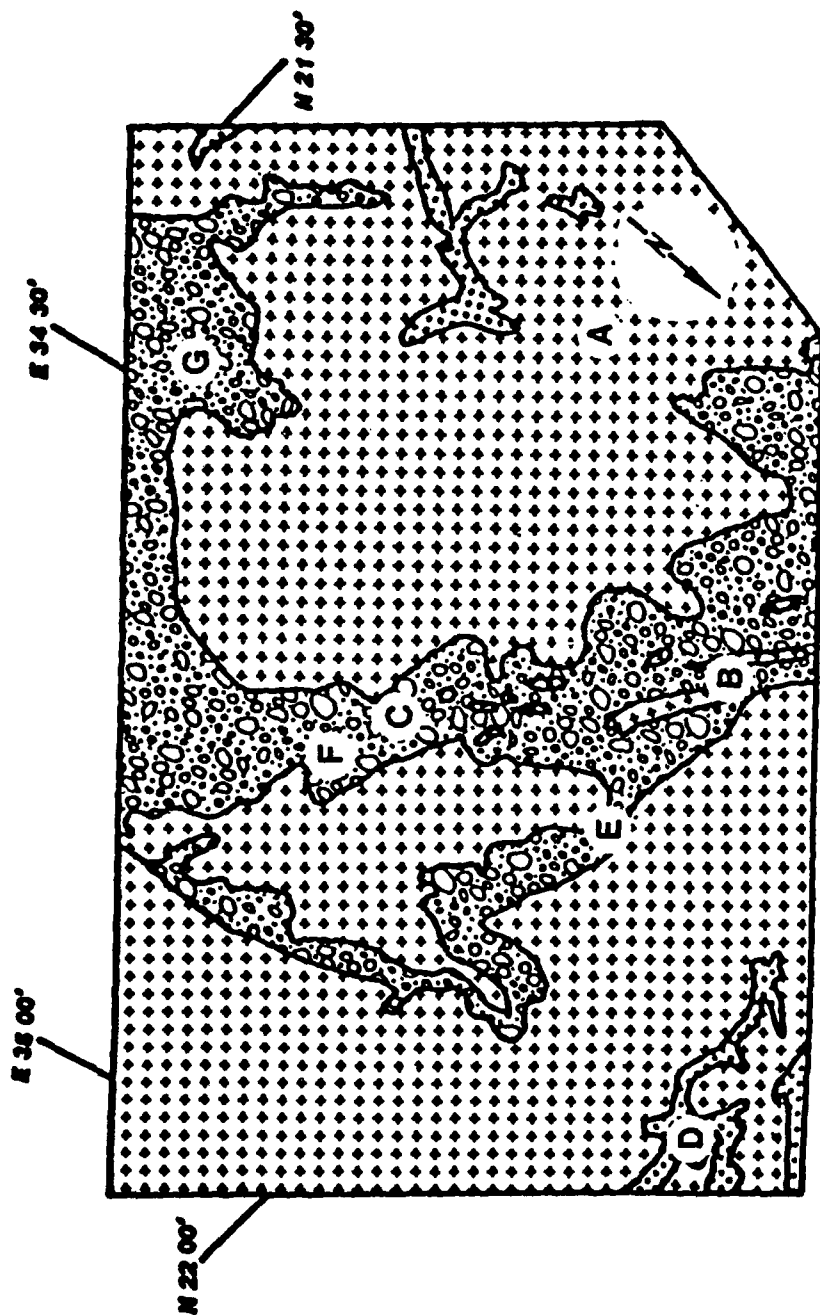detectable on the 12 November 1981 SIR-A imagery

54

Figure 31. Landsat-2 imagery of test site 9, 7 December 1975, MSS band 5, solar elevation 35°, solar azimuth 143°, ID No. 82311907261500

Figure 32. SIR-A imagery of test site 9, 12 November 1981, orbit 10/11, data take 7

Figure 33. Reconnaissance geologic map of test site 9 inferred from the
12 November 1981 SIR-A imagery

LEGEND

QUATERNARY/RECENT WINDBLOWN SANDS AND SURFICIAL DEPOSITS

QUATERNARY ALLUVIUM, WADI FILL

PRECAMBRIAN BASEMENT COMPLEX

light tones related to high spectral reflectance. The SIR-A image, on the other hand, was found to be the most useful for geologic mapping.

71. A complex pattern of subangular stream channels can be identified on the SIR-A imagery (B of Figure 32). Although these fluvial patterns are not readily apparent on the Landsat imagery, their positions on the SIR-A imagery correspond exactly to the stream patterns that appear on Vail's (1978) Geologic Map of Sudan. These patterns were mapped prior to the availability of shuttle imaging radar; therefore, they can hardly be called "radar rivers" even though they are not apparent on the best available Landsat imagery. When this Landsat image was obtained, the reflectance properties of channel and interchannel materials were obviously so similar that little or no contrast was provided on the imagery.

72. The number of lineaments that can be mapped on the Landsat image (Figure 34) is approximately half that inferred from SIR-A interpretation (Figure 35). Lineaments extending more than 10 km are easily inferred on the radar imagery, but are not detectable on the Landsat imagery, especially in the Quaternary alluvium (locations E and F). The Quaternary alluvium should serve as an important medium for surface water infiltration and, combined with the capability to map fluvial channels and lineaments, could allow for selecting high priority sites for ground-water exploration. For example, location G, as shown on the SIR-A imagery (Figure 35) would be of special interest because it is within a channel that intersects numerous lineaments. Thus, location G has both the potential for ground-water recharge and the probability of being a productive well site.

Egypt-Sudan Border, Test Site 10

73. Test site 10, centered at latitude 22°23' N and longitude 35°22' E, is near the Egypt-Sudan border on the western shore of the Red Sea (Figure 4). The interpretive guides and techniques used to infer lithologic units on the Landsat image (Figure 36) and the SIR-A image (Figure 37) were similar to those previously discussed for test sites 8 and 9. Figure 38 is a reconnaissance geologic map derived from the interpretation of the SIR-A imagery.

74. Geologic contacts, lineaments, and stream channels in the Precambrian Basement Complex (A and B, Figures 36-38) and in the Tertiary Coastal Deposits (C) can be mapped equally well on the Landsat and SIR-A imagery.
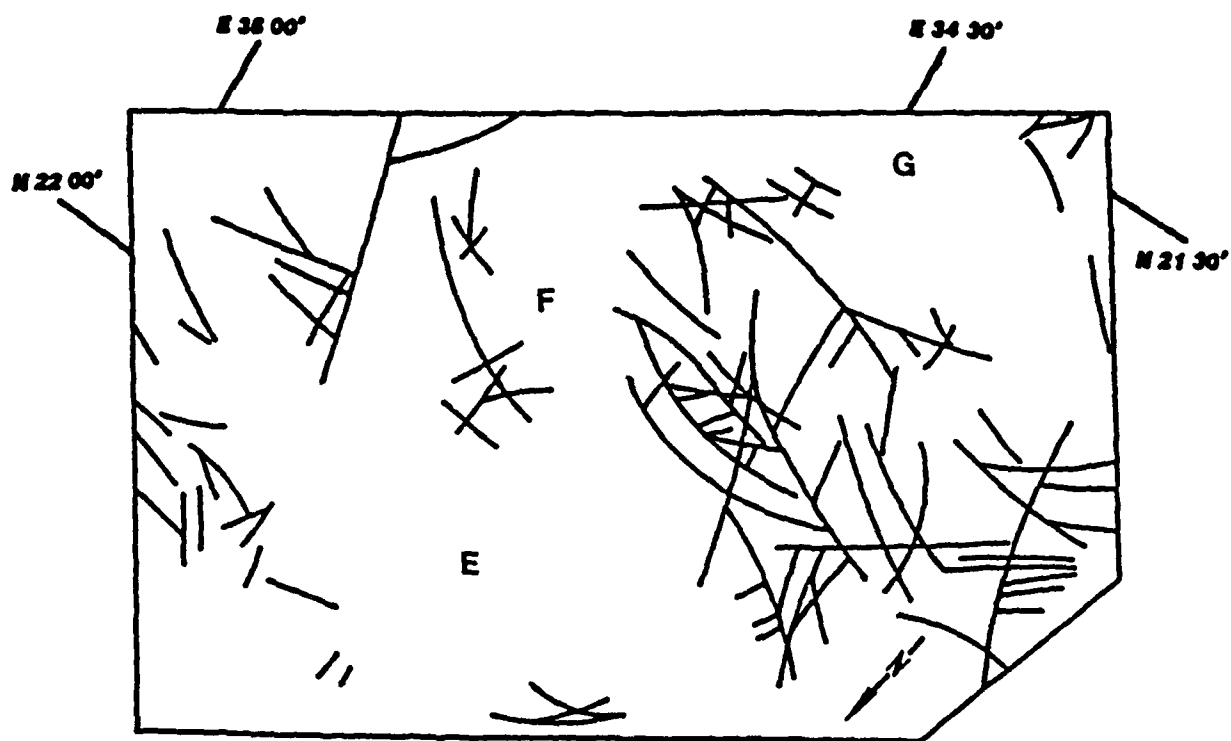
58

Figure 34.   Interpretation of linear and curvilinear features detectable
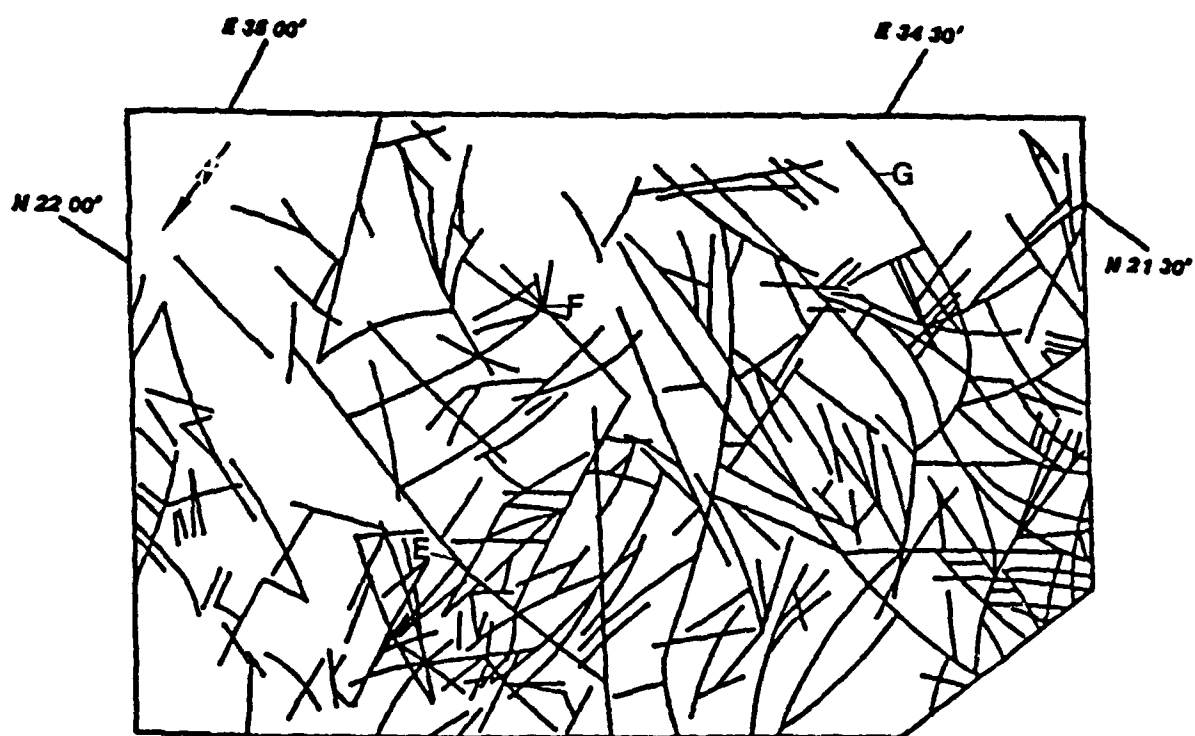on the 7 December 1975 Landsat-2 imagery

Figure 35.   Interpretation of linear and curvilinear features detectable
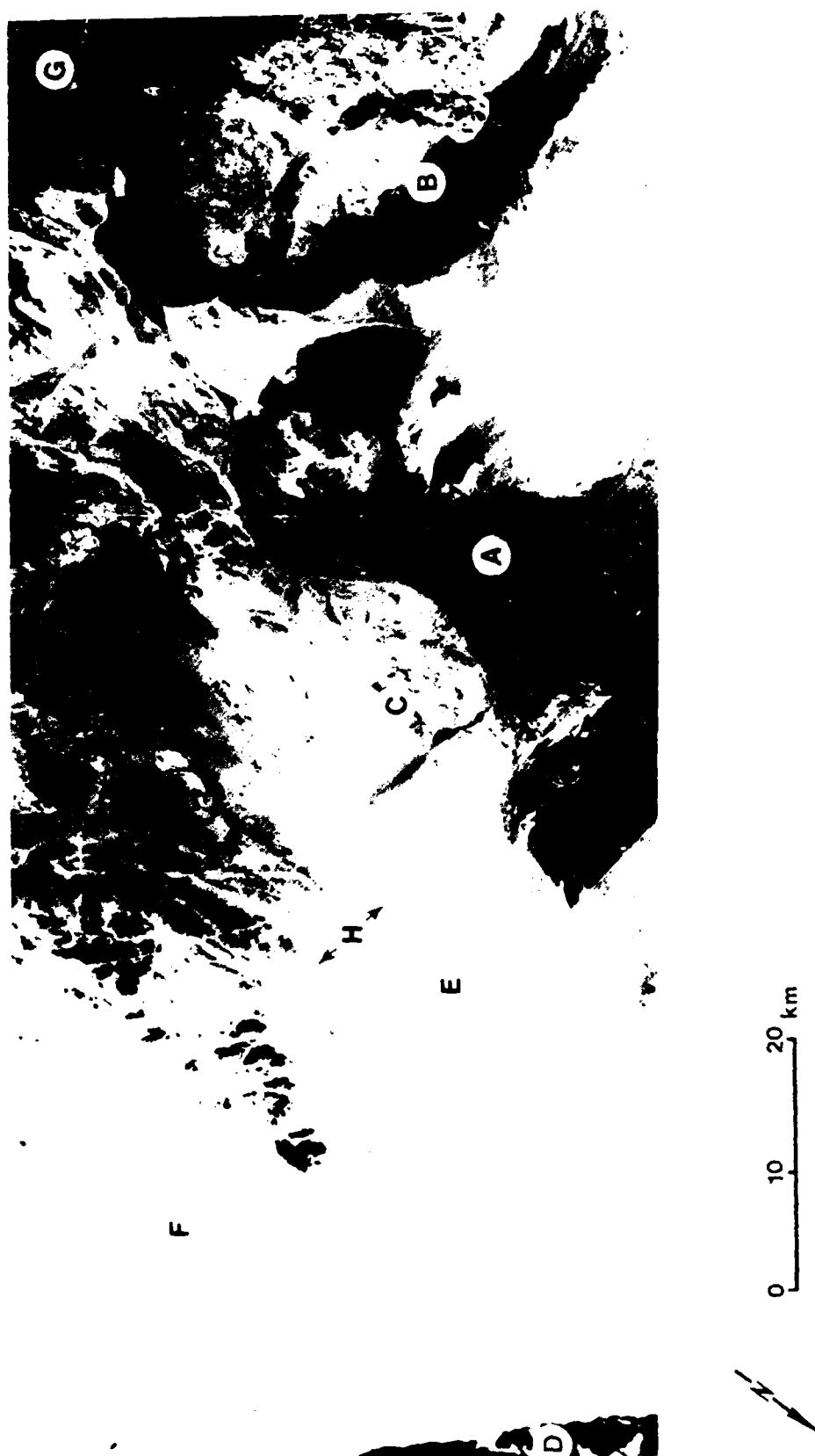on the 12 November 1981 SIR-A imagery

Figure 36. Landsat-1 images of test site 10, left 12 March 1973, MSS band 7, solar elevation 48°, solar azimuth 125°, ID No. 81232073342500; right 5 May 1973, MSS band 7, solar elevation 61°, solar azimuth 95°, ID No. 81286073344500
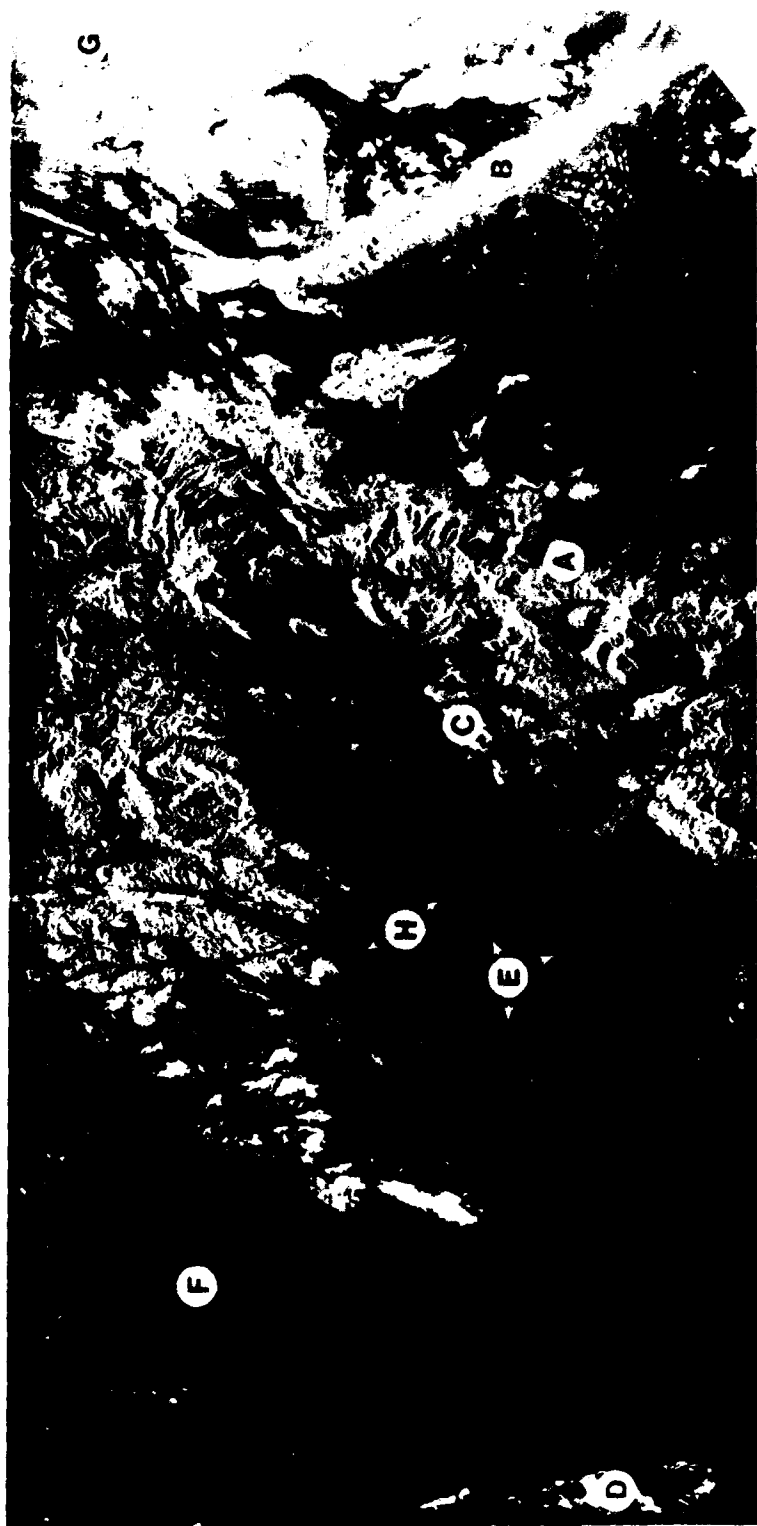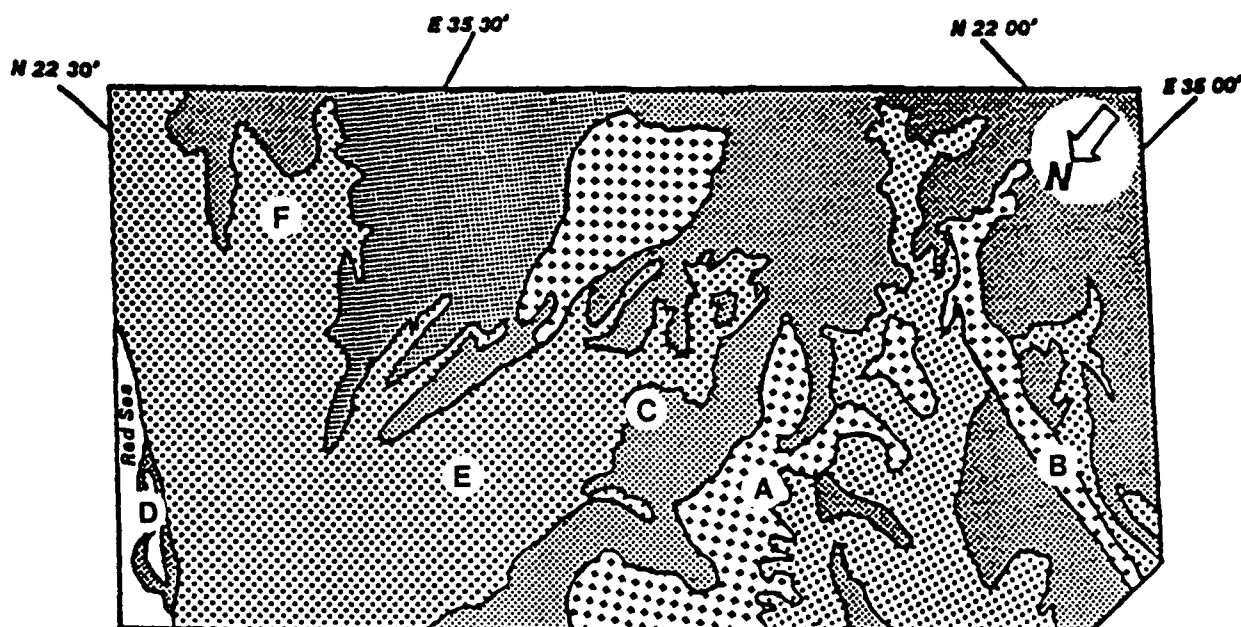
Figure 37. SIR-A imagery of test site 10, 12 November 1981, orbit 10/11, data take 7

LEGEND

```
[::::] QUATERNARY/RECENT WINDBLOWN SANDS AND SURFICIAL DEPOSITS

[::::] TERTIARY COASTAL DEPOSITS OF THE RED SEA MARGIN

[++++] PRECAMBRIAN BASEMENT COMPLEX
```
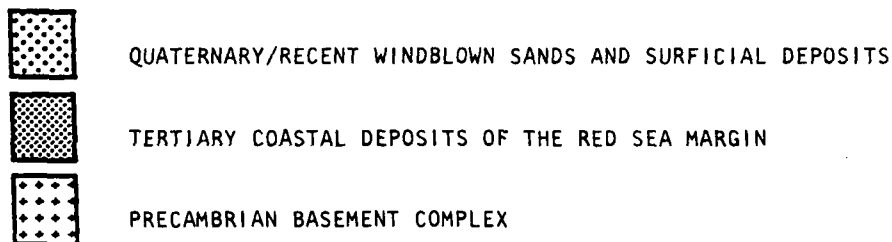
Figure 38.   Reconnaissance geologic map of test site 10 inferred from the
12 November 1981 SIR-A imagery

However, the numerous lineaments and fluvial channels that appear in the
Quaternary and Recent surficial deposits on the SIR-A map (E, Figure 38) can-
not be inferred from Landsat interpretation.   The large southeast-trending
lineament (H on Figure 37) that cuts across an extensive alluvial fan appears
to be an attractive site for further ground-water exploration because of its
potential for being in a recharge area.   This lineament cannot be mapped on
the Landsat image (H of Figure 36).

PART V: POTENTIAL FOR USING AIRCRAFT RADAR IMAGERY FOR
"RADAR RIVER" DETECTION

75. Previous discussions (Part IV) have pointed out that relict fluvial channels in arid and hyperarid environments are sometimes difficult to detect on Landsat MSS imagery because surficial materials can possess relatively uniform spectral characteristics. However, the 23.5-cm-wavelength signals of the shuttle radar have apparently penetrated unconsolidated eolian and alluvial materials in some cases, thus revealing the presence of buried fluvial systems.

76. One aspect of ground-water exploration in arid environments that has not been previously recognized is the potential for using shorter wavelength imaging radars for the detection of "radar rivers." Aircraft X-band (3-cm-wavelength) radar imagery was obtained for northeastern Sudan. Because of numerous aircraft turns (resulting in image smear and distortions), the imagery was not of commercial quality. Nonetheless, comparisons with Landsat-type imagery were quite revealing.

Location

77. On 16 January 1981, aircraft radar coverage was obtained by an AN/APS-94 system for northeastern Sudan, which encompasses part of the southern portion of the Sahara Desert. The system used records two 25-km-wide swaths simultaneously, which are imaged by antennas mounted on each side of the aircraft. The flight line (consisting of two different swaths) extended in a northeasterly direction from the confluence of the Atbarah and Nile rivers at the southwest to Port Sudan at the northeast (Figure 39).

Geographic Setting

78. The desert terrain of northeastern Sudan consists of broad areas of sand and "flint rock" with occasional hills and low relief exposures of basalt, granite, and limestone; these exposures are often surrounded with banks of windblown sand. Dry air masses from the northern deserts of Libya, Egypt, and Saudi Arabia flow southward over Sudan to create an arid climate.
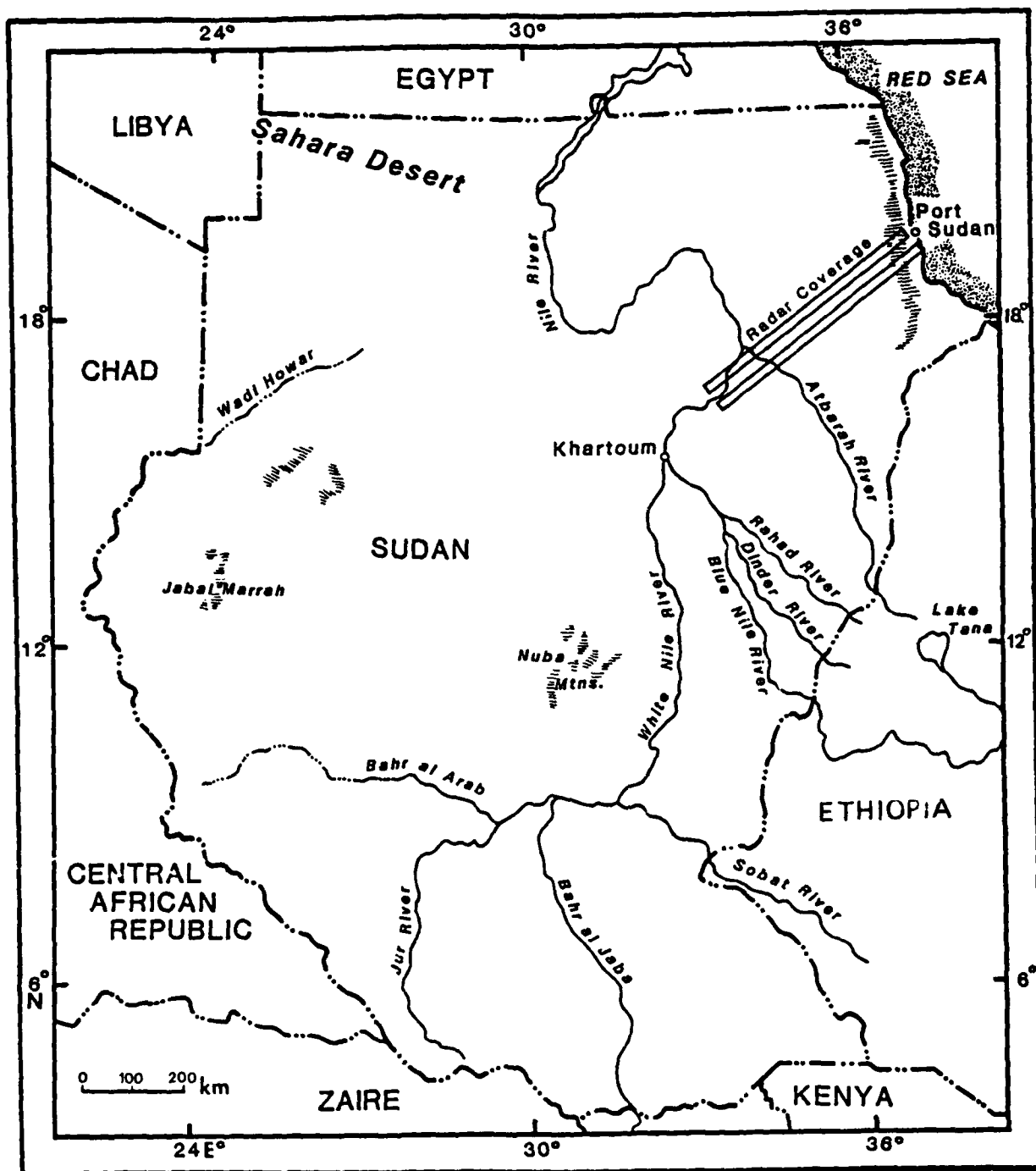
Figure 39. Location of aircraft radar coverage, northeastern Sudan

Aircraft Radar and Landsat Imagery Comparisons

79.   Initial imagery comparisons of the X-band SLAR and Landsat MSS
bands 4 through 7 (e.g., Figure 40) were made for a sand-covered area along
the flight line. These comparisons suggested that imagery generated from this
relatively short-wavelength radar revealed fluvial patterns strikingly similar
to the "radar rivers" detected by the shuttle long-wavelength radar in north-
ern Sudan and southern Egypt (e.g., McCauley et al. 1982); however, examina-
tion of the Landsat imagery (Figure 40b), which was obtained from the EROS
Data Center, did not display the drainage patterns that were obvious on the
X-band radar imagery (Figure 40a). Thus, the hypothesis was made that if the
fluvial patterns inferred from X-band radar imagery were, in fact, similar to
those appearing on shuttle radar, then analysis of short-wavelength military
reconnaissance radar imagery could provide an important ground-water explora-
tion tool for many desert regions of the world. Unfortunately, the SIR-A and
-B ground tracks failed to coincide with the X-band coverage.

80.   For several areas along the X-band radar flight line, however, mul-
tiple Landsat data sets incorporating yearly and seasonal variations are
available. To investigate the possibility that the fluvial channels detected
on the X-band imagery were either not detectable or were less obvious on
Landsat imagery, 20 different Landsat-1, -2, and -3 MSS and RBV images
spanning the period 1973 through 1979 were obtained from the EROS Data Center.
The variation in the amount of terrain information that could be interpreted
from the different MSS images was quite remarkable. For example, although the
February 1973 Landsat-1 MSS image illustrated in Figure 40b is nearly fea-
tureless, the two March 1979 Landsat images shown in Figure 41 allow for the
interpretation of considerably more terrain detail. The Landsat-1 image (Fig-
ure 40) and the Landsat-2 and -3 images (Figure 41) reflect the dry season
conditions. In addition, because the imaging dates of the two MSS images
shown in Figure 41 were only 9 days apart, the terrain conditions were prob-
ably very similar. Figure 42 compares drainage patterns interpreted from the
X-band radar and MSS images illustrated in Figure 41. The drainage complexes
detectable on the radar are much more extensive than those on the Landsat
scenes. The Landsat-3 scene (Figure 41b) also has more tonal contrast than
the Landsat-2 image (Figure 41c). Because the MSS systems on Landsat 1 and
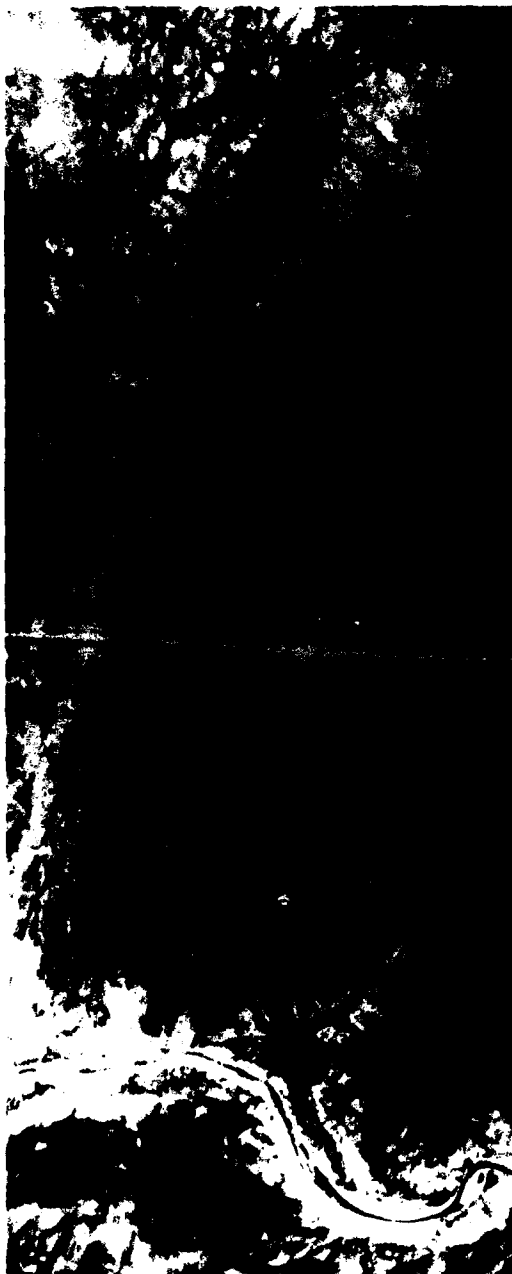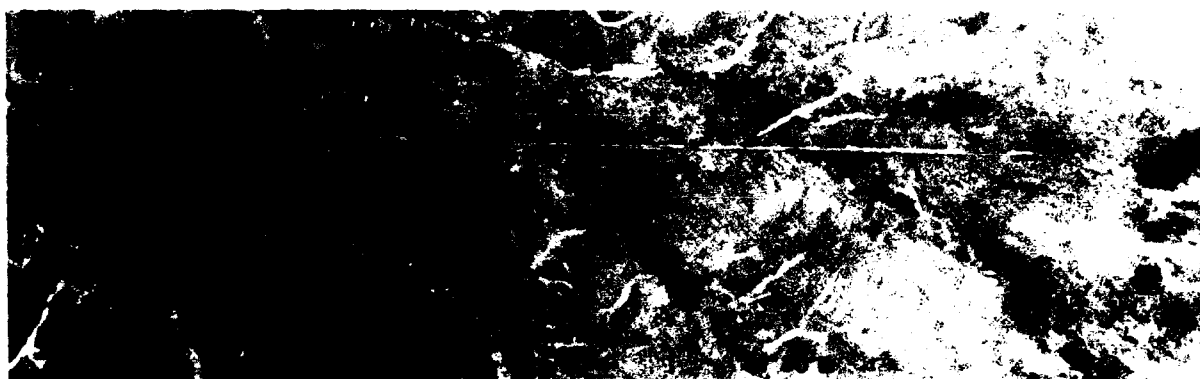
a. Aircraft X-band radar
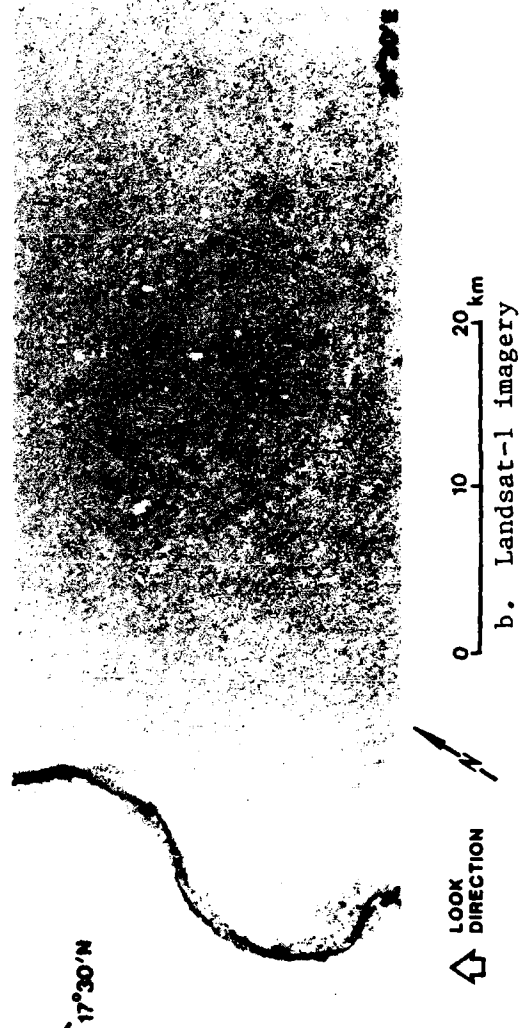
b. Landsat-1 imagery

Figure 40. Comparison of Aircraft X-band radar (a) and Landsat-1 imagery (b), 22 February 1973, MSS band 5, solar elevation 45°, solar azimuth 126°, ID No. 81214073555500

a. Aircraft X-band radar
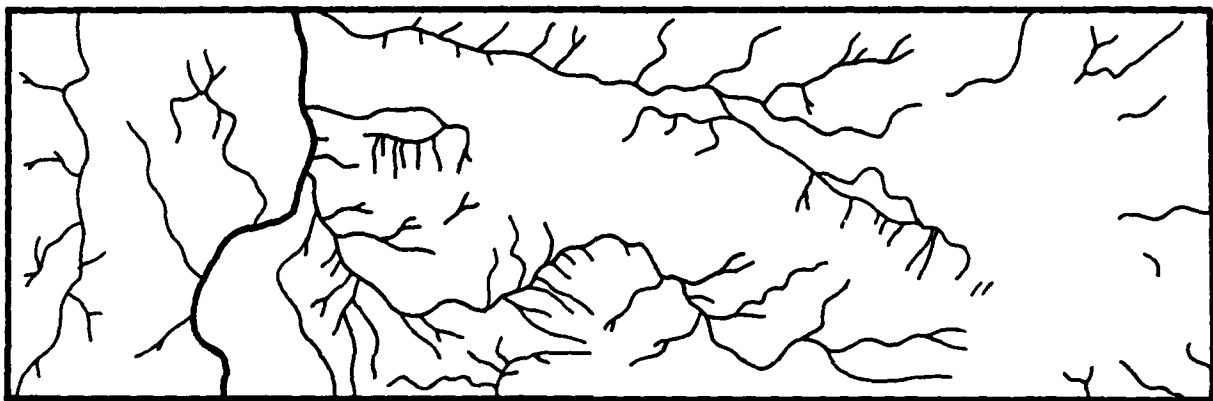

b. Landsat-3 imagery

LOOK DIRECTION

0   10   20 km

c. Landsat-2 imagery

Figure 41. Comparison of Aircraft X-band radar (a); Landsat-3 imagery, 17 March 1979, MSS band 7, solar elevation 49°, solar azimuth 114°, ID No. 83037707241500 (b); Landsat-2 imagery, 26 March 1979, MSS band 7, solar elevation 49°, solar azimuth 114°, ID No. 82152407134500 (c)

67

a. Aircraft X-band radar
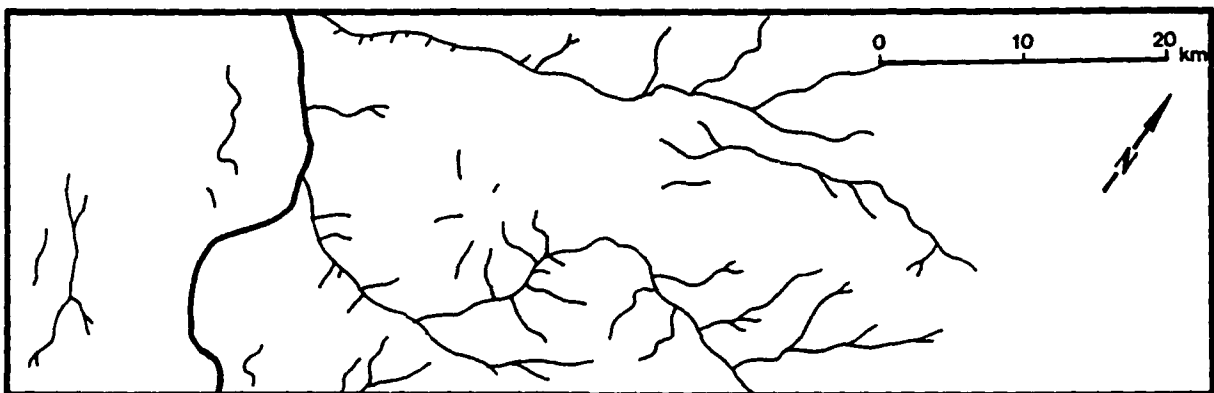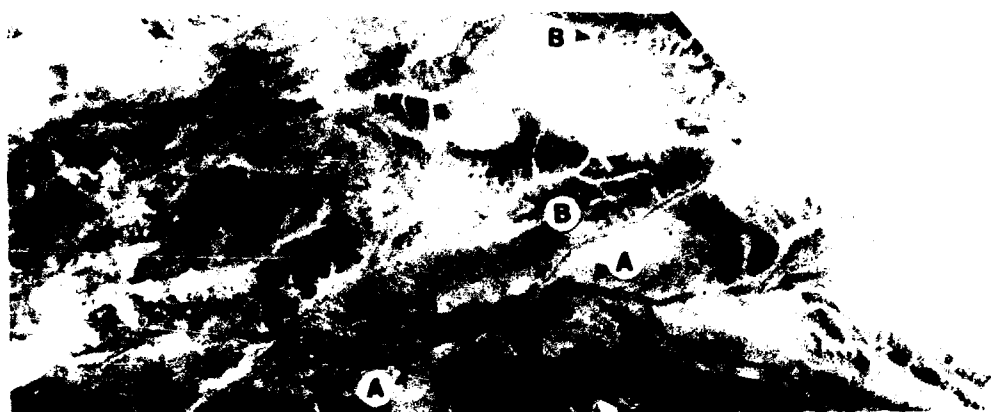

b. Landsat-3 imagery

c. Landsat-2 imagery

Figure 42.   Comparison of drainage patterns interpreted from
radar and Landsat MSS imagery

and 2 were nearly identical, differences in image quality are probably related to differences in processing.

81. Comparison of Landsat MSS images showed that band 7 was often superior to bands 4 and 5 for the detection of fluvial complexes (Figure 43). Figure 44 provides an identical scene comparison of drainage patterns interpreted from separate MSS bands obtained on 4 April 1979. Of the band-7 images examined, certain stream channels appear darker on the imagery when compared with the interfluve areas (A, Figure 43a). In certain instances, differences in soil moisture within and outside the stream channels have resulted in tonal differences on the imagery. The infrared absorption by soil moisture causes damp ground to appear darker than dry ground. However, other channels are imaged as light-toned features (B, Figure 43a), suggesting that soil moisture is not always responsible for the enhancement of these features. The light-toned patterns imaged on band 7 are commonly related to differences in lithologies and soil types in and adjacent to the channels. Alluvium within the channels has a higher reflectivity in the band 7 range, causing it to be imaged in brighter tones. Vegetation growing adjacent to the fluvial channels can also affect the imaged light-toned patterns. Distinctive types of native vegetation commonly display upstream extensions of drainage patterns, existing in areas of high soil moisture. Local vegetation patterns can indicate the location of ground-water springs or seeps that, individually, are below the resolution limits of the MSS scanner.

82. Several Landsat-3 RBV images were evaluated to determine their potential for detecting radar rivers. The Landsat-3 RBV system has a resolution twice that of the MSS system and potentially allows for an improvement in the detection of intricate stream patterns. The panchromatic spectrum of the RBV system provides a "composite" of spectral wavelengths, which is also an apparent advantage for detecting surficial streams. A comparison of RBV and MSS band 5 images (Figure 45) acquired on 4 January 1979 illustrates the usefulness of RBV imagery in portraying stream complexes. The poor quality of the MSS image makes it almost unusable for interpreting fluvial patterns. Comparison of X-band radar imagery with Landsat imagery (Figure 45), all of which were obtained during the dry season, reveals that stream patterns are most obvious on the radar image.

a. MSS band 7
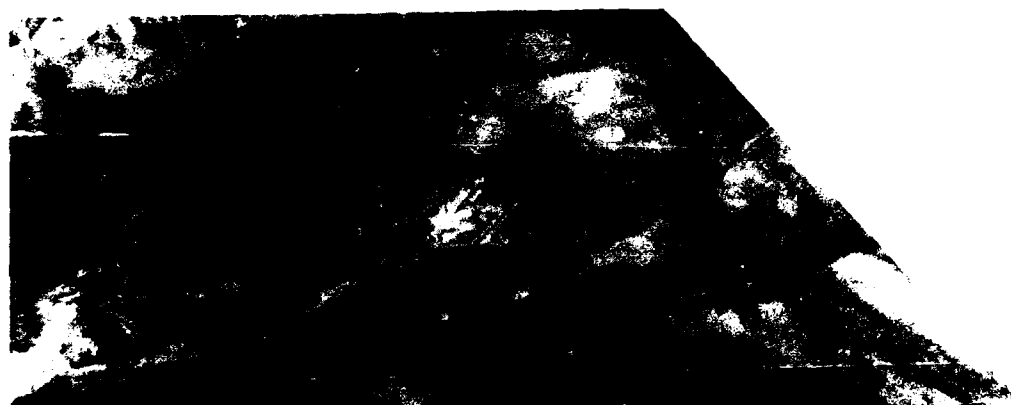
b. MSS band 5
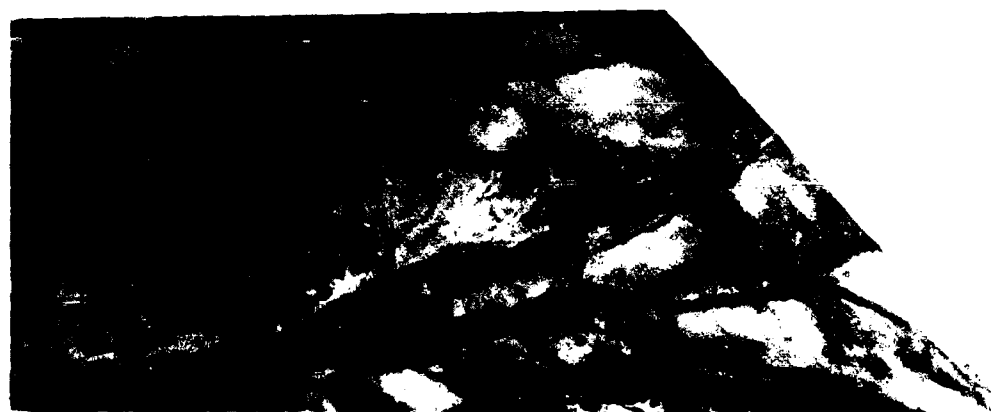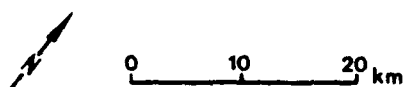
c. MSS band 4

Figure 43. Landsat-3 imagery, 4 April 1979, solar elevation 53°,
solar azimuth 104°, ID No. 83039507242500

70
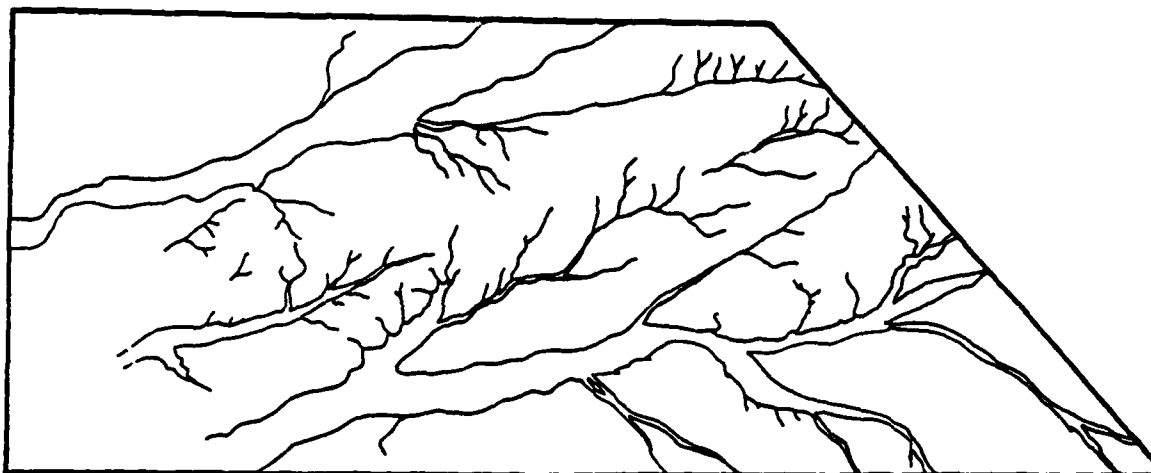
a.   MSS band 7

b.   MSS band 5

c.   MSS band 4

Figure 44.   Comparison of drainage patterns interpreted from Landsat
imagery

a. Aircraft X-band radar

b. Landsat-3 RBV imagery
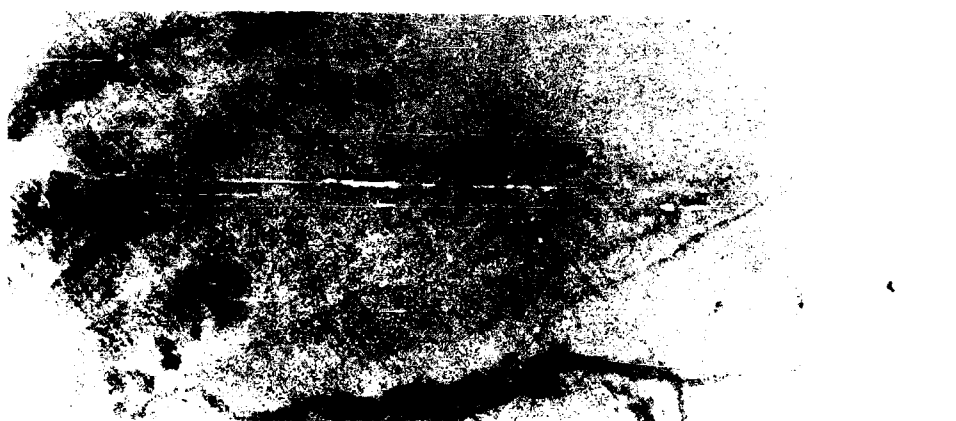
c. Landsat-3 imagery

Figure 45.   Comparison of Aircraft X-band radar (a); Landsat-3 RBV
imagery (b), 4 January 1979, solar elevation 36°, solar azimuth
138°, ID No. 83030507243XB; and Landsat-3 imagery (c), 4 January
1979, MSS band 5, solar elevation 37°, solar azimuth 138°, ID
No. 83030507244500

83. On Landsat 3, the RBV systems consist of two panchromatic cameras that produce two side-by-side images. The shuttering arrangement of the two vidicon cameras of the Landsat-3 RBV system allows the cameras to be shuttered alternately, twice each, resulting in four RBV "subscenes" for every MSS scene acquired. Subscenes "A" and "C" are acquired by one camera, and "B" and "D" by the other camera. In this study, inspection of the Landsat-3 RBV images revealed that fluvial patterns were better portrayed on all near-identical RBV "B" subscenes than on adjacent "C" subscenes despite the fact that image "pairs" were obtained on the same date. Because the "B" and "C" subscenes were obtained by different cameras, the quality degradation in the "C" sub-scenes could possibly be attributed to a camera malfunction in the RBV system. Inquiries to the EROS Data Center, from whom the imagery was acquired, revealed that malfunctions in the RBV system are common and many of the poor quality images are not always related to the film processing. Figure 46 compares an RBV "C" subscene and X-band radar imagery of the same area.

84. Pronounced wet and dry seasons exist in northeastern Sudan. Images acquired on different dates were examined to determine the effects of seasonal differences on the detection of fluvial systems. Rainfall data over the past 30 years indicate that about 90 percent of the 2 to 10 cm of annual precipitation within the study area occurs during the months of July, August, and September. During these wetter months, intermittent streams contain small amounts of surface water, and the increase in soil moisture immediately adjacent to these streams is sufficient to support vegetation. The reflectance from live vegetation is known to help outline existing fluvial systems on Landsat imagery. Inspection of the Landsat images revealed that increases in vegetation density along some stream channels did occur during the wetter months as was expected. The growth of vegetation during the wet season is helpful in locating certain fluvial channels on the Landsat imagery. However, in areas devoid of vegetation, the relation of seasonal effects to the detection of fluvial systems was minimal. Soil moisture levels of stream channels did not appear to vary significantly between wet and dry months.

85. Many of the older streams have become incised into the bedrock and filled with windblown sand. Within these incised streams, the high permeability of the sand deposits would allow for the immediate downward percolation of any precipitation, leaving little or no moisture on the surface. Because spectral characteristics between the bedrock and sand-filled channels are

a. Aircraft X-band radar
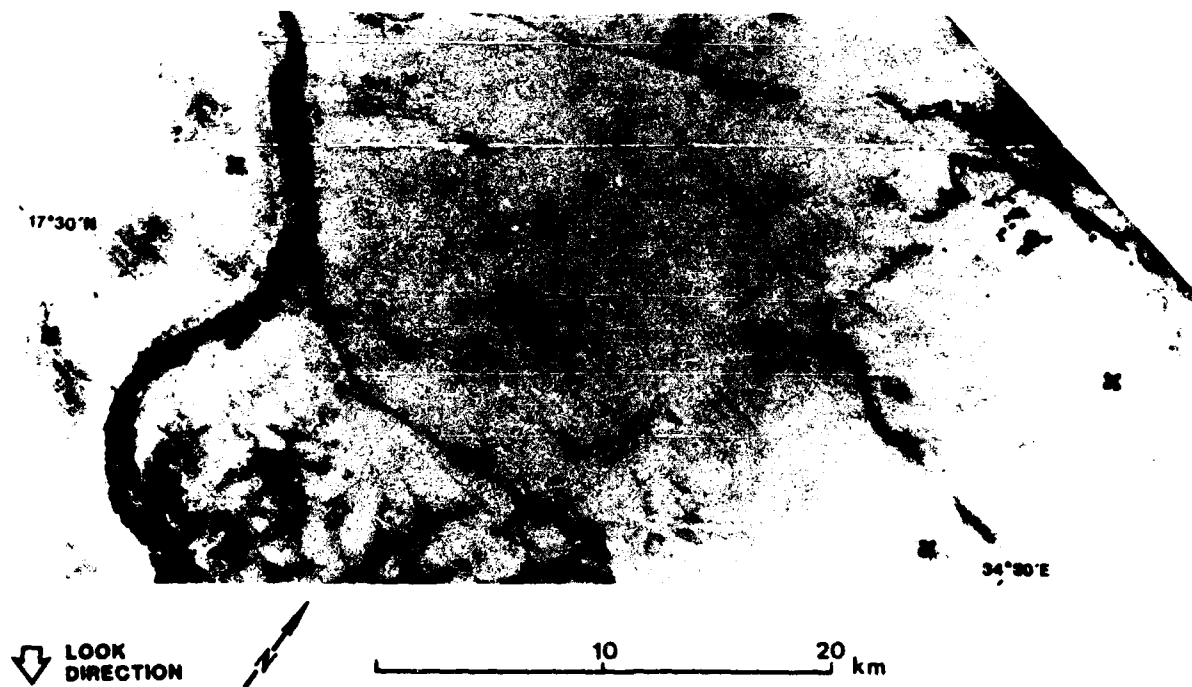
b. Landsat-3 radar "C" subscene

Figure 46. Comparison of Aircraft X-band radar (a) and Landsat-3 RBV "C" subscene (b), 22 January 1979, solar elevation 37°, solar azimuth 134°, ID No. 83032307243XC

often quite similar, detection of these channels on Landsat imagery is diffi-
cult. Aircraft radar, on the other hand, is sensitive to surface roughness
and not reflected light. Radar imagery is, therefore, a useful tool for
stream detection in desert areas because of the differences in surface
roughness between sand-filled channels, bedrock, and vegetation.

PART VI: CONTRAST ENHANCEMENT OF DIGITAL MULTISPECTRAL SCANNER DATA

86. A multitude of image enhancement procedures have evolved to deal with Landsat MSS data in their computer-compatible tape (CCT) format. The CCT's contain the image data in digital form. Image enhancement algorithms are applied to MSS digital data to improve the appearance of an image for visual interpretation or for subsequent machine analysis. One single image enhancement technique is not suitable for all purposes; the choice of techniques selected should be a function of the user's requirements. For this study, simple contrast enhancement techniques greatly increased the amount of information that could be visually interpreted from a Landsat image format.

Contrast Enhancement

87. The Landsat MSS was designed to accommodate a wide range of scene brightness values (pixels) from black volcanic flows to high-reflectance desert regions. Few individual terrain scenes have a brightness range that uses the full brightness range of the MSS detectors in the visible and near-infrared portion of the electromagnetic spectrum; consequently, only a small range of brightness values is used, resulting in a low-contrast scene. In addition, the EROS Data Center's photographic reproduction of Landsat imagery commonly varies in quality, with, of course, the least desirable products being those that lacked adequate contrast (discussed in Parts IV and V of this report). Maximum use of as much of this brightness range as possible can, however, produce an image with the optimum contrast ratio. The technique used to expand the range of brightness values so that they are displayed over a larger range is known as contrast enhancement or contrast stretch.

Comparison of Contrast-Enhanced Landsat Imagery with SIR-A Imagery

88. The Landsat scene illustrated in Figure 47 is a contrast-enhanced, MSS band 7 image obtained in northwestern Sudan near test site 2 (Figure 4). An attempt was made to make the gray tones on the Landsat image look similar to those on the SIR-A image of the same area (Figure 48). Consequently, a negative print, rather than the usually positive print, was produced. This negative print causes the sand-filled fluvial channels on the Landsat image to
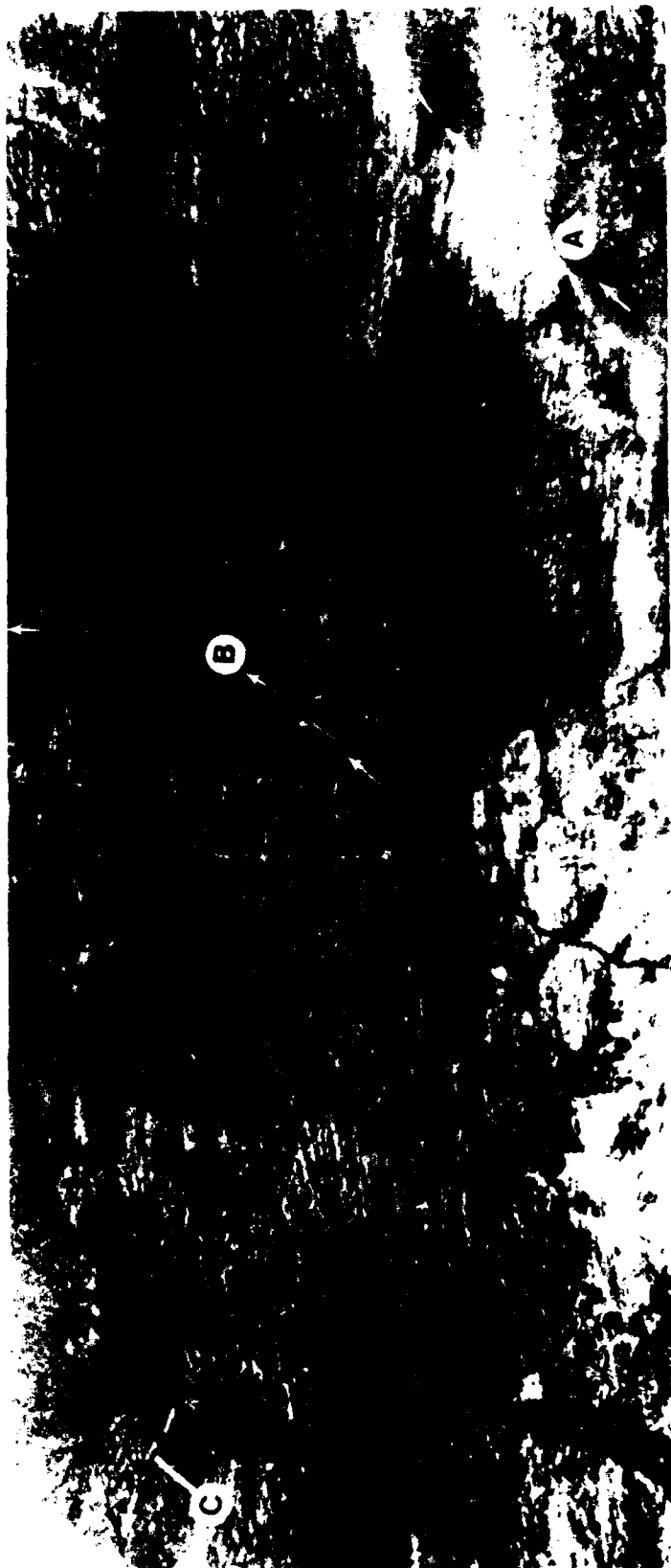
Figure 47. Contrast-enhanced Landsat-1 imagery of test site 2, 11 February 1973, MSS band 7, solar elevation 41°, solar azimuth 132°, ID No. 81203081515
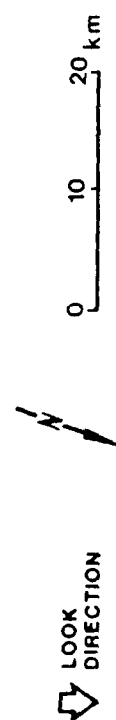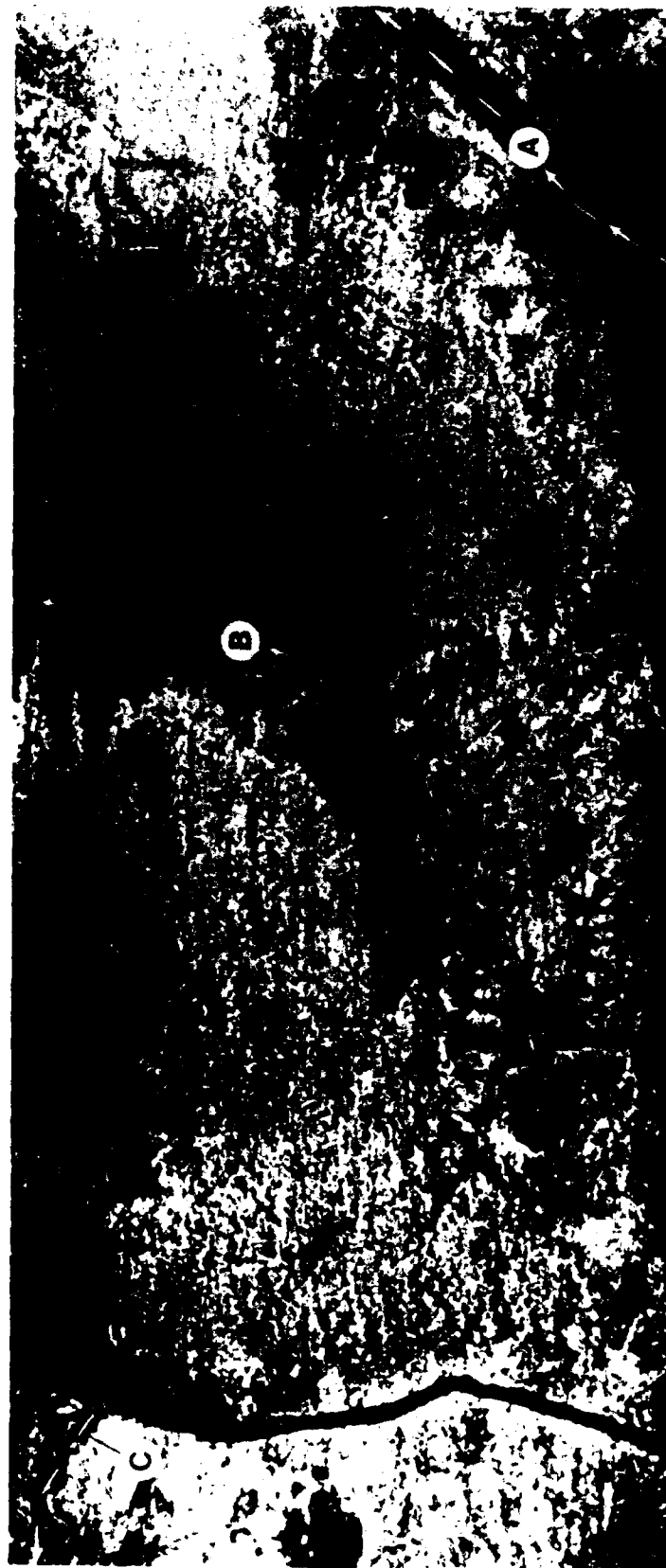
Figure 48. SIR-A imagery of test site 2, 13 November 1981, orbit 27, data take 28

appear dark, which is somewhat similar to the gray tone of the "radar rivers" on the SIR-A image. Nonetheless, the relict stream valleys at A and B and the incised channel at C are much more obvious on the SIR-A image (Figure 48) than on the Landsat image (Figure 47).

89. The capability to map on a regional scale (i.e., beyond the 50-km-swath width coverage of SIR-A) is needed when relict fluvial systems are used to prioritize potential well-drilling sites. Using the test site 2 location (Figure 4), fluvial channels were first located on the SIR-A image swath that traversed the central part of a contrast-enhanced Landsat scene (Figure 49). Drainage patterns were then extended beyond the SIR-A coverage using only the Landsat image. Two major valleys that converge at C appear to originate some 100 km to the north-northwest. Inferred flow directions have been annotated in some of the larger stream valleys. The two incised channels (A) extend well beyond the SIR-A coverage (Figure 48) and are easily mapped on the Landsat. The largest incised channel "flows" to the south-southeast, emptying onto a flat sand plain in the vicinity of area E. The accurate delineation of fluvial patterns in the sand plain is difficult.

Figure 49. Contrast-enhanced Landsat-1 imagery in vicinity of test site 2, solar elevation 41°, solar azimuth 132°, ID No. 81203081515

PART VII: CONCLUSIONS AND RECOMMENDATIONS

Conclusions

90. This report provides (a) an evaluation of the suitability of Land-sat imagery to bridge the gap between shuttle radar flight lines, (b) a discussion of the circumstances under which one remote sensor can be superior to the other for detecting relict drainage systems, and (c) an assessment of the value of imaging radar for ground-water exploration in arid regions, which is critical to the successful conduct of military operations. Based on the comparisons and analyses presented in this report, the following general conclusions can be drawn:

 a. Shuttle imagery of arid regions of northeastern Chad, north-western Sudan, and south-central Egypt allows for the mapping of stream channels and other drainage features that are, in part, covered with windblown sand. These features represent potential sources of ground water that can be tapped by military well-drilling units.

 b. Desert terrains, characterized by a veneer of eolian drift sand, commonly possess relatively uniform spectral characteristics. Consequently, the inference of relict fluvial channels using visible and near-infrared Landsat imagery is often difficult; however, digital techniques for enhancing the contrast can significantly improve the interpretability of the imagery.

 c. Photographic reproductions of Landsat MSS images from arid terrains produced by the EROS Data Center typically lack adequate contrast. This problem is compounded by film processing inconsistencies.

 d. In comparison with Landsat analysis, structural elements in the terrain that influence ground-water movement (lineaments) are more easily detected and can be mapped with greater accuracy when using shuttle radar imagery. Similarly, radar imagery is generally more useful than Landsat imagery for determining lithology.

 e. During the wet season, vegetation growth can aid in locating certain fluvial channels on Landsat imagery. Soil moisture differences, which can sometimes define stream patterns, are more easily inferred on Landsat band 7 than on bands 4 and 5.

 f. The Landsat-3 RBV system with a 30-m resolution and a broad spectral band recording allows for the mapping of considerably more terrain detail than can be inferred from MSS imagery.

g. Relative to Landsat short-wavelength (3-cm) aircraft radar imagery provides an improved means for mapping fluvial channels in arid regions. Although such channels are preferentially highlighted on the radar imagery because of the presence of fine-grained sand, rocky soil, and in some cases, sparse vegetation within the channels, aircraft radars could have considerable applicability in sand-covered terrains where differences in surface morphology and texture define relict fluvial channels--a capability important to military planners.

h. If a Landsat imagery data base is properly selected and processed, relict fluvial channels initially mapped on shuttle imagery can be extended and mapped on a regional basis. Used in a complementary mode, radar imagery and Landsat data can provide an important ground-water exploration tool in arid regions throughout the world. Given the current military significance of Southwest Asia and the necessity for identifying ground-water resources in arid regions, the use of such a tool could make the difference between success and failure on the battlefield.

Recommendations

91. The following recommendations are made for improving ground-water exploration by US forces in arid regions:

a. Using shuttle radar and Landsat data in a complementary mode, a ground-water test site should be selected in a hyperarid area, and a geophysical/well-drilling program should be conducted to determine the validity of including "radar river" mapping as an integral part of the Army Water Resources Data Base.

b. Landsat-4 and -5, Thematic Mapper, and SPOT satellite data should be evaluated for potential application to mapping relict fluvial channels in arid environments.

c   Military reconnaissance aircraft radar (short-wavelength) imagery should be obtained for an arid environment with a veneer of eolian drift sand and compared with shuttle imagery of the same area. The "penetration advantage" of the relatively long wavelength shuttle radar should then be evaluated.

d. Imagery interpretation and enhancement techniques presented and discussed herein should be included in a remote sensing manual dealing with ground-water location/exploration for use by US Army Terrain Teams.

e. The use of remote sensing techniques as part of an integrated approach to ground-water location/exploration should be considered in future military efforts in arid regions.

REFERENCES

Blom, R. G., Crippen, R. J., and Elachi, C. 1984. "Detection of Subsurface Features in Seasat Radar Images of Means Valley, Mojave Desert, California," Geology, Vol 12, pp 346-349.

Breed, C. S. 1983. "Subsurface Imaging with SIR-A in the Egyptian Desert," Proceedings of the Seventeenth International Symposium on Remote Sensing of the Environment, Ann Arbor, MI, pp 11-12.

Elachi, C., Brown, W. E., Cimino, J. B., Dixon, T., Evans, D. L., Ford, J. P., Saunders, R. S., Breed, C., Masursky, H., McCauley, J. P. Schaber, G. G., Dellwig, L., England, A., MacDonald, H. C., Martin-Kaye, P., and Sabins, F. 1982. "Shuttle Imaging Radar Experiment," Science, Vol 218, pp 996-1003.

Elachi, C., Roth, L. E., and Schaber, G. G. 1984. "Spaceborne Radar Subsurface Imaging in Hyperarid Regions," IEEE Transactions on Geoscience and Remote Sensing, Vol GE-22, No. 4, pp 383-388.

Ford, J. P., Blom, R. G., Bryan, M. L., Dailey, M. I., Dixon, T. H., Elachi, C., and Xenos, E. C. 1980. "Seasat Views North America, the Caribbean, and Western Europe with Imaging Radar," Publication 80-67, Jet Propulsion Laboratory, Pasadena, CA.

Ford, J. P., Cimino, J. B., and Elachi, C. 1983. "Space Shuttle Columbia Views the World with Imaging Radar: the SIR-A Experiment," Publication 82-95, Jet Propulsion Laboratory, Pasadena, CA.

Ford, J. P., Cimino, J. B., Holt, B., and Ruzek, M. R. 1986. "Shuttle Imaging Radar Views the Earth from Challenger: the SIR-B Experiment," Publication 86-10, Jet Propulsion Laboratory, Pasadena, CA.

Jado, A. R., and Zotl, J. 1984. Quaternary Period in Saudi Arabia, Vol 2, Springer-Verlag, Vienna, Austria, pp 264-266.

Kaupp, V. H., Waite, W. P., and MacDonald, H. C. 1982. "Incidence Angle Considerations for Spacecraft Imaging Radar," IEEE Transactions on Geoscience and Remote Sensing, Vol GE-20, No. 3, pp 384-390.

MacDonald, H. C. 1969. "Geologic Evaluation of Radar Imagery from Darien Province, Panama," Modern Geology, Vol 1, No. 1, pp 1-63.

_____. 1980. "Historical Sketch-Radar Geology," Radar Geology: An Assessment, Publication 80-16, Jet Propulsion Laboratory, Pasadena, CA, pp 23-33.

McCauley, J. F., Schaber, G. G., Breed, C. S., Grolier, M. J., Haynes, C. V., Issawi, B., Elachi, C., and Blom, R. 1982. "Subsurface Valleys and Geoarcheology of the Eastern Sahara Revealed by Shuttle Radar," Science, Vol 218, No. 4576, pp 1004-1020.

Pravdo, S. H., Huneycutt, B., Holt, B. M., and Held, D. N. 1983. "Seasat Synthetic-Aperture Radar Data User's Manual," Publication 82-90, Jet Propulsion Laboratory, Pasadena, CA.

Rodis, H. G., Hassan, A., and Wahadan, L. 1963. "Availability of Ground Water in Kordofan Province, Sudan," Geological Survey of Sudan Bulletin, No. 12, pp 1-16.

Rodis, H. G., and Iskander, W. 1963. "Ground Water in the Hahud Outliner, the Nubian Series, Kordofan Province, Sudan," Paper 475-B, Article 49, US Department of the Interior, Geological Survey, Washington, DC, pp 179-181.

Russell, O. R., and Zall, L. 1981. "Landsat Imagery for Regional Ground-Water Exploration," Preprint 81-121, American Society of Civil Engineers, New York.

Said, R. 1962. The Geology of Egypt, Elsevier, Amsterdam.

Salama, R. B. 1976. "Ground-Water Resources of Sudan," Democratic Republic of Sudan, Rural Water Corporation, Khartoum, Sudan.

Schaber, G. G., Breed, C. S., McCauley, J. F., and Billingsley, G. 1985. "Physical Controls on SIR-A Signal Penetration and Subsurface Scattering in Mars-Like Eastern Sahara," Sixteenth Lunar and Planetary Conference, Vol 16, pp 732-733.

Schaber, G. G., McCauley, J. F., Breed, C. S., and Olhoeft, G. R. 1986 (July). "Shuttle Imaging Radar: Physical Controls on Signal Penetration and Subsurface Scattering in the Eastern Sahara," IEEE Transactions on Geoscience and Remote Sensing, Vol GE-24., No. 4, pp 603-623.

Shata, A. A. 1982. "Hydrology of the Great Nubian Sandstone Basin, Egypt," Quarterly Journal, Engineering Geology, Vol 15, pp 83-103.

Vail, J. R. 1978. "Overseas Geology and Mineral Resources," Institute of Geological Sciences, No. 49, pp 1-67.

Whiteman, A. J. 1971. The Geology of the Sudan Republic, Clarendon Press, Oxford.

Wright, E. P., Benfield, A., Edmunds, W., and Kitching, R. 1982. "Hydrology of the Kufra and Sirte Basins, Eastern Libya," Quarterly Journal, Engineering Geology, Vol 15, pp 83-103, London.

MILITARY HYDROLOGY REPORTS

Report No.	No. in Series	Title	Date
TR EL-79-2	-	Proceedings of the Military Hydrology Workshop, 17-19 May 1978, Vicksburg, Mississippi	May 1979
MP EL-79-6 (Military Hydrology Series)	1	Status and Research Requirements	Dec 1979
	2	Formulation of a Long-Range Concept for Streamflow Prediction Capability	Jul 1980
	3	A Review of Army Doctrine on Military Hydrology	Jun 1981
	4	Evaluation of an Automated Water Data Base for Support to the Rapid Deployment Joint Task Force (RDJTF)	Nov 1981
	5	A Quantitative Summary of Groundwater Yield, Depth, and Quality Data for Selected Mideast Areas (U)	Mar 1982
	6	Assessment of Two Currently "Fieldable" Geophysical Methods for Military Ground-Water Detection	Oct 1984
	7	A Statistical Summary of Ground-Water Yield, Depth, and Quality Data for Selected Areas in the CENTCOM Theatre of Operations (U)	Oct 1984
	8	Feasibility of Using Satellite and Radar Data in Hydrologic Forecasting	Sep 1985
	9	State-of-the-Art Review and Annotated Bibliography of Dam-Breach Flood Forecasting	Feb 1985
	10	Assessment and Field Examples of Continuous Wave Electromagnetic Surveying for Ground Water	Jun 1986
	11	Identification of Ground-Water Resources in Arid Environments Using Remote Sensing Imagery	
	12	Case Study Evaluation of Alternative Dam-Breach Flood Wave Models	Nov 1986
	13	Comparative Evaluation of Dam-Breach Flood Forecasting Methods	Jun 1986
	14	Breach Erosion of Earthfill Dams and Flood Routing (BEED) Model	
	15	The Seismic Refraction Compression-Shear Wave Velocity Ratio as an Indicator of Shallow Water Tables A Field Test	Jun 1987
	16	Assessment of Shuttle Imaging Radar and Landsat Imagery for Ground-Water Exploration in Arid Environments	Jun 1984
	17	A Quasi-Conceptual Linear Model for Synthesis of Direct Runoff with Potential Application to Ungaged Basins	
Unnumbered		Proceedings of the Ground Water Detection Workshop, 12-14 January 1982, Vicksburg, Mississippi	Dec 1984